“Advances in core spectroscopy”

Impurities in the core of burning plasmas: PFCs, radiation, stability, transport and diagnostic challenges

Luis F. Delgado-Aparicio *et al*.

Princeton Plasma Physics Laboratory (PPPL)

Princeton University, PPPL, 08/14/2018

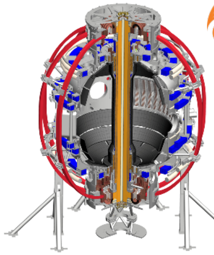

Outline

① Magnetically confined fusion (MCF) plasmas and the Z-challenge

② Z-studies

③ Radiation and the need of spectroscopy?

④ Novel x-ray diagnostics

⑤ Summary

Tokamaks (and stellarators) around the world study different plasma parameters and shapes

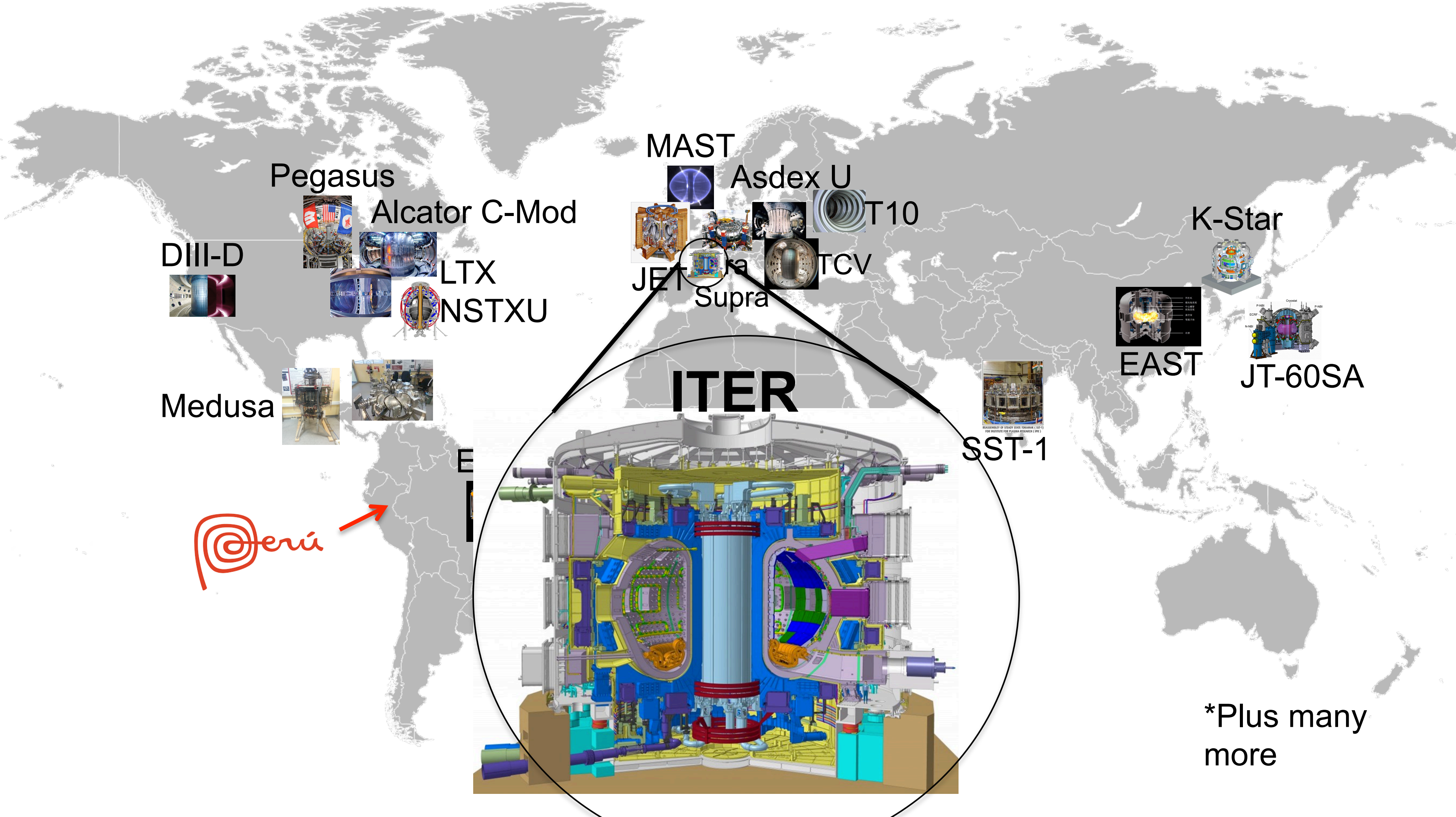

*Plus many more

ITER will be the first time we have net energy (more energy OUT than IN)

ITER is a collaboration between USA, EU, China, Japan, Korea, India and Russia

It's expected to produce 500MW of power using 50MW to run…this is the 1st time in history where $P_{out} > P_{in}$

First plasmas expected by ~ 2025

Many challenges ahead!

The Z-challenge? (low-Z vs high-Z)

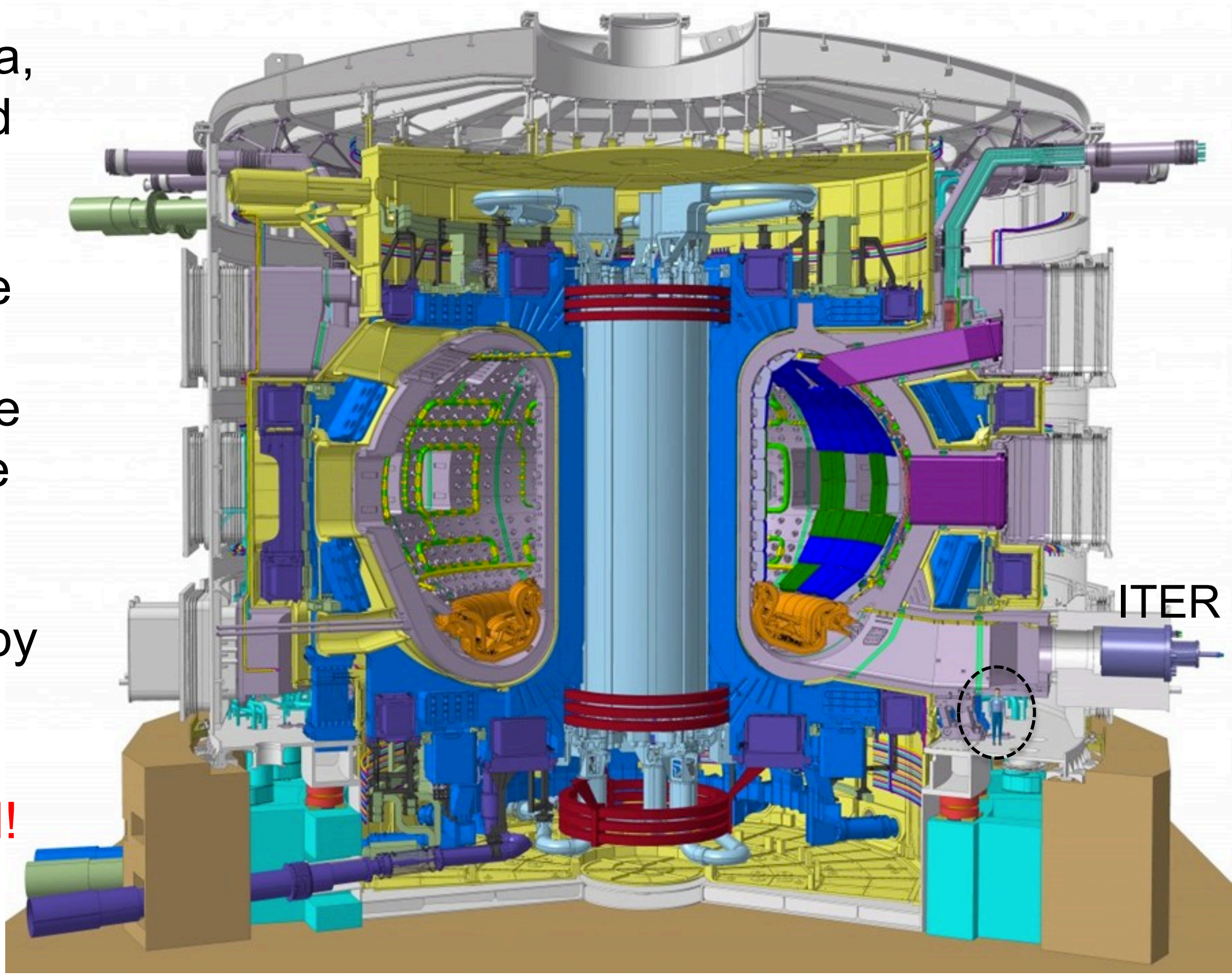

The low-Z (Li, Be, C, B) vs high-Z (Fe, Mo, W) plasma facing component (PFC) challenge

Both low- & high-Z materials are currently being used for the **PFCs**, but each has technological hurdles.

MAST, CCFE, Oxfordshire, UK

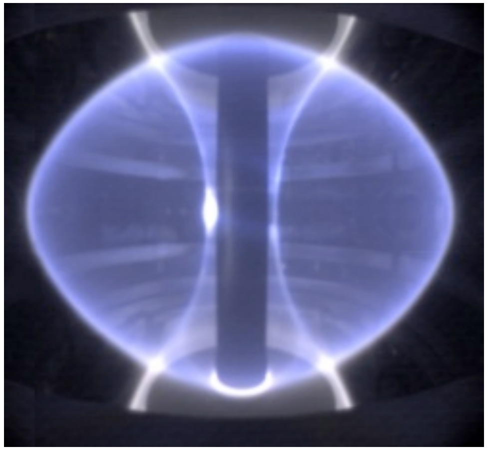

① Low-Z materials:

a) Typically have higher erosion rates

b) Their injection into the main chamber will result in an increase of Z_{eff} and collisionality ($\nu_{e,Z}$).

c) H-, D- & T-retention is a difficult issue!

NSTX-U @ PPPL, Princeton University, Princeton, NJ

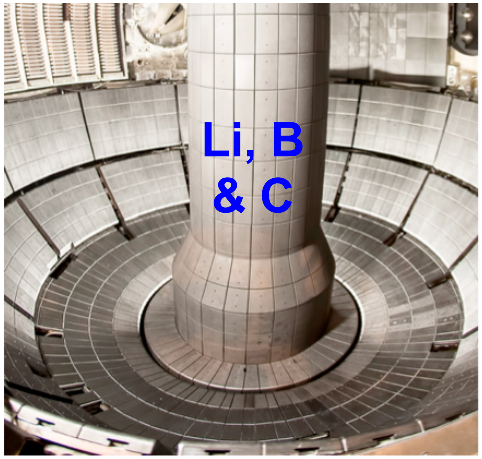

② Augment of Z_{eff} will lead to:

a) Reduce fuel purity (n_D/n_e) and reactivity ($S_n \propto n_D^2$ or $n_D n_T$).

b) But contributing less to radiated power density:

$P_{rad}=n_e n_D L_D+n_e n_C L_c+\Sigma n_e n_Z L_Z$

The low-Z (Li, Be, C, B) vs high-Z (Fe, Mo, W) plasma facing component (PFC) challenge

③ Conversely, high-Z materials have good properties as a PFCs:
a) Low H/D/T retention.
b) High-heat tolerance (e.g. high melting points)
c) Low erosion (sputtering) rates.
d) Small contribution to Z_{eff}:

$$Z_{eff}=n_D/n_e+36n_C/n_e+\Sigma(n_Z/n_e)Z^2$$

④ However, if high-Z impurities accumulate to any substantial level:
a) Exponentially enhance the radiation power losses ($\propto Z^4$).
b) Reduce the heating efficiency and modifying the overall power balance.

⑤ High-n_Z/n_e can lead to radiation collapse

Tore Supra/WEST in France

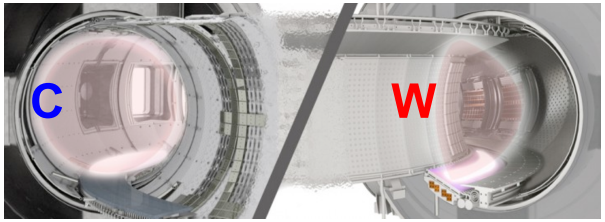

EAST in China

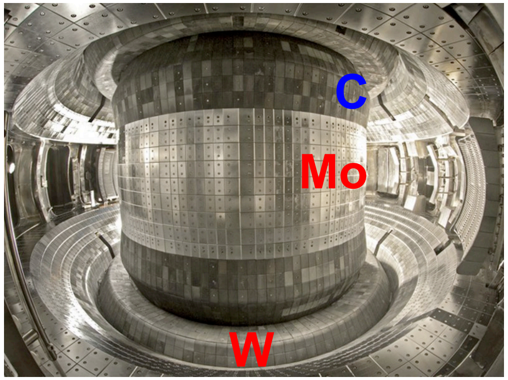

C-Mod in Cambridge, MA, USA

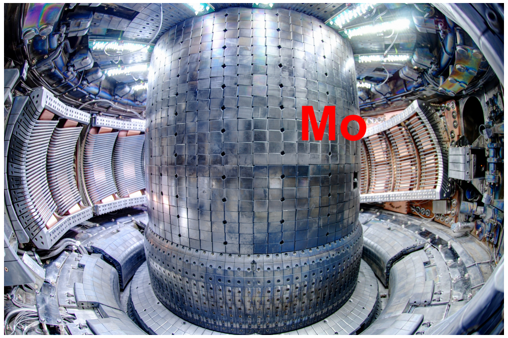

Present and future tokamaks deal with the difficulties associated with metallic walls

PSFC MIT

C-Mod (MIT), WEST (France), JET (UK), ASDEX (DE), EAST(China) have metallic PFCs

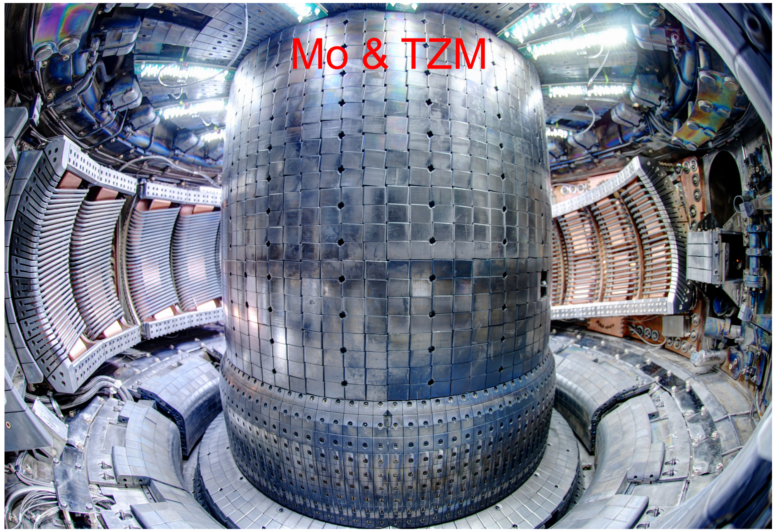

Low-Z
Boron (fully stripped)
Carbon (fully stripped)

Medium-Z
Argon (He- and H-like)

High-Z
Molybdenum (Ne-like)

Nominal 5-7 year plan steps for implementation of high-Z wall in NSTX-U

NSTX-U

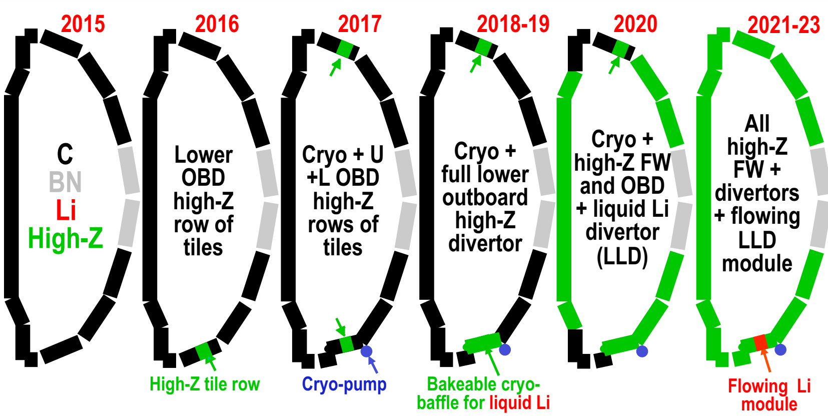

PPPL

ITER will have Be & W PFCs

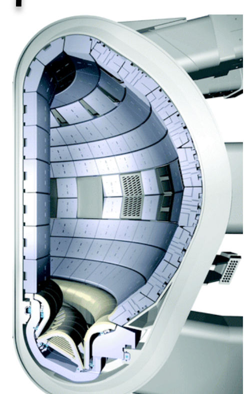

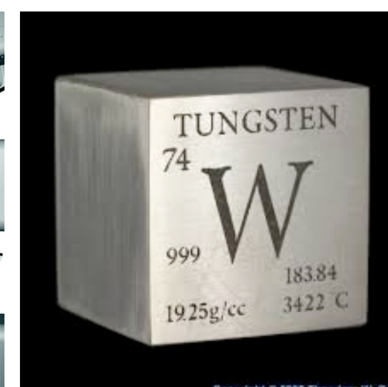

With the help of detailed simulations ITER decided on a wall with low- and high-Z PFCs

Simulations of plasma flows and plasma-wall interaction have had a decisive influence on the design of ITER wall.

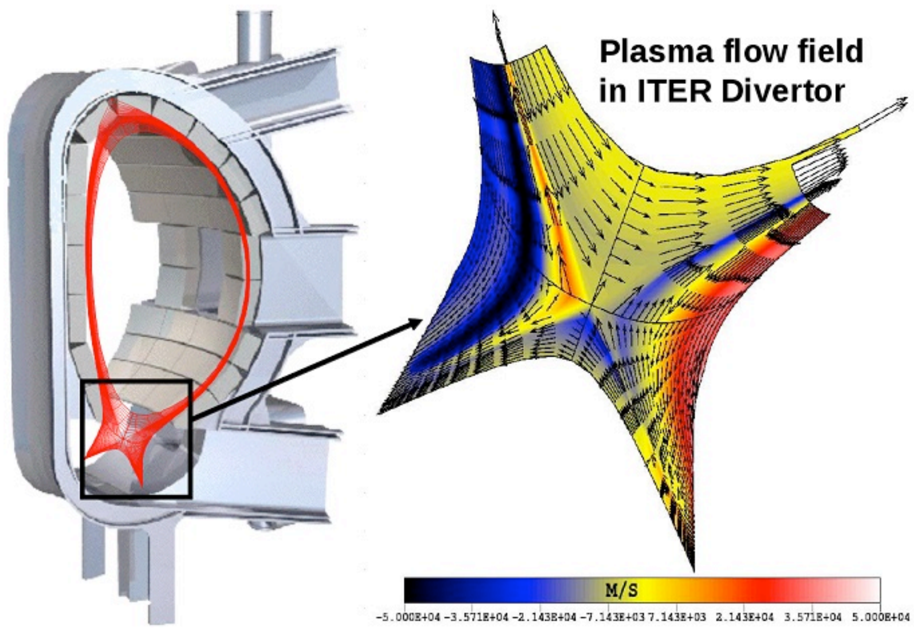

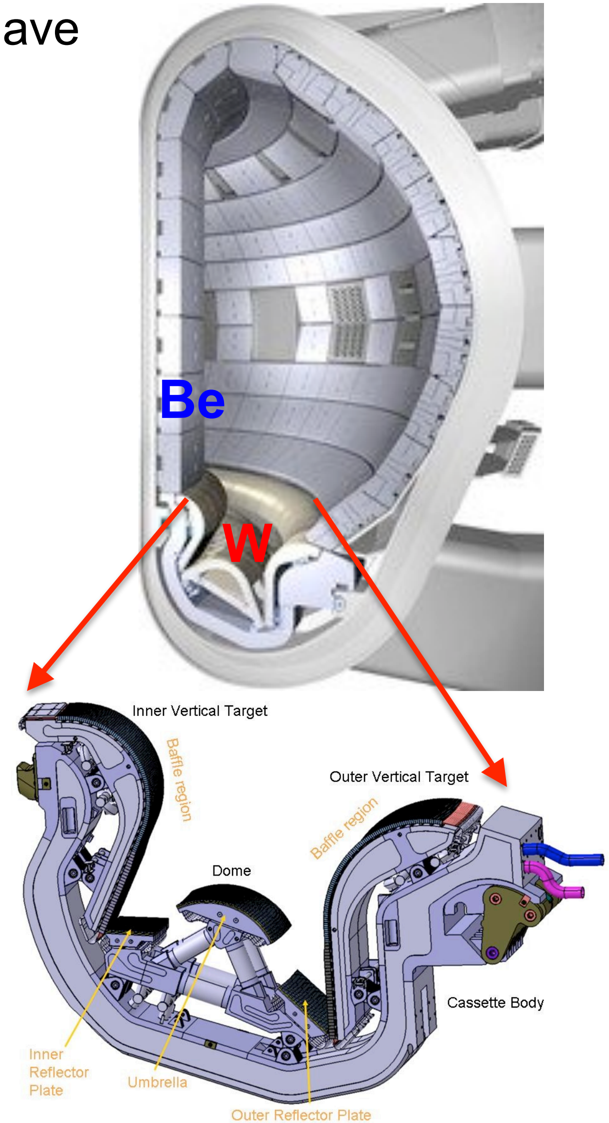

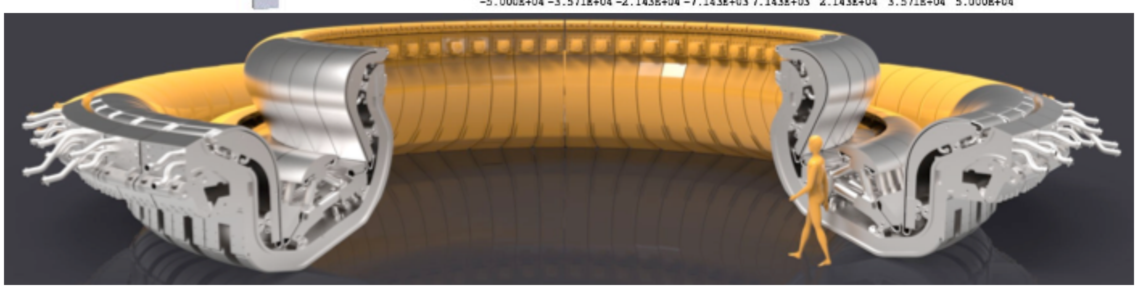

Edge localized modes (ELMs) and disruptions can impact integrity of divertor cassettes

Summary 1: Its is important to understand, tailor and control Z-transport & accumulation

① Understanding the sources, transport/confinement of high-Z impurities is crucial to ITER success:

- Degradation of energy confinement
- Impurity-induced macroscopic instabilities
- Fuel dilution

② Controlling Z-transport to avoid accumulation in the core is necessary to achieve and maintain high fusion performance.

STUDY: - Neoclassical transport
- Turbulent-induced transport
- Effect of RMPs!

③ For the near future: **Novel diagnostics** should become an essential part of a control algorithm coupled to physics & engineer actuators for minimizing impurity accumulation in tokamaks (diagnostic development in-line with OFES mission).

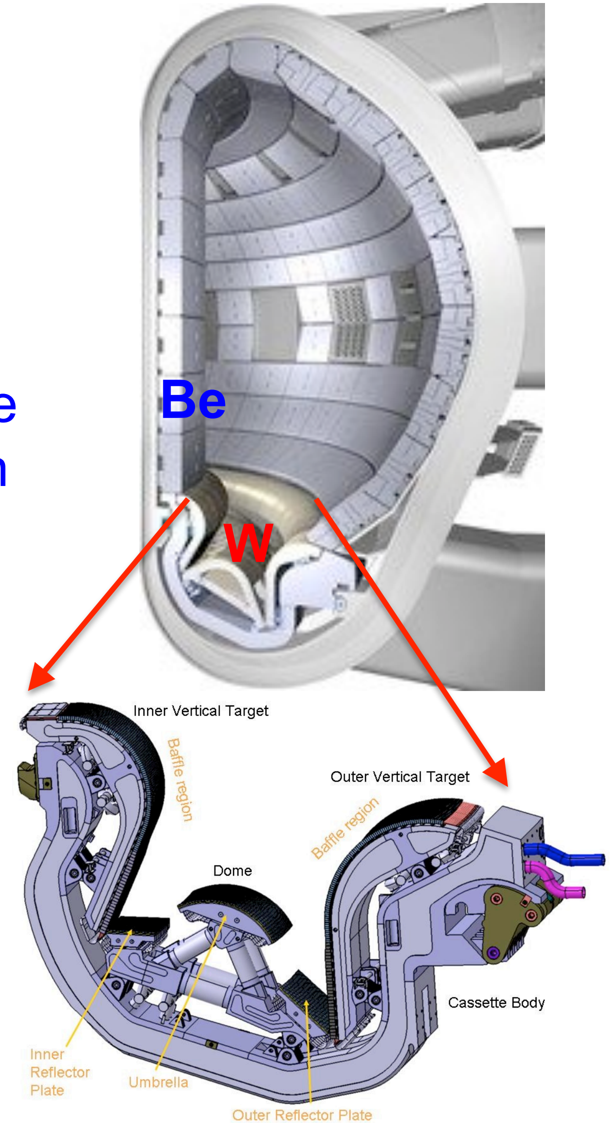

Outline

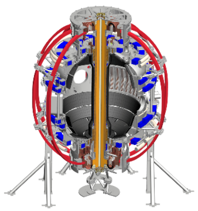

① Magnetically confined fusion (MCF) plasmas and the Z-challenge

② Z-studies

③ Radiation and the need of spectroscopy?

④ Novel x-ray diagnostics

⑤ Summary

Outline

② Examples of Z-studies:

a) Transport & asymmetries
b) Core stability
c) Density-limit

Outline

② Examples of Z-studies:

a) Transport & asymmetries

b) Core stability

c) Density-limit

Impurity transport can be complicated but now its much simpler than before (using modern diagnostics + codes)

Conventional transport equations (Z)

$$\frac{\partial n_Z(r,t)}{\partial t} = -\nabla \cdot \Gamma_Z + \left[n_{(Z-1)} S_{(Z-1)\to Z} + n_{(Z+1)} S_{(Z+1)\to Z}\right] - n_Z \left[S_{Z\to(Z-1)} + S_{Z\to(Z+1)}\right]$$

$$\Gamma_Z(r,t) = -D_Z(r,t)\frac{\partial n_Z(r,t)}{\partial r} + n_Z(r,t)V_Z(r,t)$$

Degree of Z-peaking:

$$\frac{1}{n_Z}\frac{\partial n_Z}{\partial r}(r,t) = \frac{V_Z}{D_Z}(r,t)$$

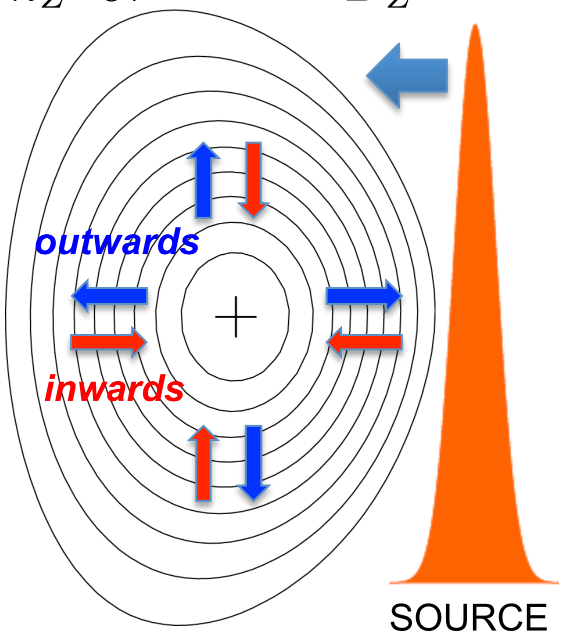

Impurity transport studies require:

① Adequate radial COVERAGE (0<r/a<1)

② Adequate radial and time resolution (Δr/a~1/20, Δt~1-5 ms)

③ Charge-state density resolution: f(T_e) (measure emissivity from several n_Z's)

④ Filter vs photon-energy resolution & coverage

⑤ Ability to discern between between symmetric and asymmetric phenomena: (r) vs (r,θ)

⑥ Spend less time on 2D tomography and **do physics!**

New “smart” diagnostics are needed to study impurity transport and density asymmetries

L. F. Delgado-Aparicio, et. al., RSI, **85**, 11D859, (2014).
L. F. Delgado-Aparicio, et. al., to be submitted, NF, (2018).

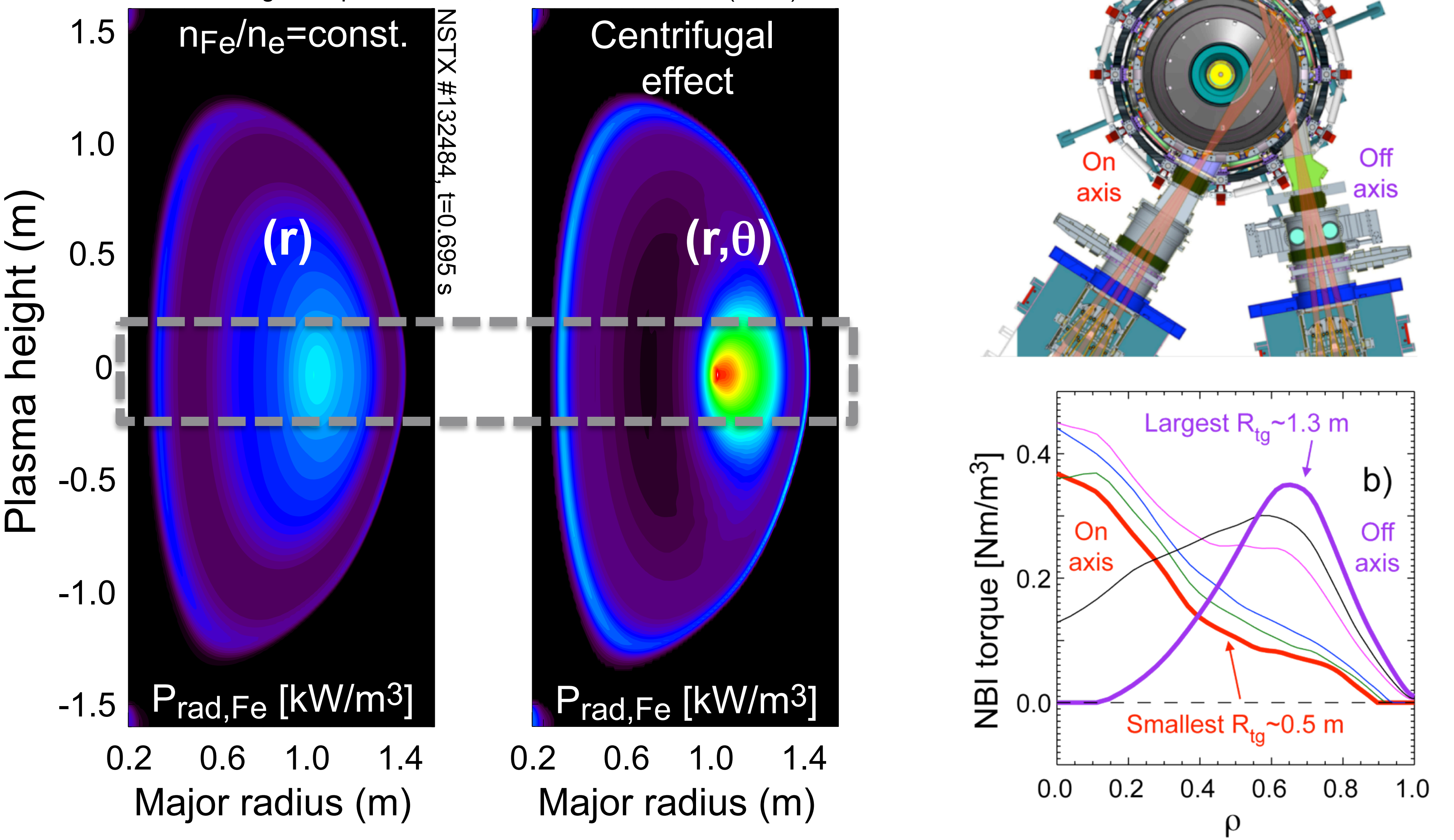

Solutions for electrostatic potential ($\Delta\Phi$) and impurity density show in/out asymmetries

2D solution for electrostatic potential

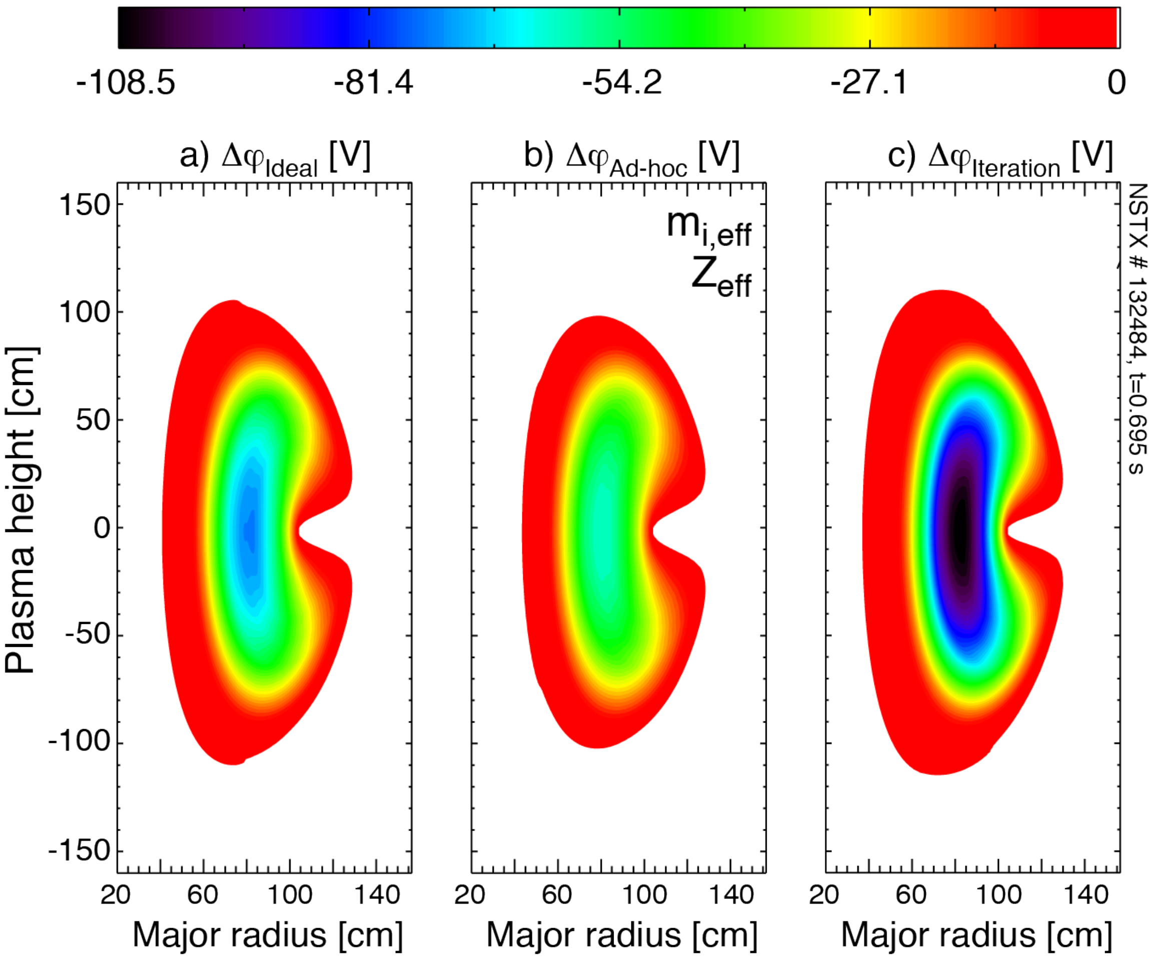

Impurity ion density in/out asymmetries

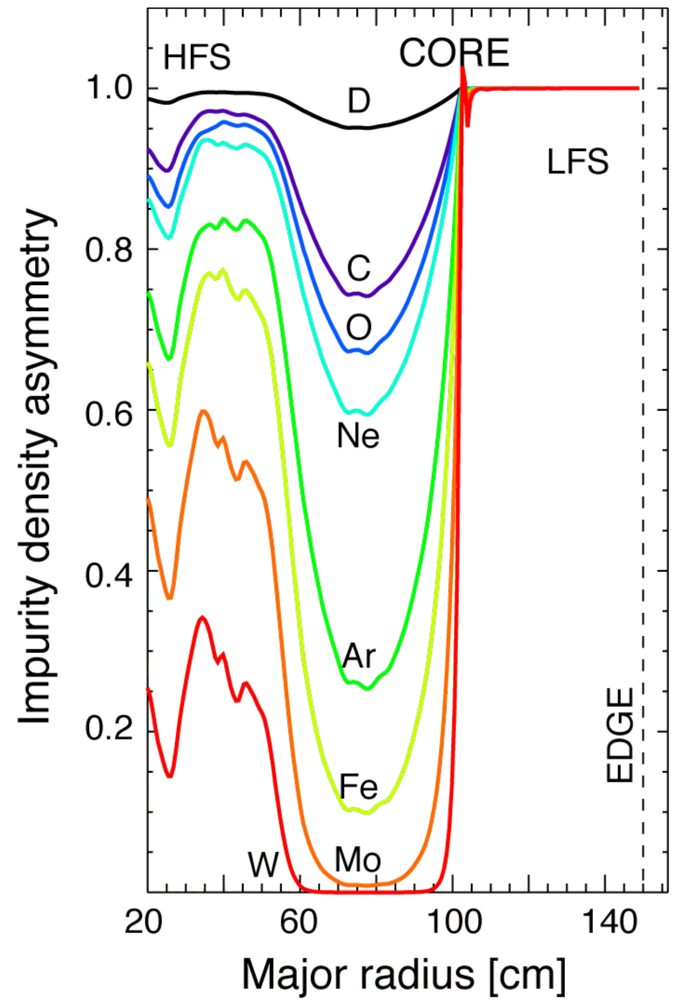

Core bremsstrahlung emission from main ion and fully stripped low-Z impurities is small

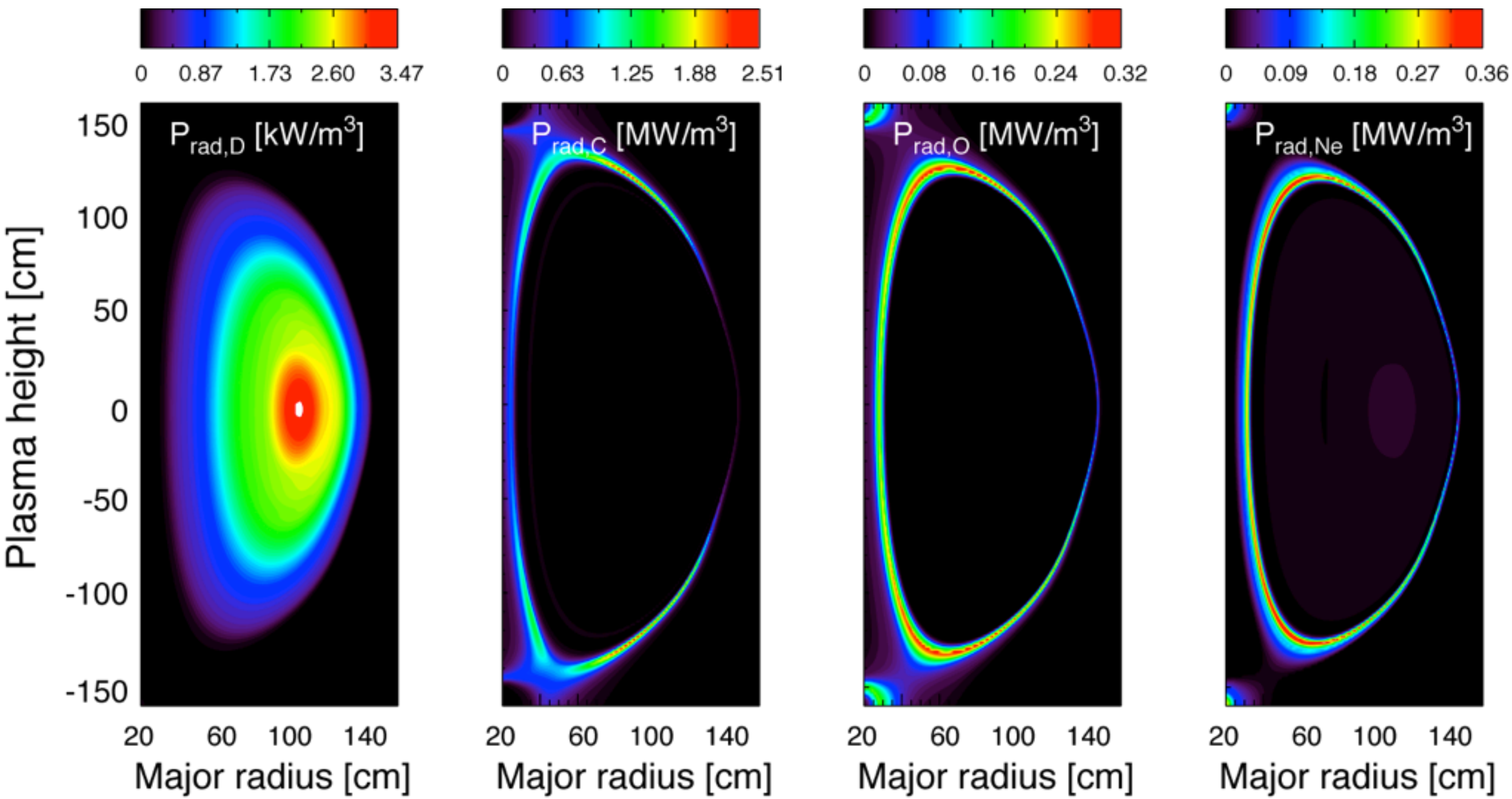

Core radiation from medium- to high-Z will be affected by centrifugal forces in NSTX-U

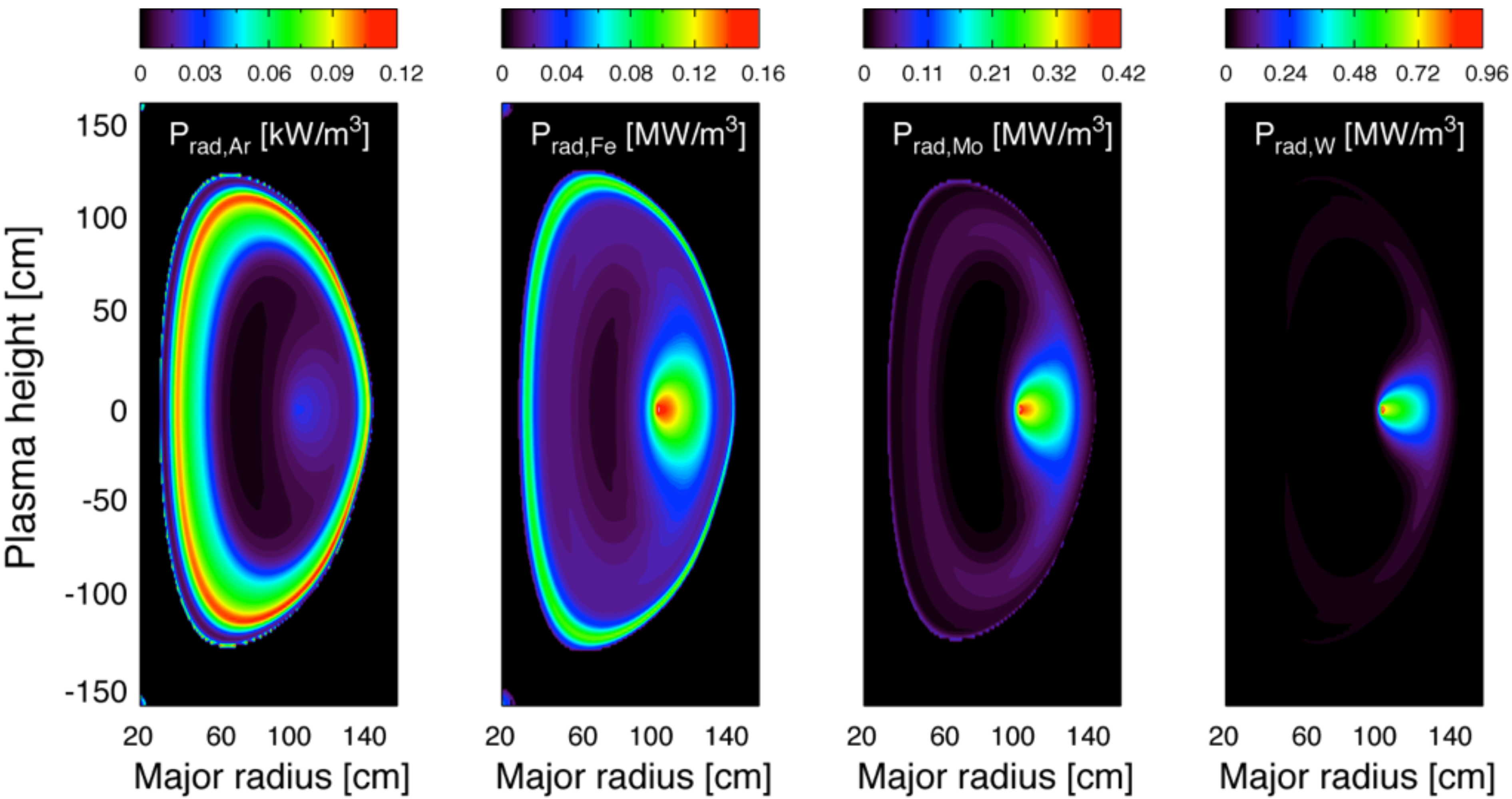

Outline

② Examples of Z-studies:

a)Transport & asymmetries

b) Core stability

c) Density-limit

Large family of macroscopic instabilities can be affected by Z-charge and radiation effects

High-Z impurities can degrade core confinement and can be the cause also of radiative density limit disruptions

Core (1/1) modes
0<r/a<0.5

Mid-radius (m/n) modes
0.3<r/a<0.9

Edge
0.9<r/a<1.1

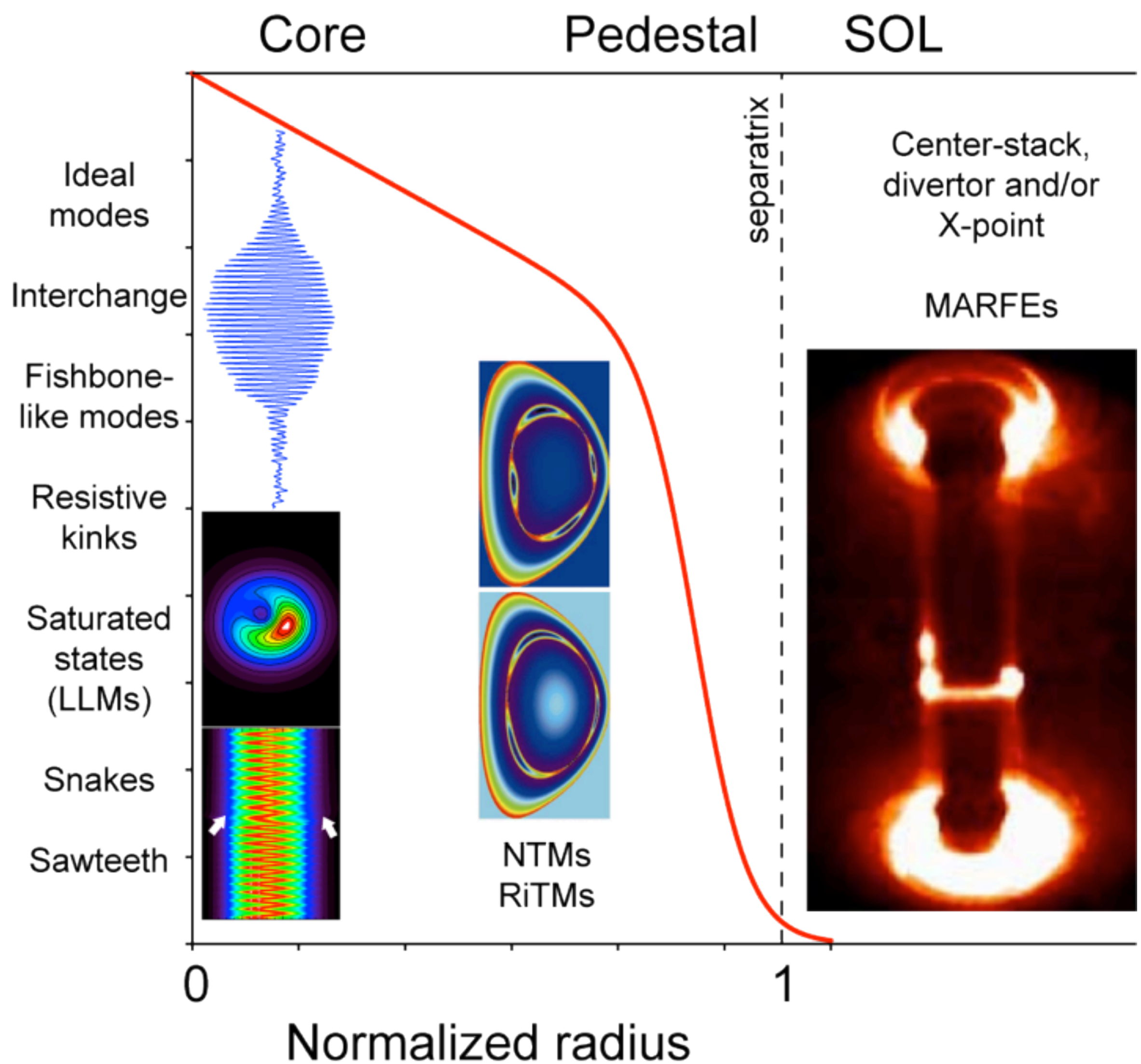

Large family of macroscopic instabilities can be affected by Z-charge and radiation effects

High-Z impurities can degrade core confinement and can be the cause also of radiative density limit disruptions

Core (1/1) modes
0<r/a<0.5

Mid-radius (m/n) modes
0.3<r/a<0.9

Edge
0.9<r/a<1.1

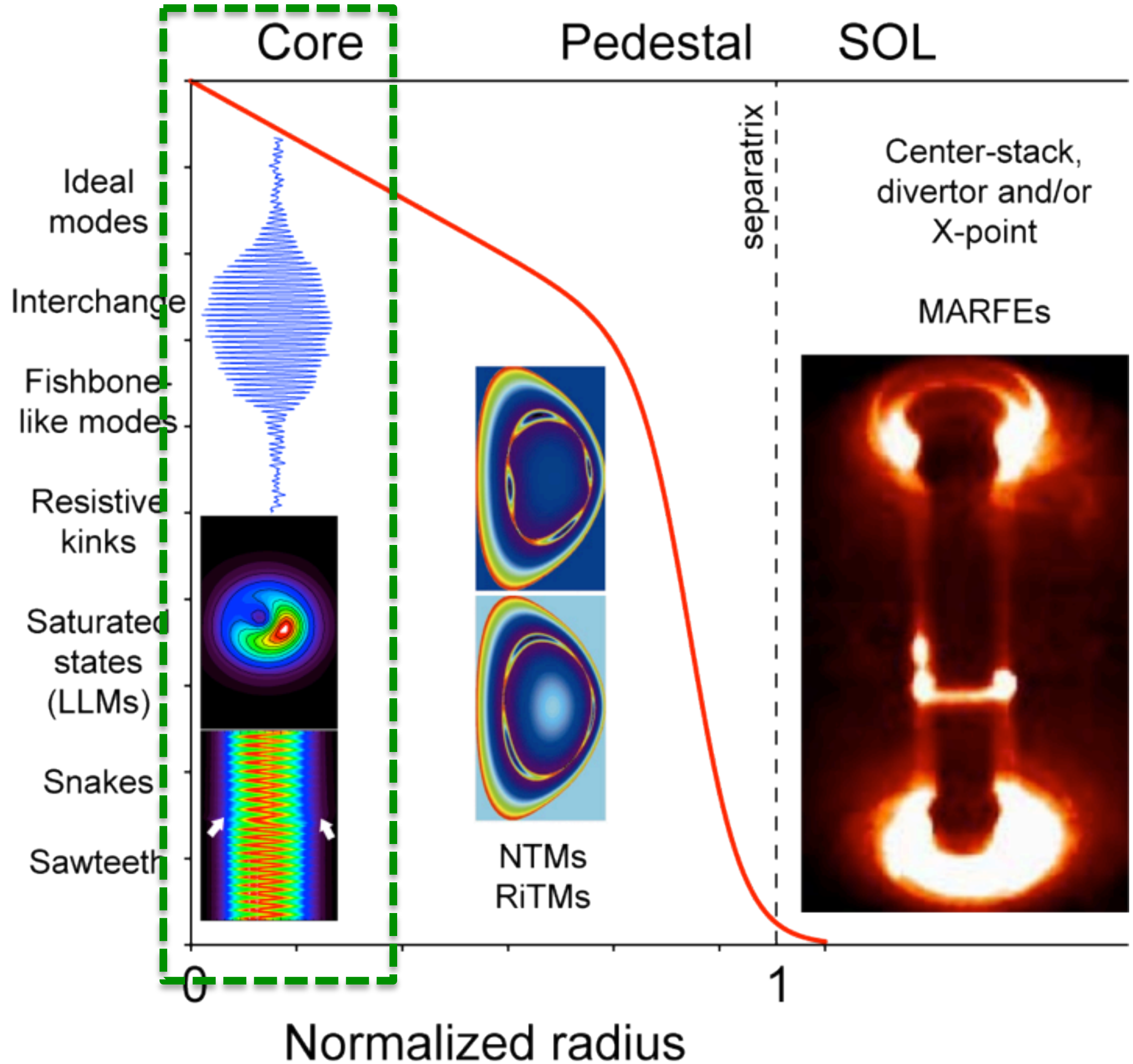

Long-lived saturated modes are routinely observed on a number of diagnostics

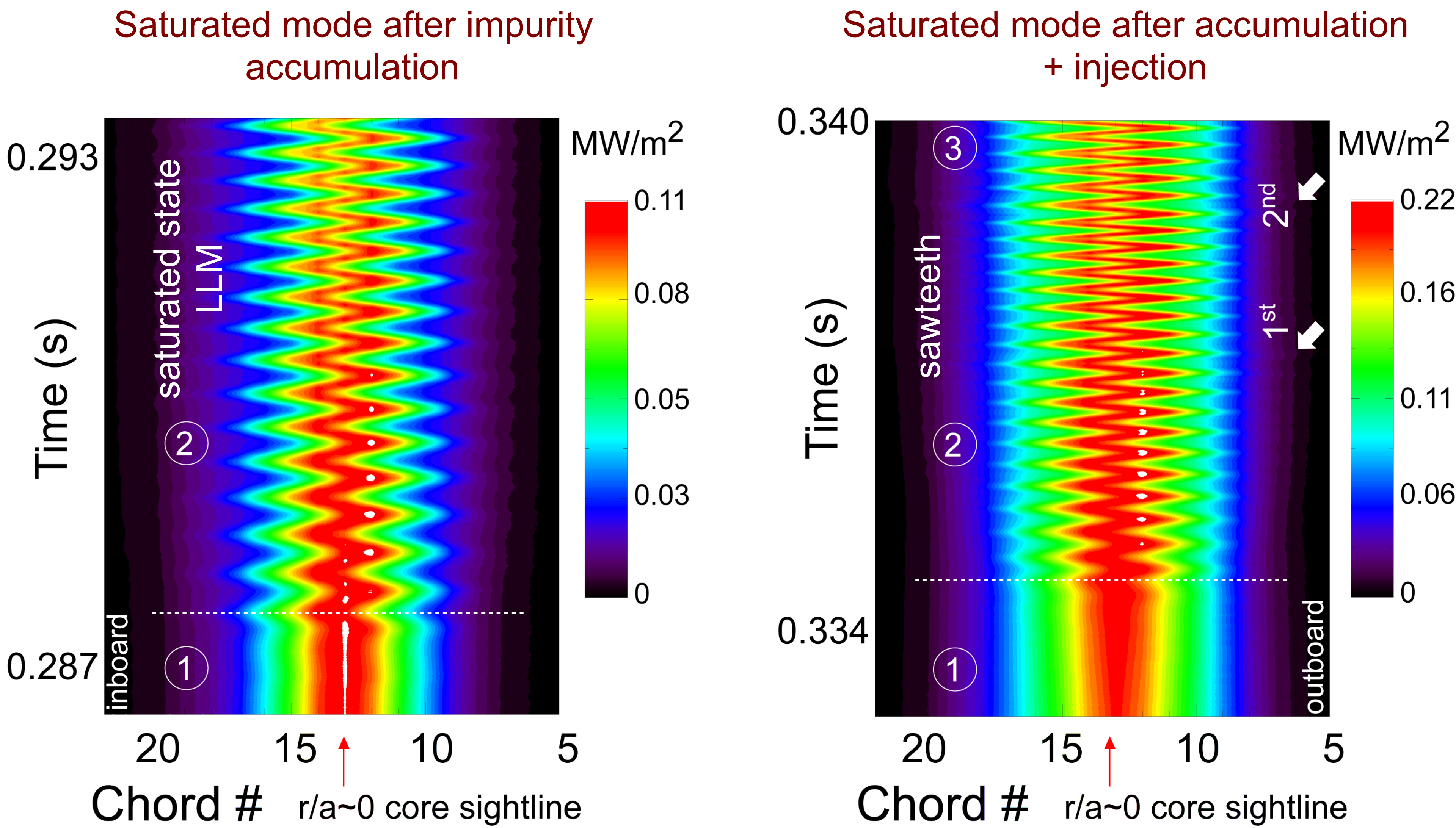

Stages resemble an ideal internal kink & magnetic island produced by a resistive (1,1) mode

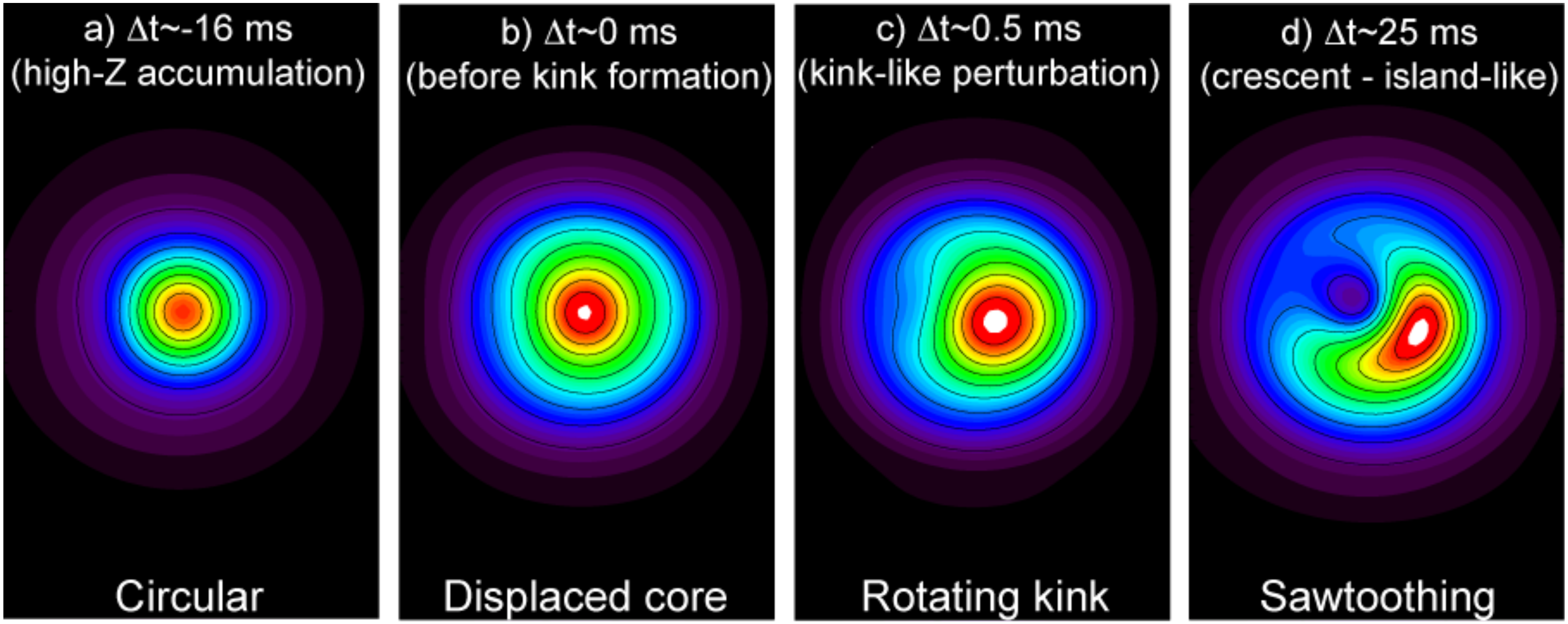

① ② ③

Co-exist with multiple sawtooth crashes

Alcator C-Mod

L. Delgado-Aparicio, et al., RSI'12, PRL'13, NF'13
L. Sugiyama, PoP'14

…surprisingly resilient to sawtooth crashes !

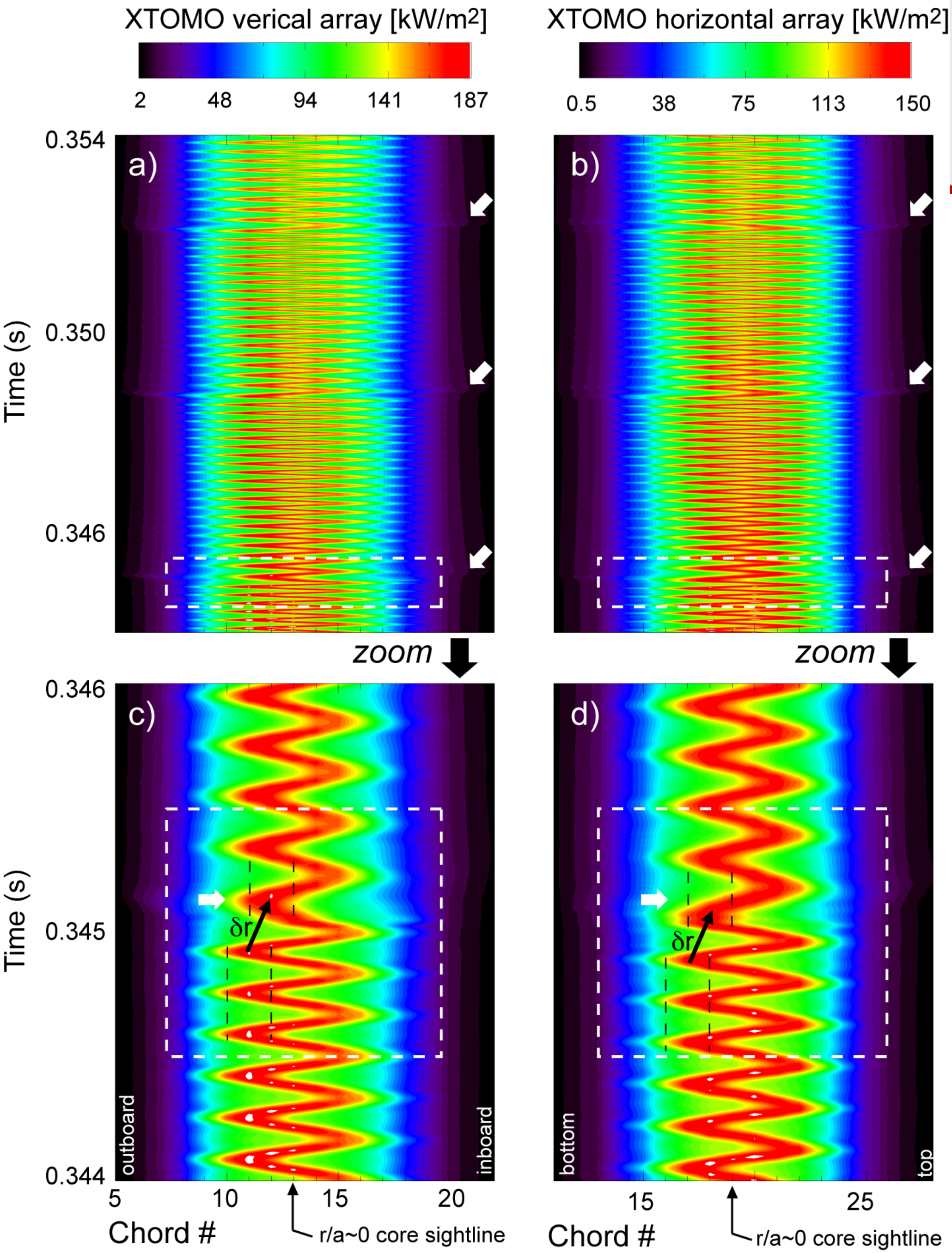

① τ_{snake}~190 μs & $\tau_{sawtooth}$~3.66 ms ⇒ ~ 20 snake periods.

② Crashes may cause a transient reduction of $r_{q=1}$ ($\delta r_1 \lesssim 1$ cm).

③ And a reduction of the v_ϕ

④ <u>During the crash</u> the small circular core moves rapidly outwards to the edge of the crescent radius.

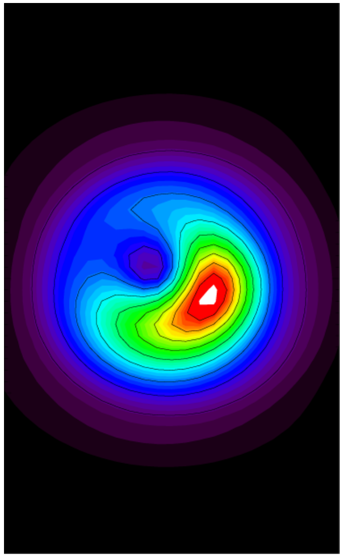

⑤ Snake density is nearly untouched by thermal crash + heat pulse.

Repetitive saturated modes are observed in long-pulse tokamaks with metal PFCs

Repetitive Z-modes have implications for ITER H-mode sustainability since available heating power is only slightly above the H-mode power threshold.

Challenges

- ITER ($r_{q=1}$~a/2)
- Reduce the effects on fast ions, J, q ⇒S_n, dilution, impurity peaking
- Develop active control tools

a) MHD control (heating vs CD vs torque)
b) Z-control (transport vs ELMs vs 3D)
c) Experiments in NSTX-U/DIII-D/EAST

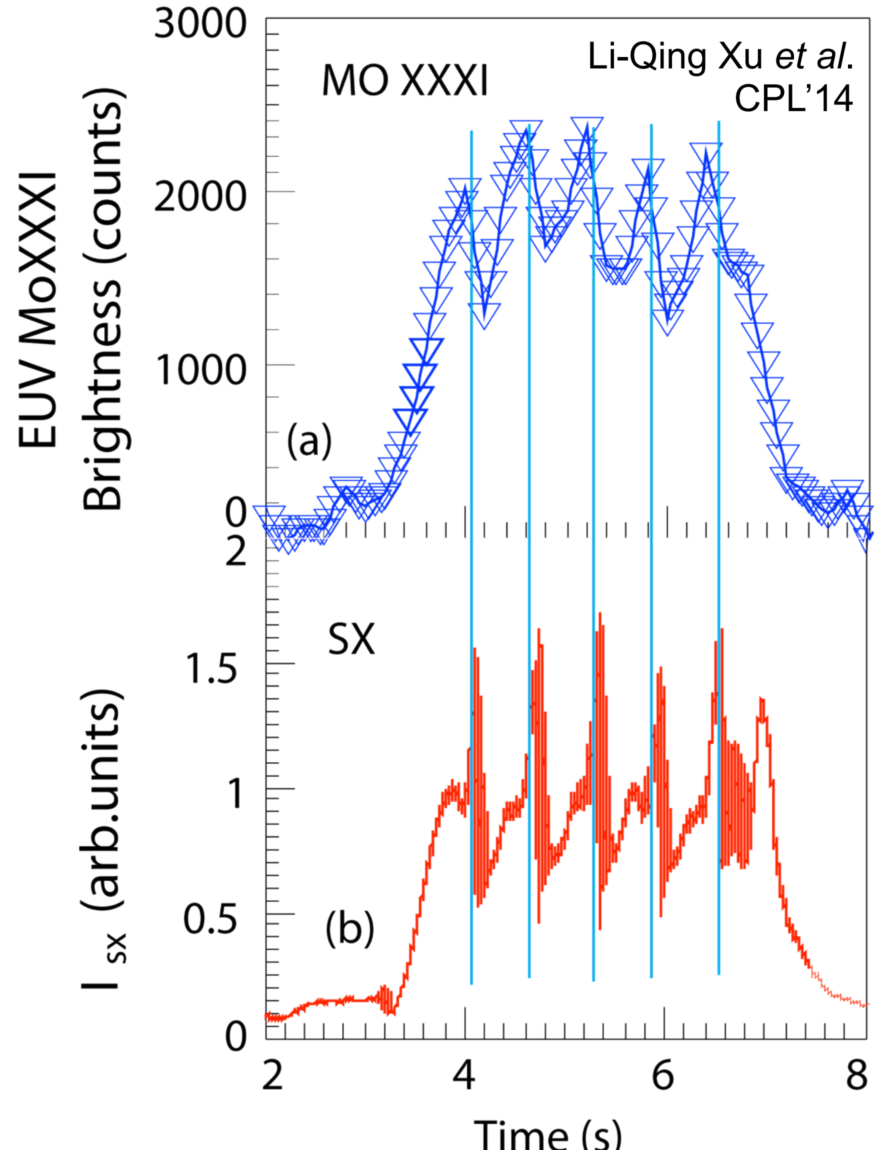

Outline

② Examples of Z-studies:

a) Transport & asymmetries

b) Core stability

c) Density-limit

Large family of macroscopic instabilities can be affected by Z-charge and radiation effects

High-Z impurities can degrade core confinement and can be the cause also of radiative density limit disruptions

Core (1/1) modes
0<r/a<0.5

Mid-radius (m/n) modes
0.3<r/a<0.9

Edge
0.9<r/a<1.1

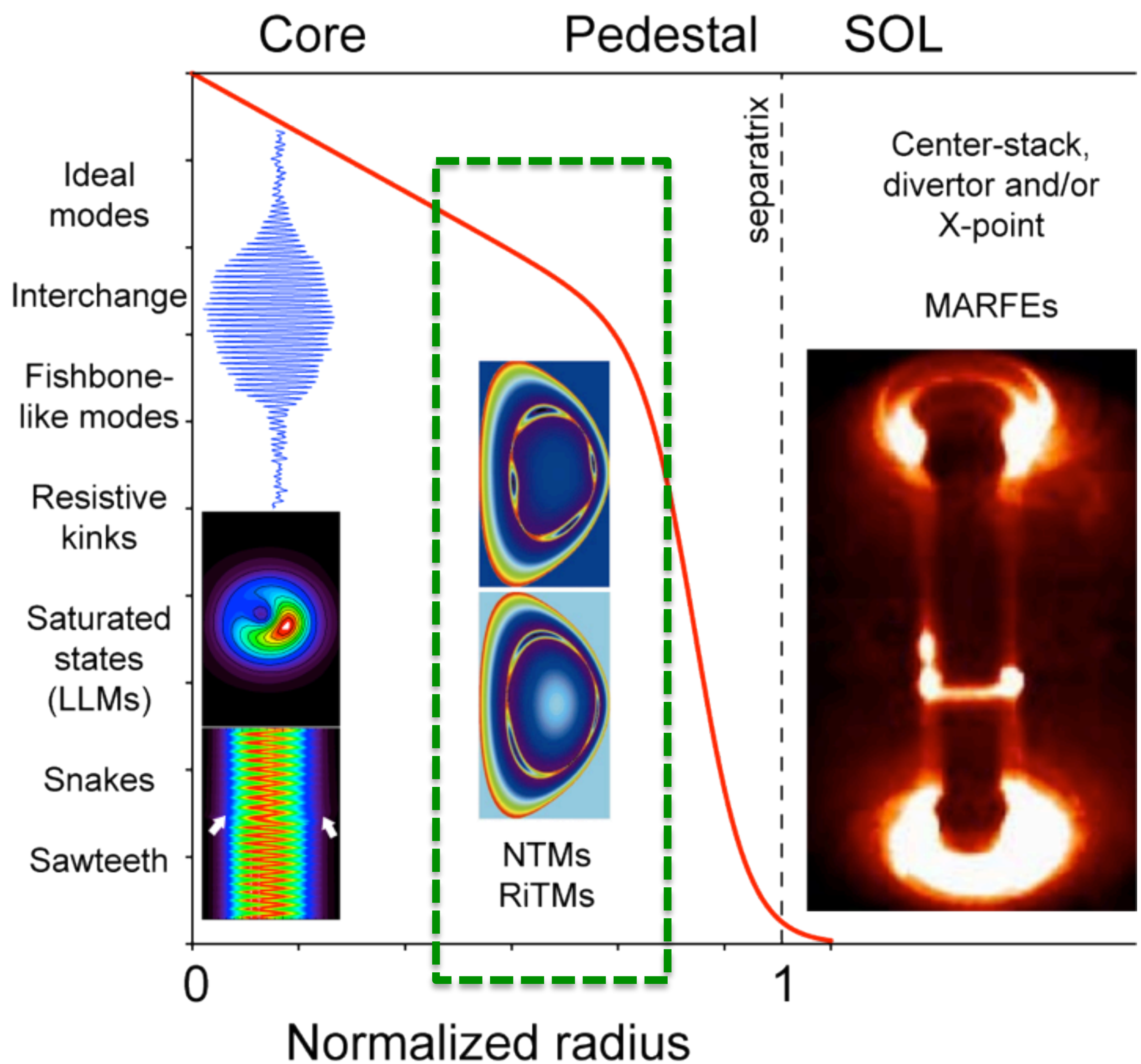

High-Z impurity radiation can contribute cooling causing TMs to grow larger & faster

- The interior region of an island contains impurities.
- Island interior is shielded from any auxiliary heating being shunted around by heat conduction parallel to the B-lines.
- Impurities radiate, cooling the island interior, causing it to grow faster and larger in comparison to the impurity-free cases.
- Radiation (≠charge) driven islands (a.k.a. radiation-induced tearing modes: RiTMs)
- MRE ⇒ onset criterion ⇒ consistent with the empirical scaling of $n_G = I_p/\pi a^2$

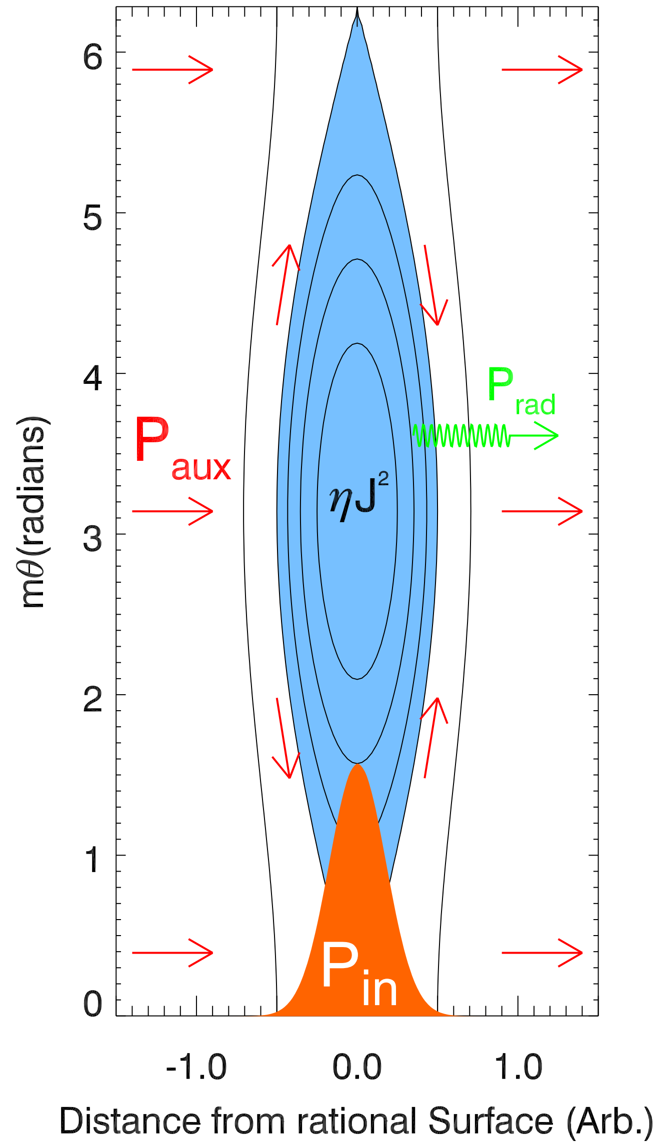

D. A. Gates and L. Delgado-Aparicio,
Phys. Rev. Letters, **108**, 165004, (2012).

Impurity effects & island asymmetries can be modeled using the extended MRE formalism

$$\frac{dw^*}{dt/\tau_R} \sim r_s\left(\Delta' - \alpha\omega^*\right) + \cancel{\frac{C_1 w^*}{w^{*2}+w_\chi^{*2}}} - \cancel{C_2\frac{\omega_\pi^{*2}}{\omega^{*3}}} - C_3 w^* + \frac{C_4(\omega)w^{*2}}{w^{*2}+w_\chi^{*2}}$$

$$C_3 = 3\tilde{P}_{rad}/\chi_{\perp,eff}^{island} n_e \langle T_e \rangle$$

$$C_4 \propto w$$

1. 3D resistivity with asymmetry adds destabilization term
2. Simple result of finite-island width in cylindrical geom.
3. Neither O-point or X-point are on the rational surface.
4. The width of the inner core-side is larger.

$$\tilde{P}_{rad} \equiv \underbrace{\eta J^2 + P_{NBI} + P_{ECRH}}_{P_{in}} - P_{rad}$$

R. White, D. A. Gates
D. P. Brennan, PoP'15

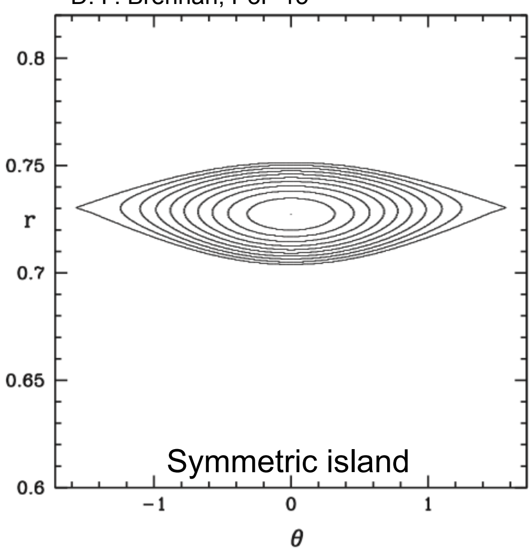

R. White, D. A. Gates
D. P. Brennan, PoP'15

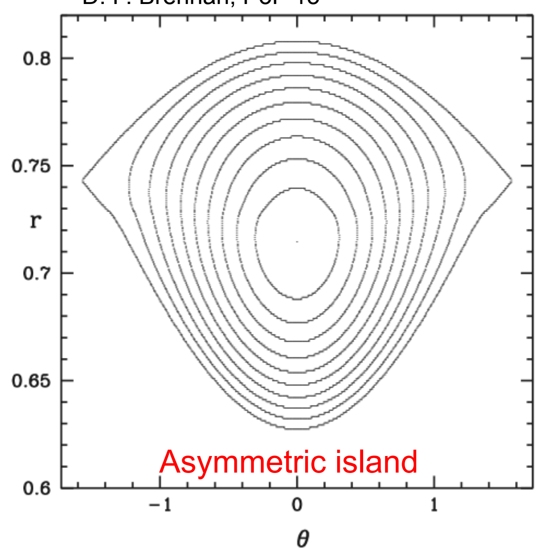

Q. Teng, D. P. Brennan,
L. Delgado-Aparicio,
D. A. Gates and J. Swerdlow, PoP'16

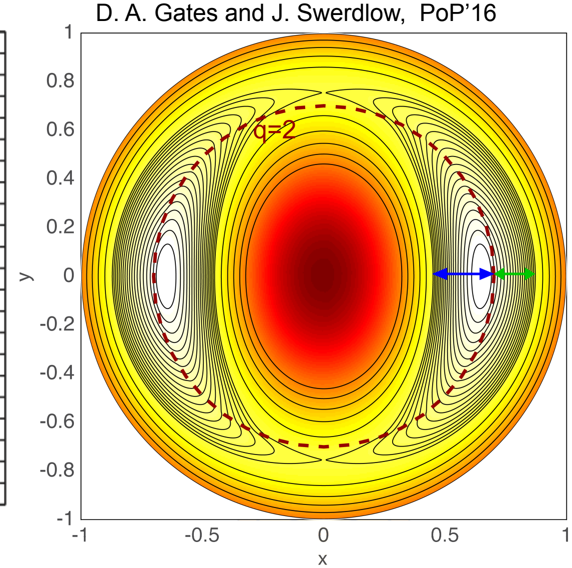

D. P. Brenan, D. Gates,
L. Delgado-Aparicio,
R. White, to be
submitted,
PoP '17

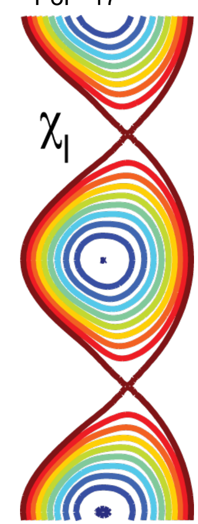

Impurity effects & island asymmetries can be modeled using the extended MRE formalism

$$\frac{dw^*}{dt/\tau_R} \sim r_s\left(\Delta' - \alpha\omega^*\right) + \cancel{\frac{C_1 w^*}{w^{*2} + w_\chi^{*2}}} - \cancel{C_2 \frac{\omega_\pi^{*2}}{\omega^{*3}}} - C_3 w^* + \frac{C_4(\omega) w^{*2}}{w^{*2} + w_\chi^{*2}}$$

$$C_3 = 3\tilde{P}_{rad}/\chi_{\perp,eff}^{island} n_e \langle T_e \rangle \qquad C_4 \propto w$$

1. 3D resistivity with asymmetry adds destabilization term
2. Simple result of finite-island width in cylindrical geom.
3. Neither O-point or X-point are on the rational surface.
4. The width of the inner core-side is larger.

Some approximations: [(2,1) is the most unstable]

$\Delta' r_s \approx -m$ to $\Delta' r_s > 0$ …..for m=2

$\Delta' r_s \approx -2m$ …..for m>2

What about the growth rate C_3?

$$\tilde{P}_{rad} \equiv \underbrace{\eta J^2 + P_{NBI} + P_{ECRH}}_{P_{in}} - P_{rad}$$

$$\frac{dw^*}{dt/\tau_R} \sim r_s \Delta' - C_3 w^*$$

If $C_3<0$ => exponential growth => Density-limit DISRUPTION !

Local onset criteria for RiTMs can be reduced to a non-dimensional form similar to n_G

$$\frac{m_e}{e^2}\frac{Z_{eff}}{(\tau_{e,D}n_D)}J^2 > n_e^2 L_D \hat{P}_{rad}^V$$

<u>Where</u>:

$$\tau_{e,D}n_D = 1.09\times10^{16}T_e[\mathrm{keV}]\ln\Lambda_{e,D}$$

$$L_D = 5.35\times10^{-37}T_e^{1/2}[\mathrm{keV}]\ \mathrm{W}\cdot\mathrm{m}^3$$

$$\hat{P}_{rad}^V \equiv P_{rad}^V/n_e^2 L_D$$

<u>Onset criteria at the rational surface</u>:

Parameterizing "cleanliness" ?

$$n_e[\times10^{20}\mathrm{m}^{-3}] < \mathcal{F}_{D,Z}\cdot J\left[\frac{\mathrm{MA}}{\mathrm{m}^2}\right]$$

$$\mathcal{F}_{D,Z} \approx \sqrt{\frac{0.61\cdot \boxed{Z_{eff}}\cdot\ln\Lambda_{e,D}}{T_e^2[\mathrm{keV}]\cdot\boxed{\hat{P}_{rad}^V}}}$$

$$\bar{n}_e[\times10^{20}\mathrm{m}^{-3}] < n_G \equiv \frac{I_p[\mathrm{MA}]}{\pi a^2[\mathrm{m}^2]}$$

L. Delgado-Aparicio, D. A. Gates, D. P. Brennan and R. White, to be submitted to PoP, (2018)

Summary 2: Large family of macroscopic phenomena can be affected by charge & radiation

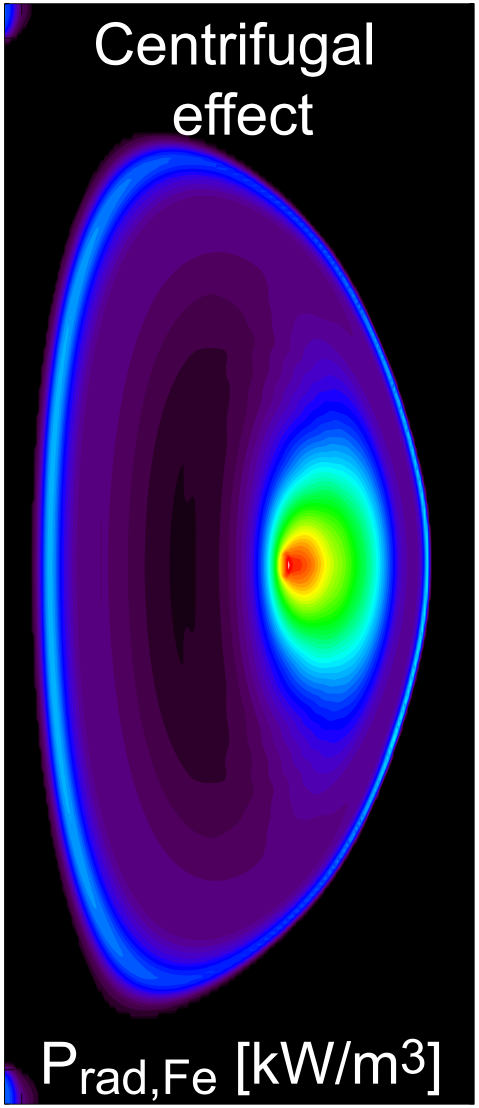

MHD

Core (1/1)

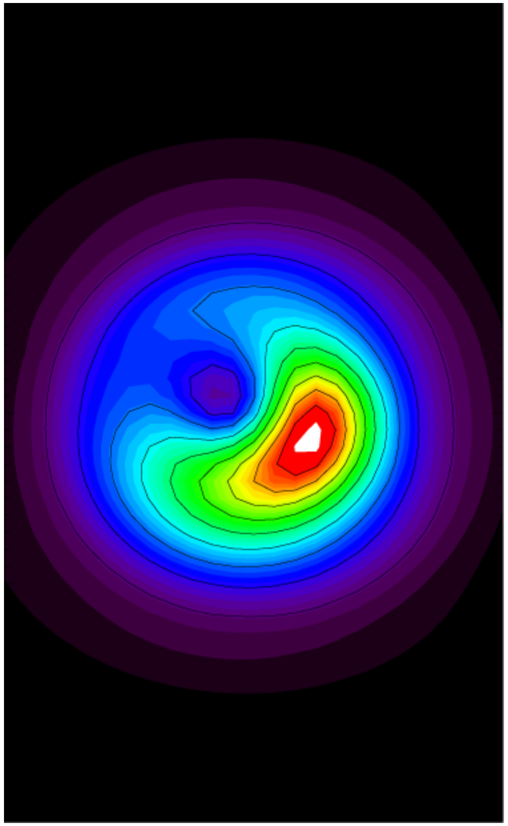

Mid-radius (2/1)

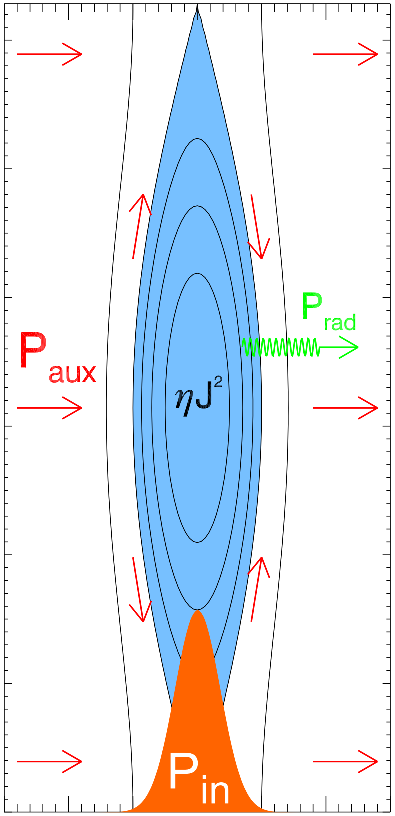

Center-stack, divertor and/or X-point

MARFEs

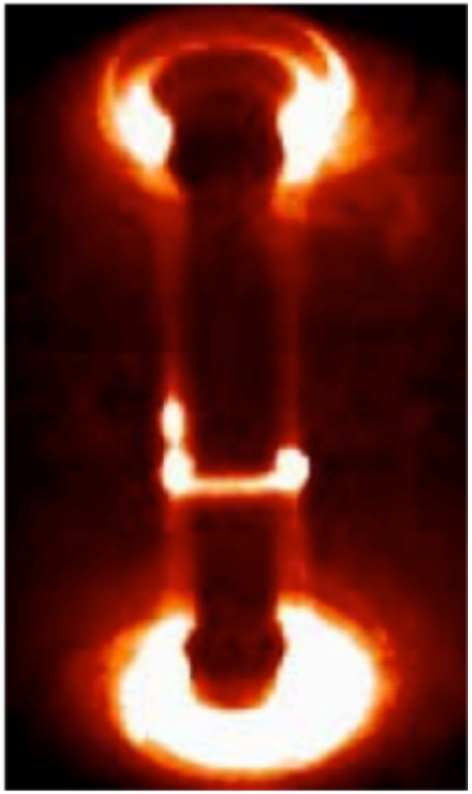

Outline

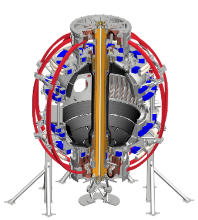

① Magnetically confined fusion (MCF) plasmas and the Z-challenge

② Z-studies

③ Radiation and the need of spectroscopy?

④ Novel x-ray diagnostics

⑤ Summary

Main radiation mechanisms: Bremsstrahlung (ff), radiative recombination (fb) & line-emission (bb)

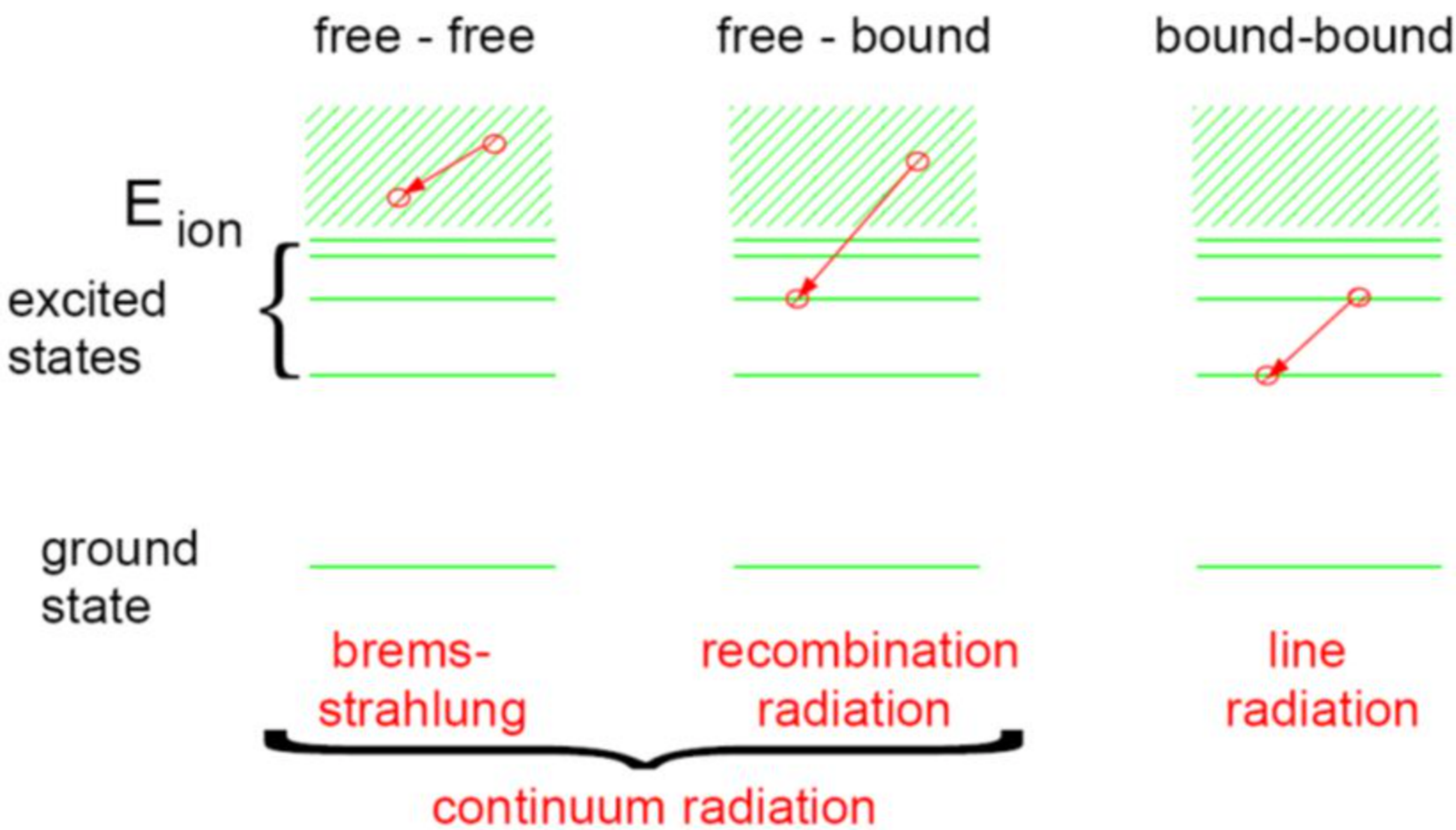

Radiation processes have to be calculated based on local plasma parameters [T_e, n_e, $n_Z(R,t)$]

1. Continuum and & line emission:

Bremsstrahlung (ff):

$$\frac{d\mathcal{P}^{ij}_{ff}(T_e,E)}{dE} \propto \frac{n_e^2 C_i (n_{ij}/n_i) Z_{ij}^2}{T_e^{1/2}} \mathcal{G}_{ff}(Z,T_e,E)\exp(-E/T_e)$$

Radiative recombination (fb):

$$\frac{d\mathcal{P}^{ij}_{fb}(T_e,E)}{dE} \propto \frac{n_e^2 C_i (n_{ij}/n_i) Z_{ij}^2}{T_e^{1/2}} \beta_{ij}(T_e,E)\exp(-E/T_e)$$

Line emission (bb):

$$\frac{\mathcal{P}^{ij}_{L}(T_e,E)}{E_L} \propto n_e^2 C_i \left(n_{ij}/n_i\right) \langle \sigma v(T_e,E)_{ij} \rangle$$

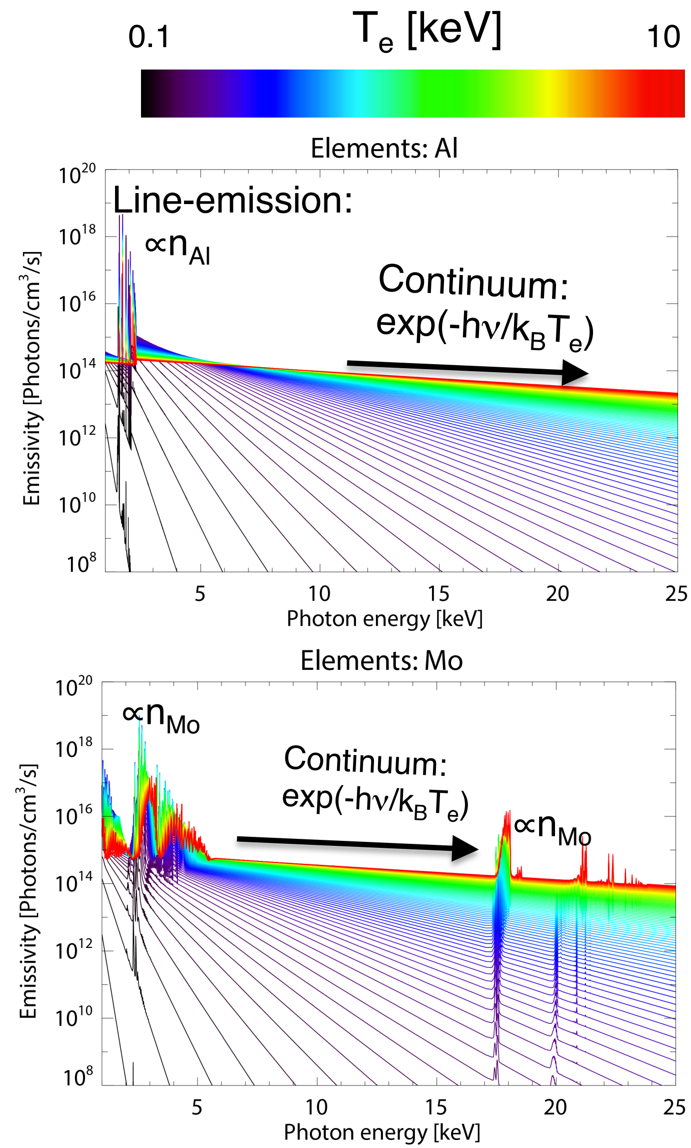

2. Visible/UV/x-ray tomography:

- Emmisivity is a flux-surface function
- Emmisivity is not a flux-surface function
- Inversion ($E=M^{-1}xB$)

Radiation processes have to be calculated based on local plasma parameters [T_e, n_e, $n_Z(R,t)$]

1. Continuum and & line emission:

Bremsstrahlung (ff):

$$\frac{d\mathcal{P}^{ij}_{ff}(T_e,E)}{dE} \propto \frac{n_e^2 C_i (n_{ij}/n_i) Z_{ij}^2}{T_e^{1/2}} \mathcal{G}_{ff}(Z,T_e,E)\exp(-E/T_e)$$

Radiative recombination (fb):

$$\frac{d\mathcal{P}^{ij}_{fb}(T_e,E)}{dE} \propto \frac{n_e^2 C_i (n_{ij}/n_i) Z_{ij}^2}{T_e^{1/2}} \beta_{ij}(T_e,E)\exp(-E/T_e)$$

Line emission (bb):

$$\frac{\mathcal{P}^{ij}_{L}(T_e,E)}{E_L} \propto n_e^2 C_i\,(n_{ij}/n_i)\,\langle \sigma v(T_e,E)_{ij}\rangle$$

2. Visible/UV/x-ray tomography:

- Emmisivity is a flux-surface function
- Emmisivity is not a flux-surface function
- Inversion ($E=M^{-1}xB$)

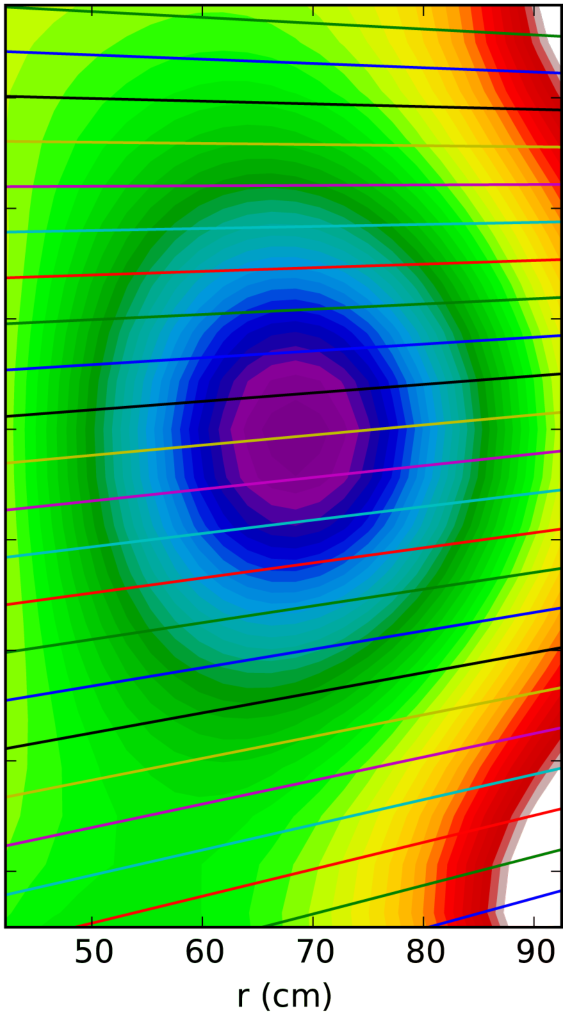

Coronal equilibrium (ionization balance)

- Commonly used in fusion plasmas and in the solar corona
- Assumes three body-recombination rate is small
- Balance between electron-impact ionization and radiative recombination

$$\underbrace{n_e n_Z \mathcal{S}_{Z\rightarrow(Z+1)}(T_e)}_{Ionization} = \underbrace{n_e n_{(Z+1)} \alpha_{Z+1\rightarrow Z}(T_e)}_{Recombination}$$

$$\Rightarrow \frac{n_{(Z+1)}}{n_Z} = \frac{\mathcal{S}_{Z\rightarrow(Z+1)}(T_e)}{\alpha_{Z+1\rightarrow Z}(T_e)}$$

- <u>Result</u>: Ionization degree is independent of density
- Charge state of ion increases with electron temperature
  - Low-Z ions (Be, B, C) are often fully stripped

Fractional abundance calculations depend only on the local electron temperature

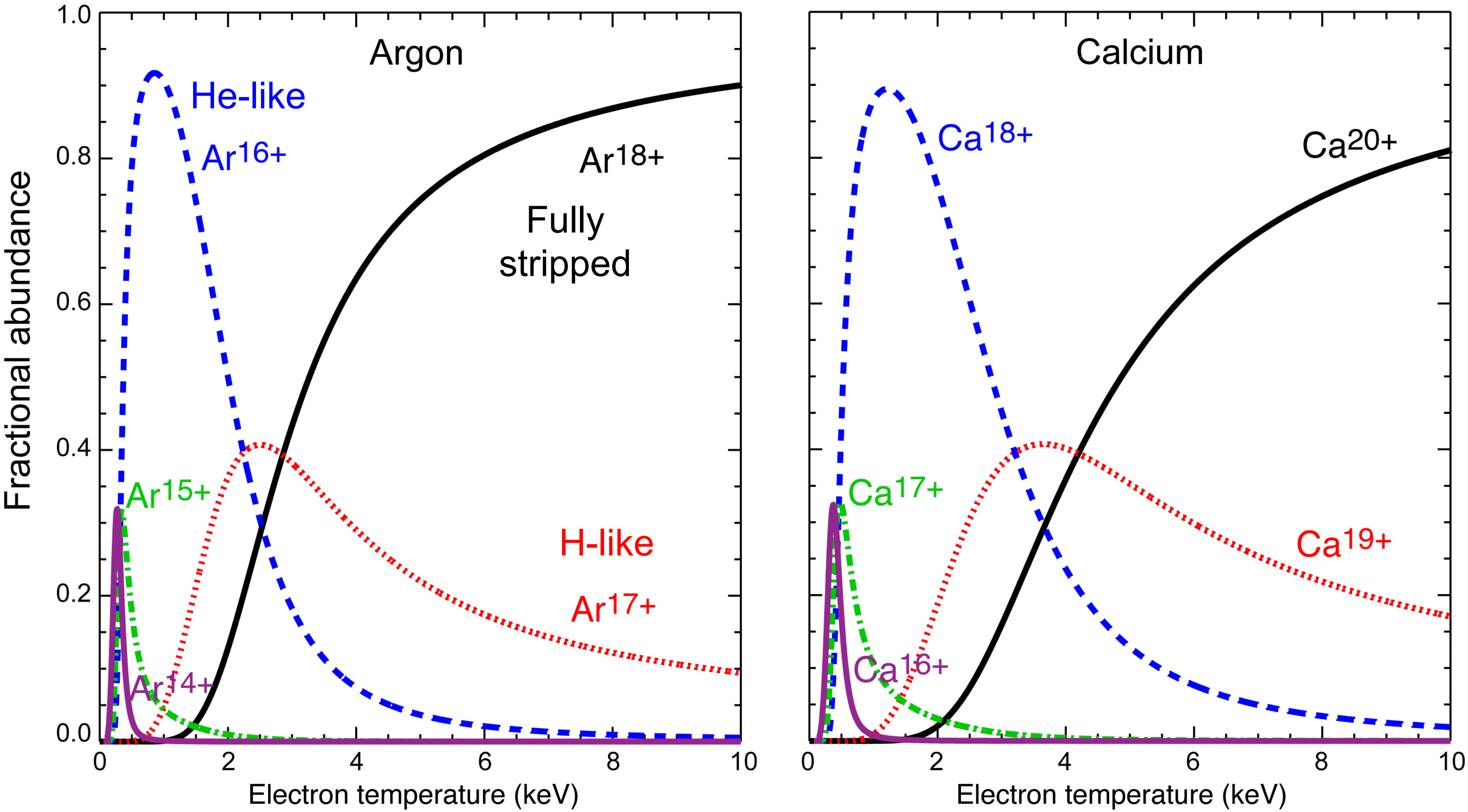

Radiative power densities (Vis/UV/x-ray) & <Z> can be obtained using coronal equilibrium

D. E. Post, *et al.*, Atomic Data and Nuclear Data Tables, **20**, 397-439, (1977).

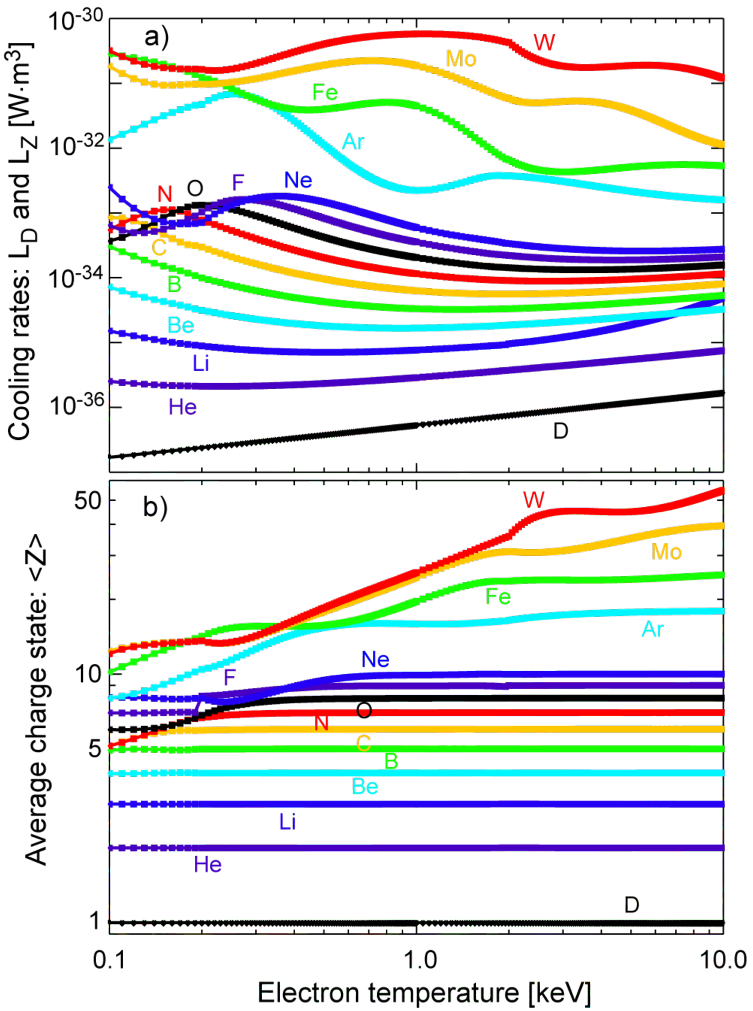

Radiated power density can be easily calculated using the cooling rates

$$P_{rad,Z} \sim n_e n_Z L_Z$$
$$\sim n_e^2 C_Z L_Z$$

Parameterizing quasi-neutrality and Zeff

$$n_e = n_D + Z n_Z$$

$$Z_{eff} = \frac{n_D}{n_e} + Z^2 \frac{n_Z}{n_e}$$

Radiative power densities (Vis/UV/x-ray) & <Z> can be obtained using coronal equilibrium

D. E. Post, *et al*., Atomic Data and Nuclear Data Tables, **20**, 397-439, (1977).

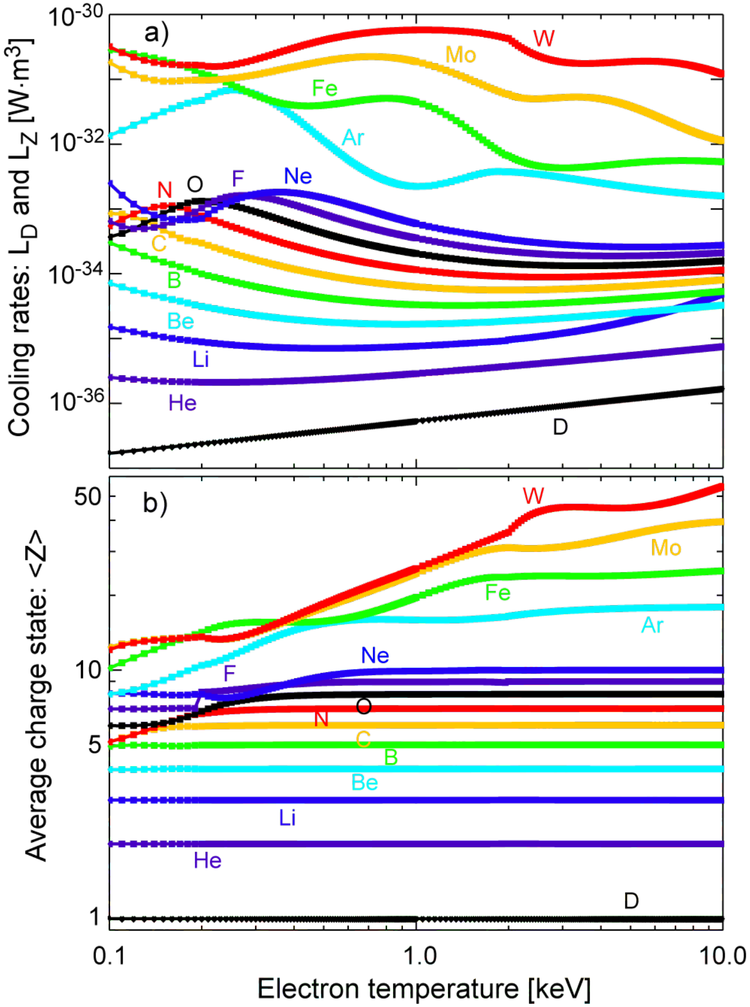

Parameterizing equations of interest for two-impurity plasma

$$1 = \frac{n_D}{n_e} + \langle Z_1 \rangle \frac{n_{Z1}}{n_e} + \langle Z_2 \rangle \frac{n_{Z2}}{n_e}$$

$$Z_{eff} = \frac{n_D}{n_e} + \langle Z_1 \rangle^2 \frac{n_{Z1}}{n_e} + \langle Z_2 \rangle^2 \frac{n_{Z2}}{n_e}$$

$$\hat{P}^V_{rad} \equiv \frac{P^V_{rad}}{n_e^2 L_D} = \frac{n_D}{n_e} + \frac{n_{Z1}}{n_e}\frac{L_{Z1}}{L_D} + \frac{n_{Z2}}{n_e}\frac{L_{Z2}}{L_D}$$

Modern references for high-Z impurities include details of the electronic structure and excitation cross sections

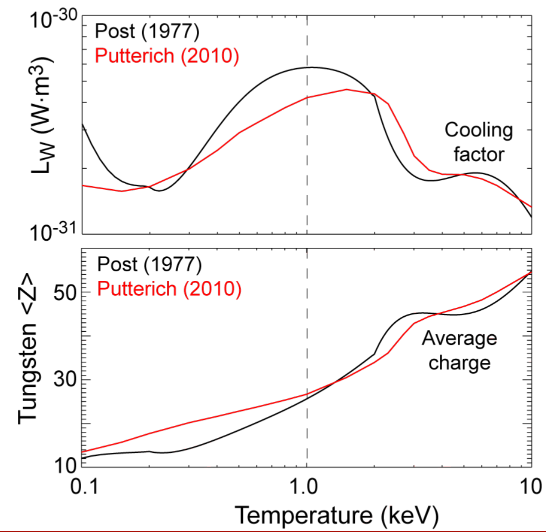

L. Delgado-Aparicio, et al., to be submitted to PoP, (2018)

Summary 3: Charge state of ion increases with T_e and we should measure ff, fb & bb radiation

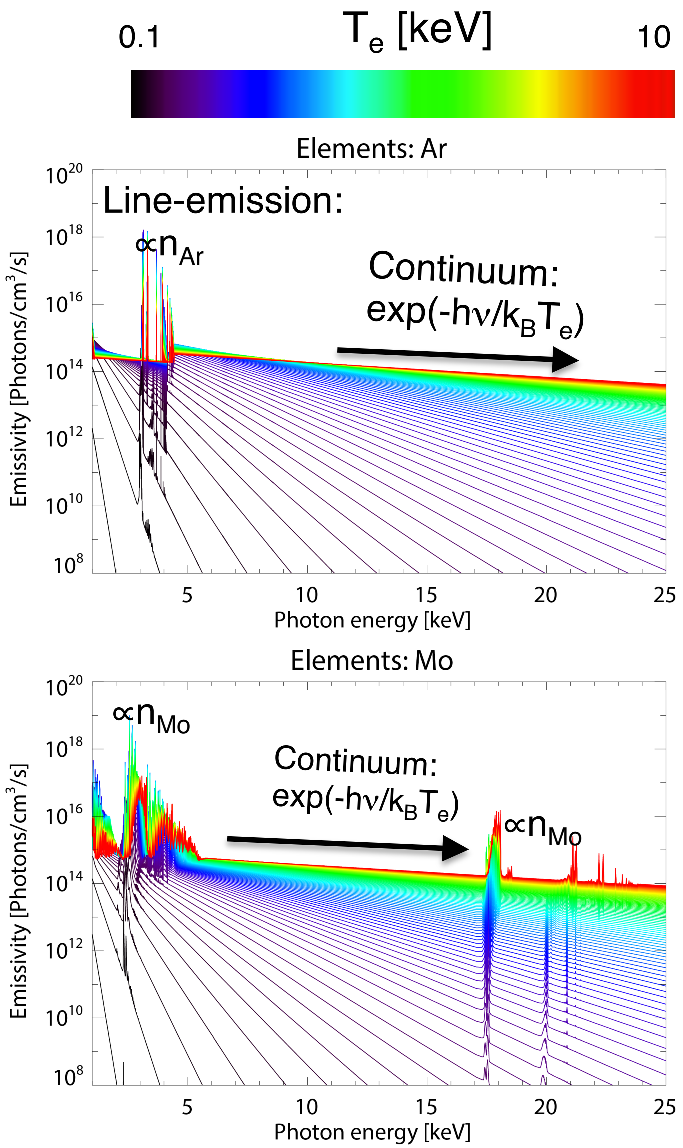

Continuum and & line emission:
Bremsstrahlung (ff)
Radiative recombination (fb)
Line emission (bb)

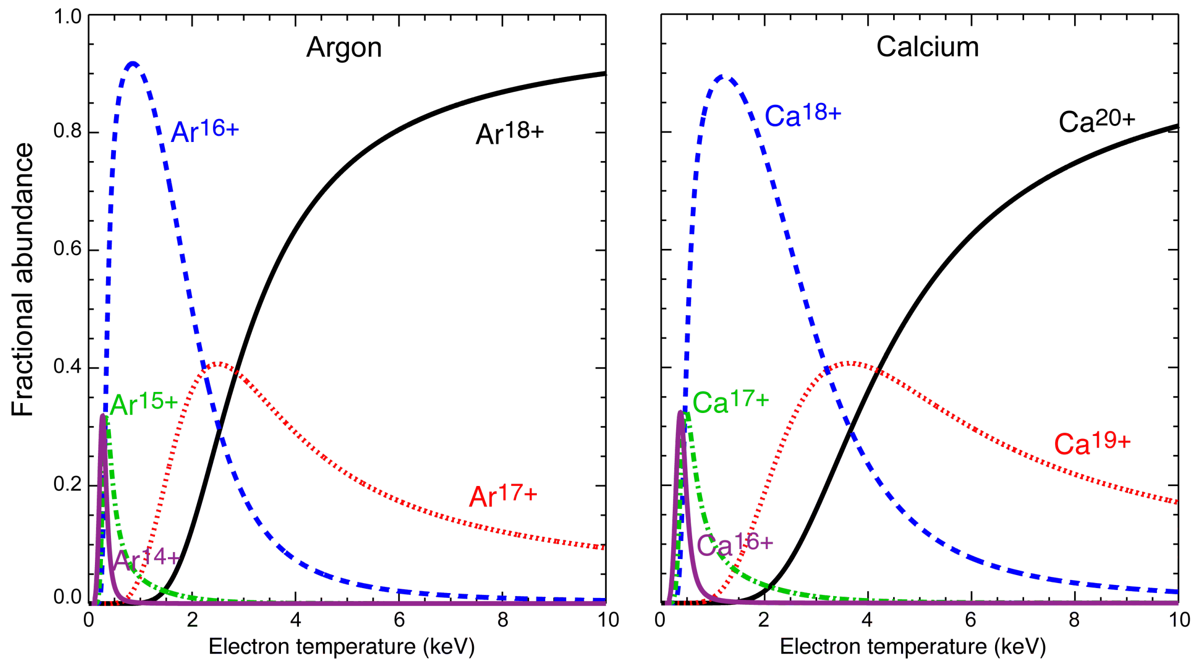

Outline

① Magnetically confined fusion (MCF) plasmas and the Z-challenge

② Z-studies

③ Why radiation & spectroscopy?

④ Novel x-ray diagnostics

⑤ Summary

Why is important to measure x-rays emitted from tokamak and stellarator plasmas ?

① A significant fraction of the power delivered to the plasma is lost in the form of radiation [even in an ideal pure H plasma].

② A subset of P_{rad}: In real conditions could be as high as 90%.

③ X-rays are the most dominant source of radiation from hot plasmas: since $h\nu \sim T_e$:

Exercise: For 100 eV $< T_e <$ 20 keV $\Rightarrow$ $0.5 < \lambda < 130$ Å $\Rightarrow$ X-rays!

④ Measurement of power losses in the x-ray range enable the characterization of parameters such as, n_e, n_Z, T_e, T_i, v_ϕ, v_θ, to be used in describing/studying:

a) MHD and reconection events (from hot core to cold edge).
b) Transport coefficients (e.g. diffusivity and pinch velocity).
c) Radial electric field (E_r)
d) Magnetic flux-surface reconstructions: $T_e(\psi) \Rightarrow J$ and q

THE X-RAY CASE: …how to diagnose x-rays from thermonuclear plasmas @ ~300million C?

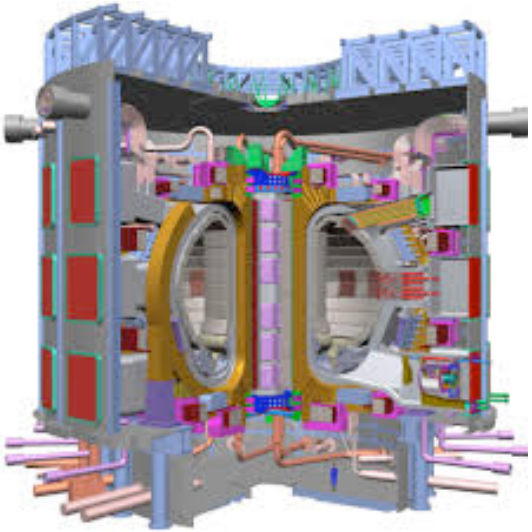

Nearly 90% of the radiated power in ITER will be in the x-ray range:

SXR: 1<E<20 keV
HXR: 20<E<400 keV

Three options in the x-ray range

① Conventional broadband x-ray measurements
(e.g. SXR tomography=>confinement, MHD, equilibrium).

② Doppler line-radiation x-ray measurements
(e.g. n_Z, T_e, T_i, v_ϕ, v_θ, => E_r).

③ Modern PHA & multi-energy measurements
(e.g. Z_{eff}, n_Z, T_e, $n_{e,fast}$).

① Conventional SXR tomography consists of an array of diodes integrating the local emissivity

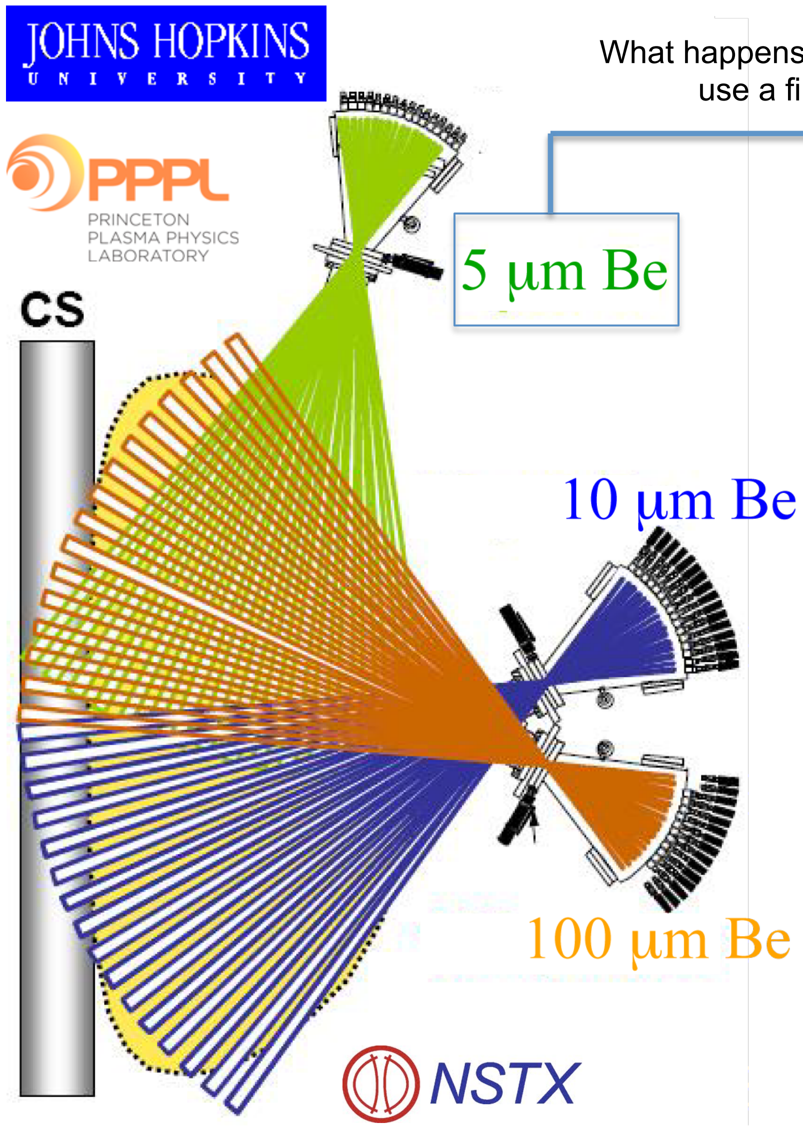

What happens if we don't use a filter?

① Essential elements:
- a) Pinhole
- b) Thin metallic filter
- c) SXR/Bolo detector + Amplifier + DAQ

② Thick filters will help discriminate between edge and core effects.

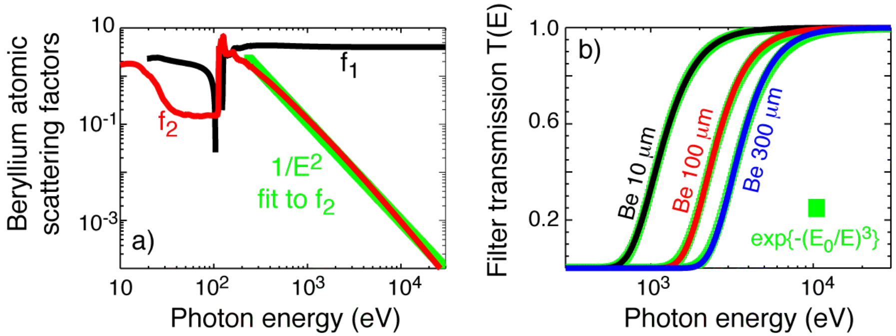

L. Delgado-Aparicio, et al., RSI, **81**,10E303, (2010).

③ Individual diodes or diode arrays.

④ Current mode: use trans-impedance amplifiers with gain of 10^4-10^7 V/A.

Conventional SXR tomography integrates in photon-energy using metal filter & diode arrays

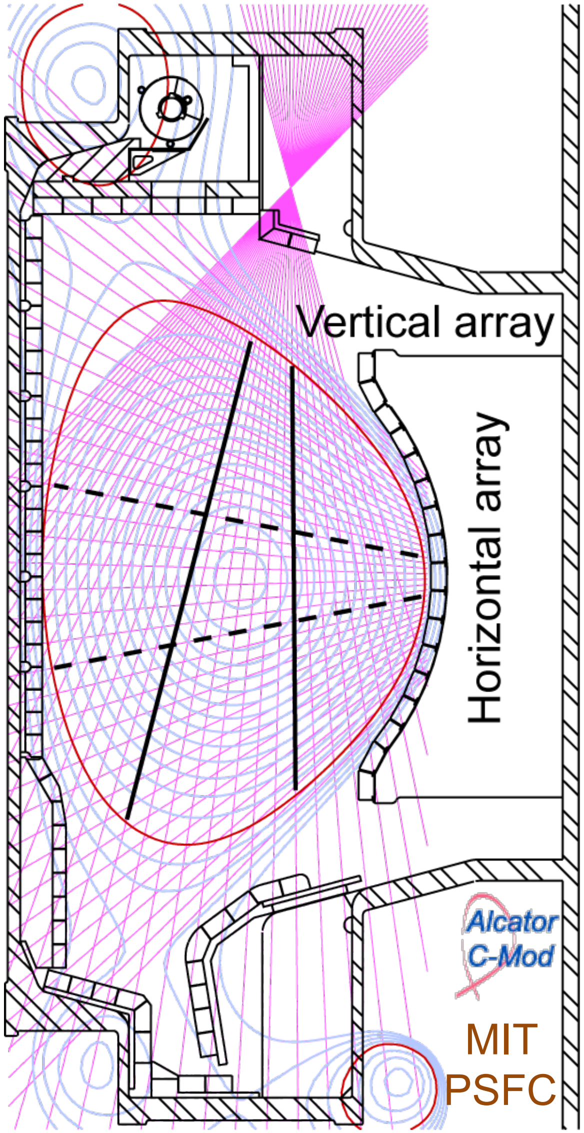

DIRECT EXAMPLES (e.g. Si)

AXUV-100

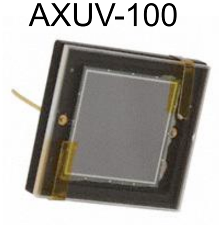

AXUV-20

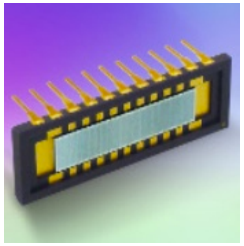

INDIRECT EXAMPLE (e.g. CsITl)

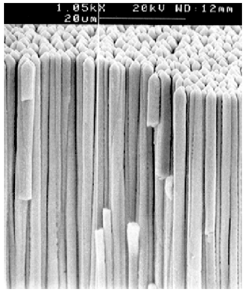

Example of spatially resolved x-ray spectra from ITER

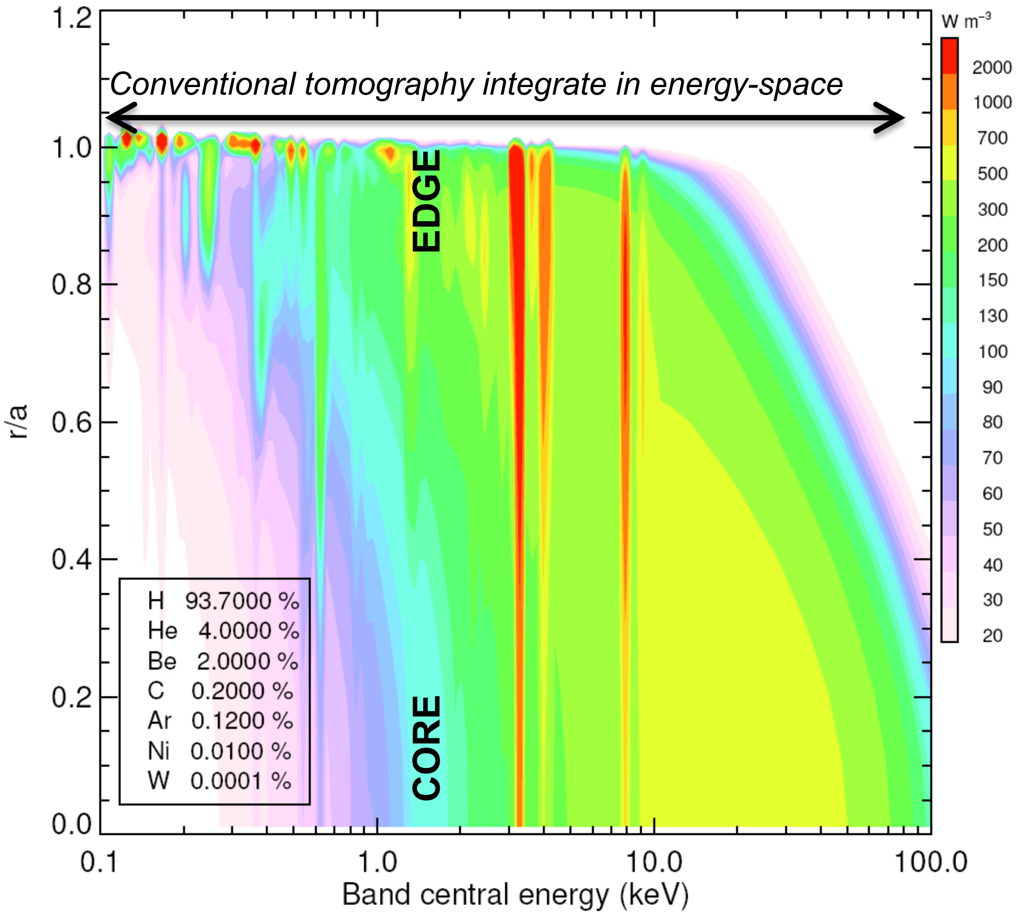

Integration means also that it is very difficult to extract local parameters from the SXR emission

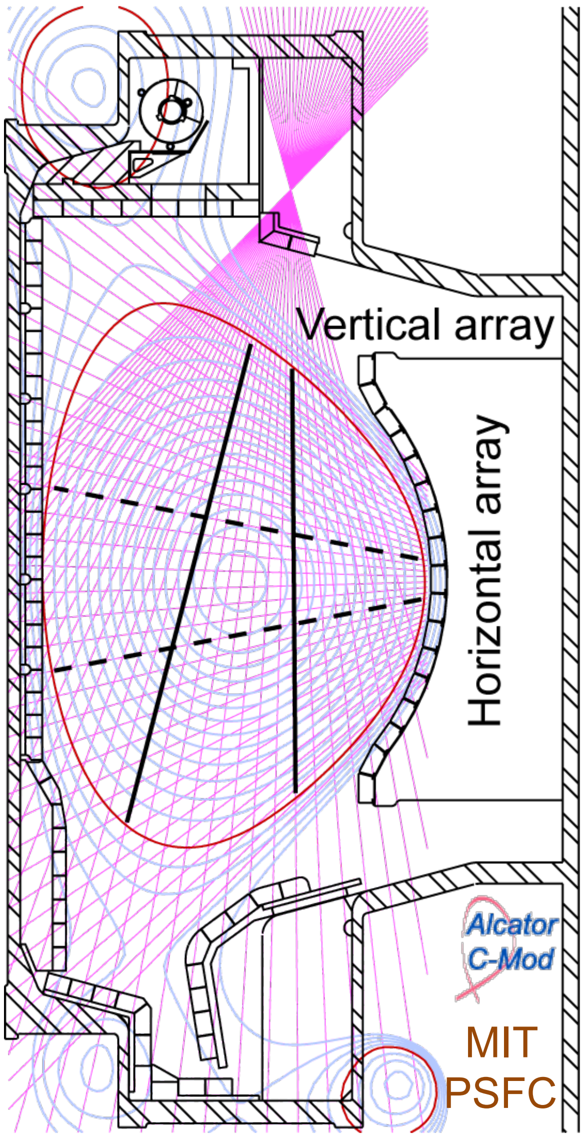

SXR tomographic systems measure the line-integrated continuum & line-emission from MCF plasmas

n_e: electron density

n_i: ion (H, D/T) density

n_Z: impurity density (He, B, C, O, Ar, Mo, W)

T_e: electron temperature

"Maxwellian" distributions $f(E_e/k_B T_e)$

θ-asymmetries as $F[v_\phi$: toroidal velocity, M_Z: ion mass$]$ (vertical or tangential views are needed)

L: Length of integration, θ: poloidal angle (radial and poloidal coverage)

Energy response

$T_{filter}(E_{ph})$: transmission function of filter

Detector response: $S(E_{ph})$

However, conventional SXR tomography is still being used for stability, MHD & transport studies

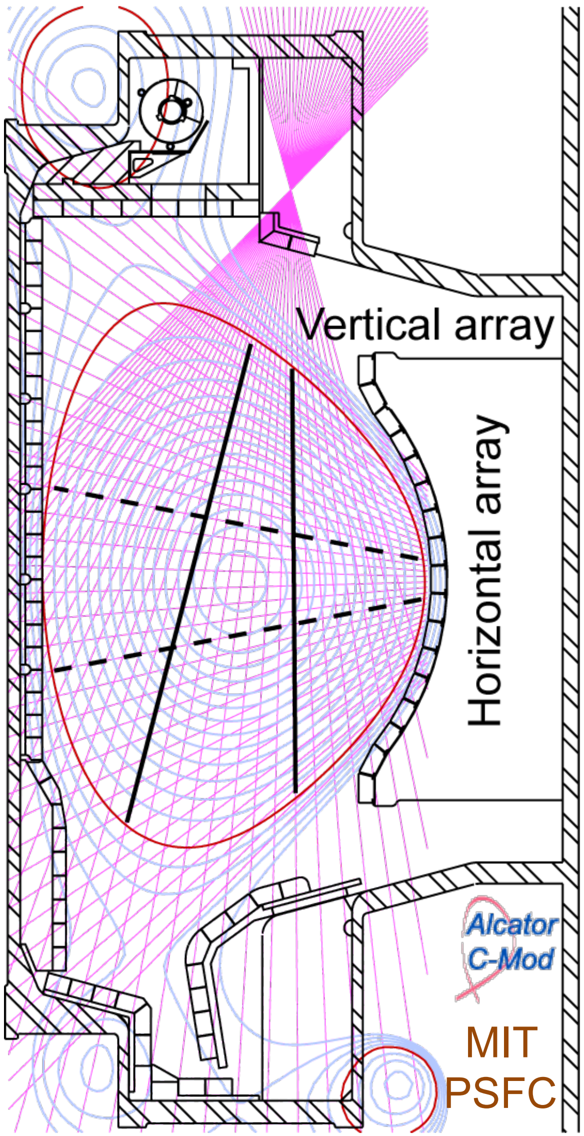

a) Stability and MHD [e.g. (m,n) modes and sawteeth]

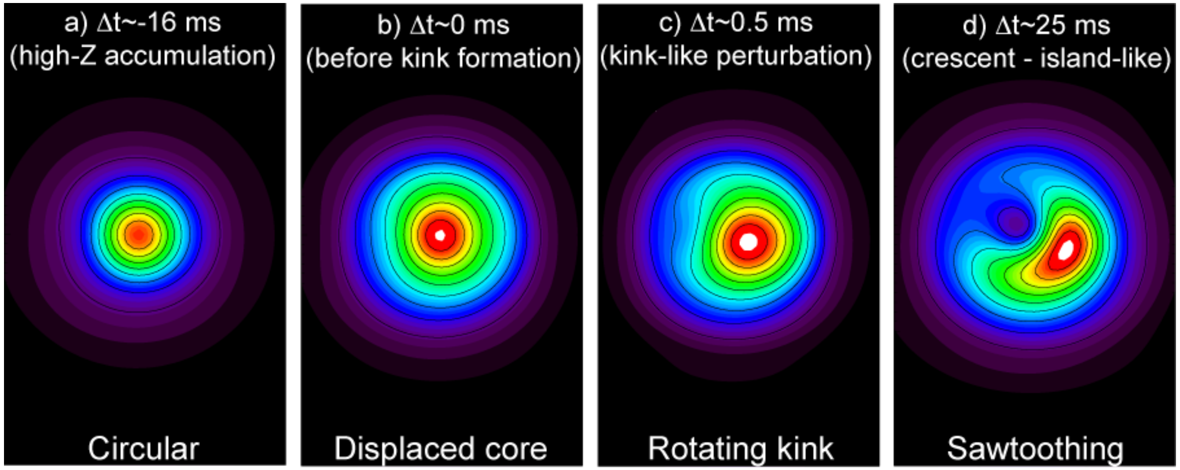

b) Impurity transport (e.g. using gas injection or LBO)

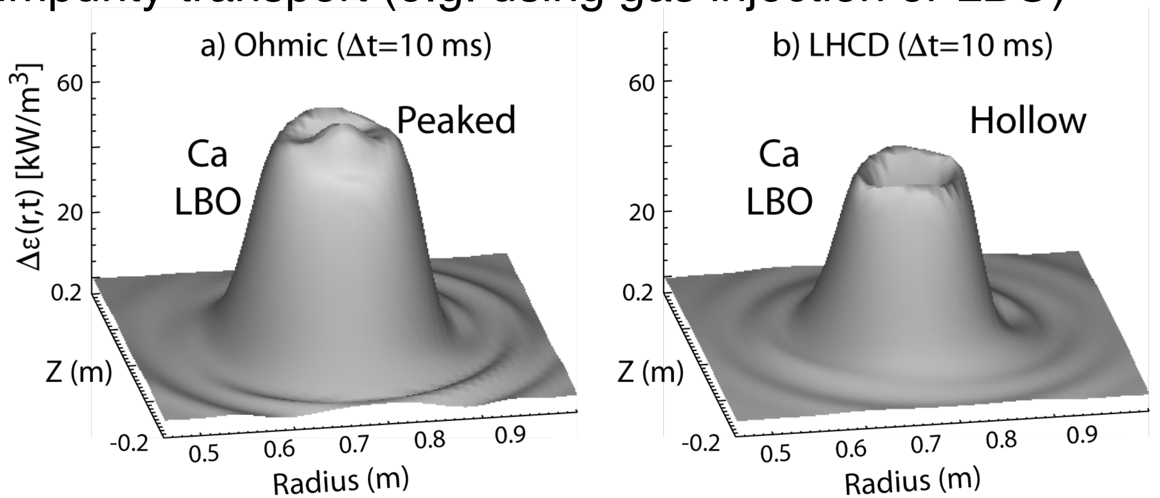

Three options in the x-ray range

① Conventional broadband x-ray measurements
(e.g. SXR tomography=>confinement, MHD, equilibrium).

② Doppler line-radiation x-ray measurements
(e.g. n_Z, T_e, T_i, v_ϕ, v_θ, => E_r).

③ Modern PHA & multi-energy measurements
(e.g. Z_{eff}, n_Z, T_e, $n_{e,fast}$).

Extract local plasma information !!!

How do we extract physics information from narrow and/or wider SXR energy bands ?

Narrow energy bands

- Doppler spectroscopy
- High-resolution spectrometers
  - $E/\Delta E \sim 10000\text{-}20000$
- Probes mainly the ion-channel
  - T_i, $V_{\phi,\theta}$, n_Z
- Obtain T_e using line-ratio

Wider energy bands

- Multi-energy spectroscopy
- Low-resolution spectrometers
  - $E/\Delta E \sim 10$
- Probes electron and ion channels
  - T_e, n_Z, ΔZ_{eff}, Z_{eff}
- $n_{e,fast}$ (e.g. LHCD, runaways)

Example of spatially resolved x-ray spectra from ITER

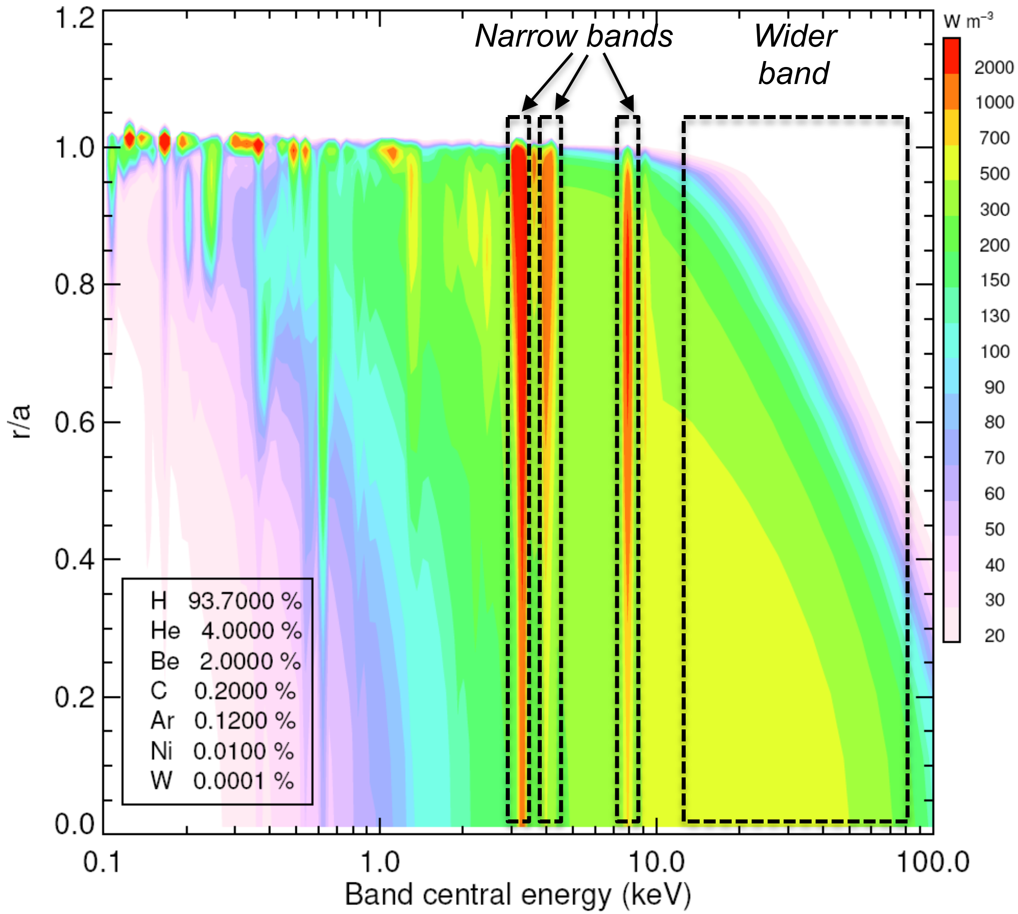

Three options in the x-ray range

① Conventional broadband x-ray measurements
(e.g. SXR tomography=>confinement, MHD, equilibrium).

② Doppler line-radiation x-ray measurements
(e.g. n_Z, T_e, T_i, v_ϕ, v_θ, => E_r).

③ Modern PHA & multi-energy measurements
(e.g. Z_{eff}, n_Z, T_e, $n_{e,fast}$).

Extract local plasma information !!!

Motivation for developing and using new x-ray crystal imaging spectrometers

① Measurement of ion-temperature (T_i), toroidal velocity (v_ϕ) and impurity density (n_Z) are important for understanding and optimizing confinement:

a) ∇T_i driven turbulence (ITG) is a leading candidate for explaining anomalous ion thermal transport.

b) V_ϕ and dV_ϕ/dr play important roles in the H-mode transition, ITB-formation, and RWM-stabilization.

c) Z-transport/accumulation needs to be studied & controlled/avoided

② Not all reactor concepts will consider NBI. Spontaneous rotation may provide the solution for stabilization.

∴ Spatially resolving x-ray crystal spectrometer enables T_i, v_ϕ and n_Z measurements via Doppler broadening & line shifts.

Choosing the appropriate (non-perturbative) extrinsic impurity to do x-ray spectroscopy

① For the temperature range of interest between 0.5 and 5 keV, He and Ne are fully stripped except in the relatively cool edge region.

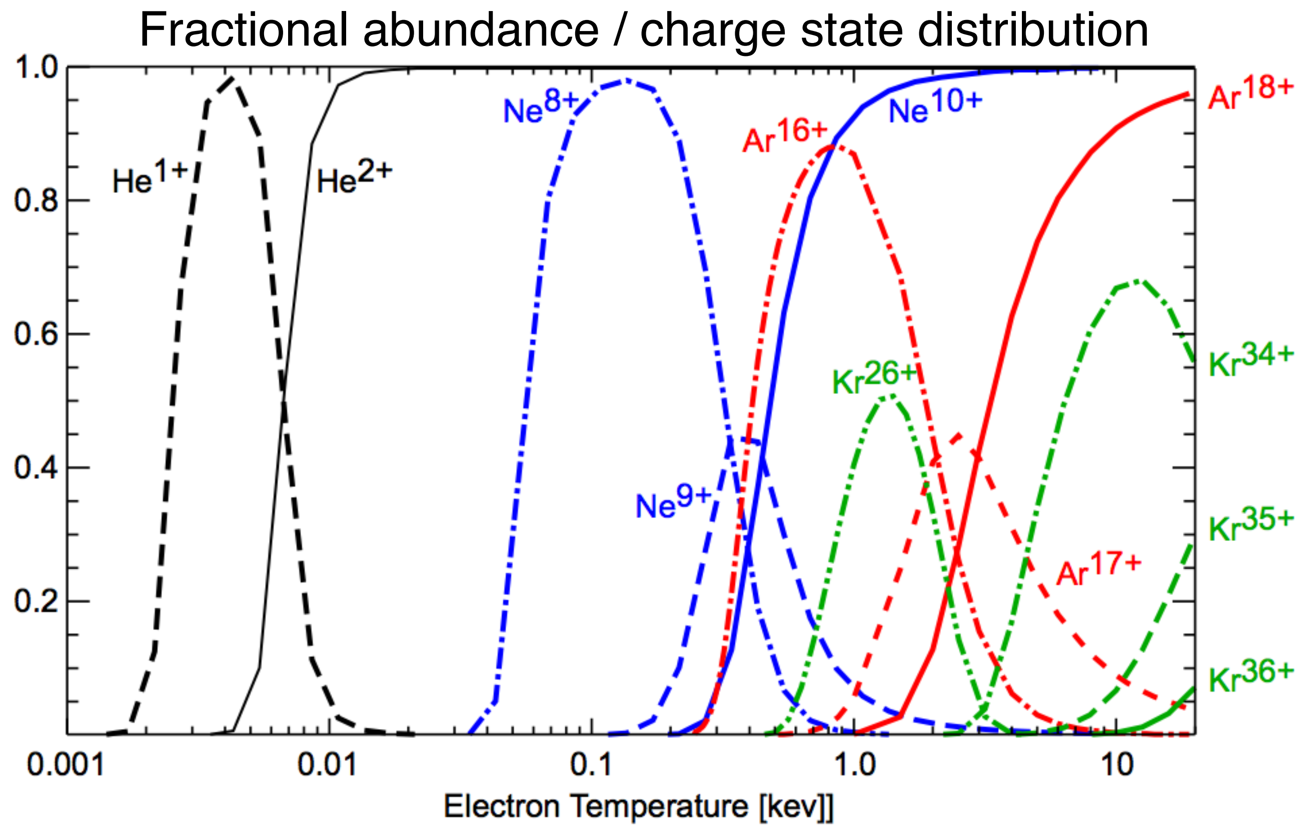

Choosing the appropriate (non-perturbative) extrinsic impurity to do x-ray spectroscopy

① For the temperature range of interest between 0.5 and 5 keV, He and Ne are fully stripped except in the relatively cool edge region.

② Argon H- and He-like charge states are dominant between 0.5 and 5 keV

Fractional abundance / charge state distribution

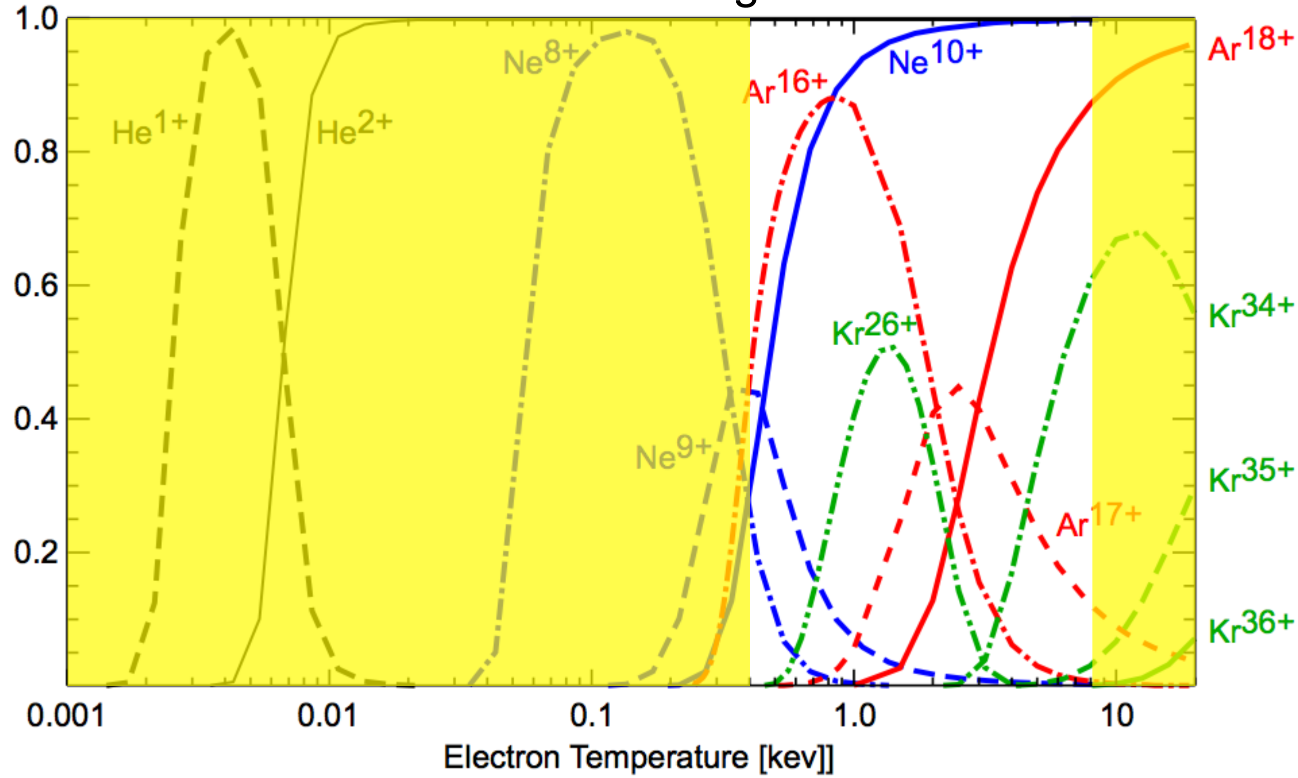

③ Kr or Xe could be used for diagnosing the core, but because they are more "*perturbative*" than Ar for the same absolute density.

X-ray crystal imaging spectrometers revolutionized our field with T_i and $V_{\phi,\theta}$ profile measurements

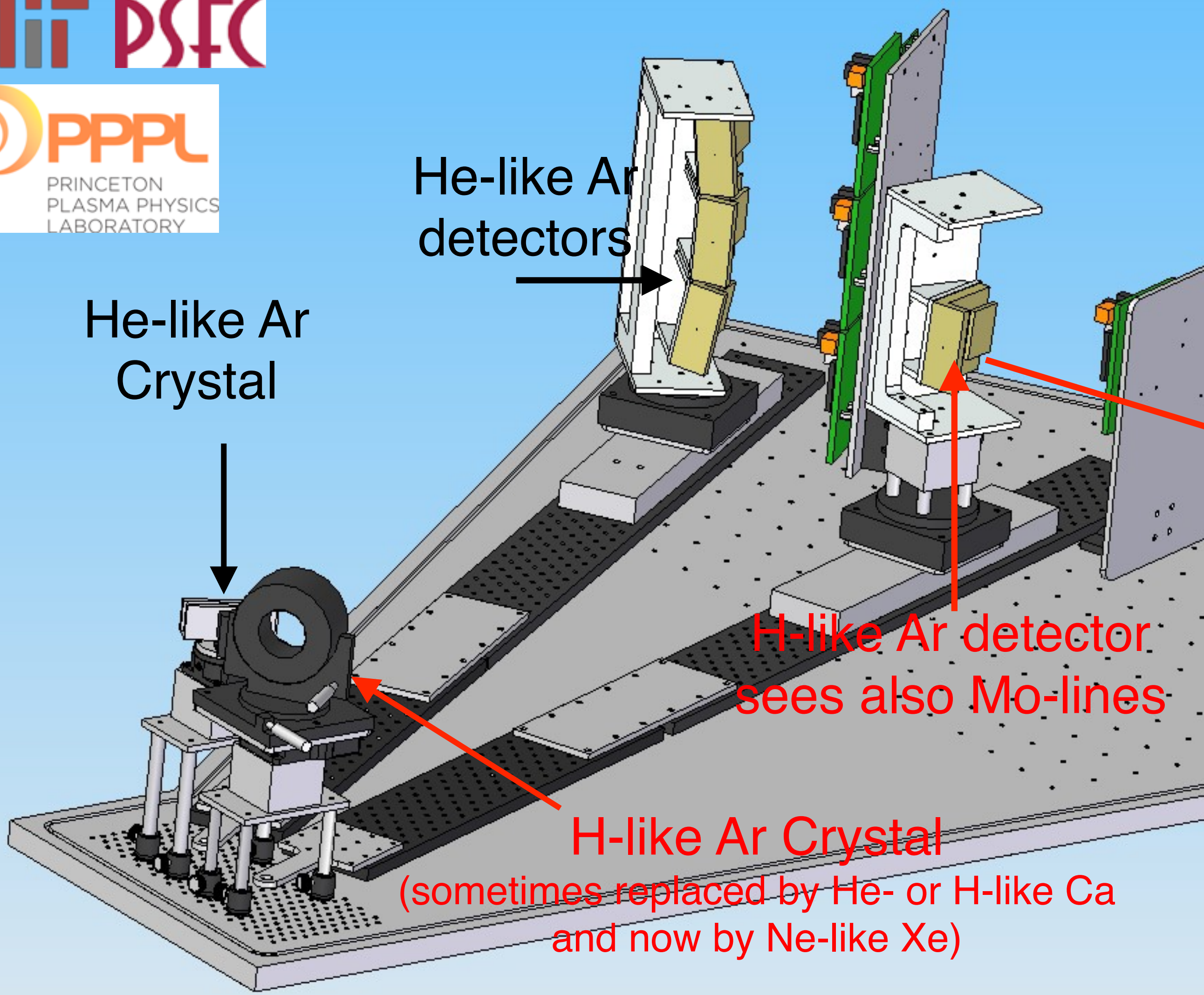

Ne-like Mo and H-like Ar fall in the spectrum

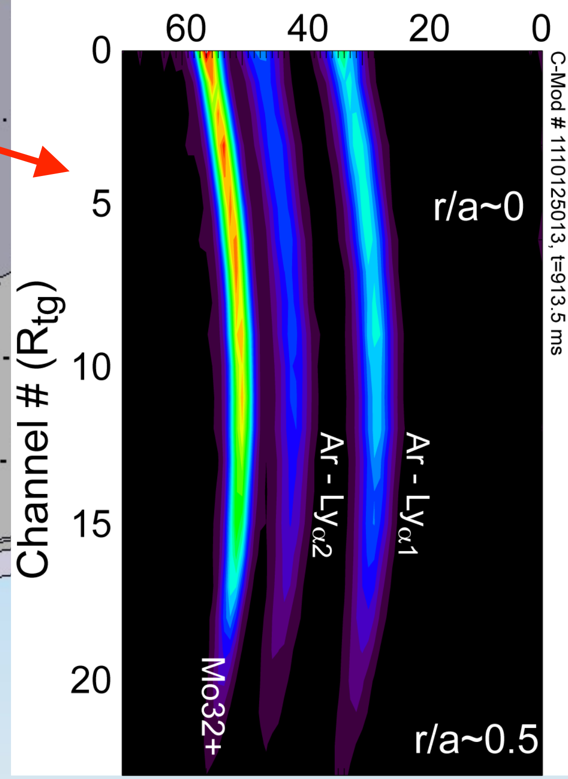

Similar systems have been installed in NSTX, KSTAR, EAST, LHD, W7 and in the future, NSTX-U, WEST, JT60SA & ITER

How crystals help us achieving high-spectral resolution ($E/\Delta E>10^4$)

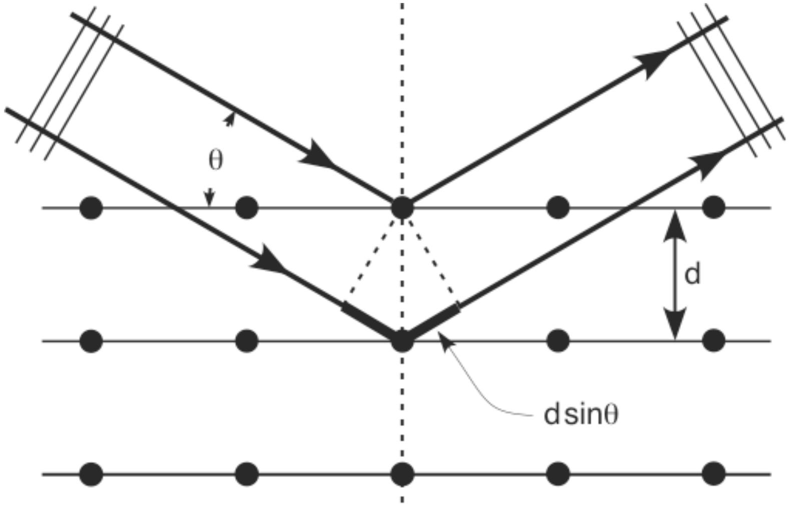

① Bragg diffraction: $2d\sin\theta = n\lambda$

② Assuming a constant "d", the observed relative wavelength shift (DS: Doppler shift) is given by:

$$\left.\frac{\Delta\lambda}{\lambda}\right|_{DS} = \frac{\Delta\theta}{\tan\theta}$$

③ The value of $\Delta\theta$ can be constrained by the Johann error, which is given by:

$$\Delta\theta = l_c^2/8R_c^2\tan\theta$$

④ Resolving power:

$$\frac{\lambda}{\Delta\lambda} = 8\frac{R_c^2}{l_c^2}\tan^2\theta$$

⑤ For lc~5 cm (crystal length), Rc~2.7 m, $\theta=54^o$, $\lambda/\Delta\lambda$~40000 !!!

Pilatus detectors enable breakthrough of 100k pixels (min.) at single/multiple energy ranges

Operates in single photon counting mode

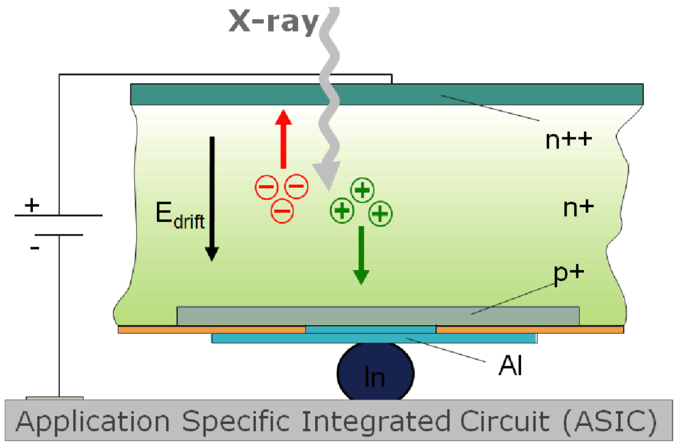

CMOS hybrid pixel technology developed originally for synchrotrons (CERN + PSI + DECTRIS)

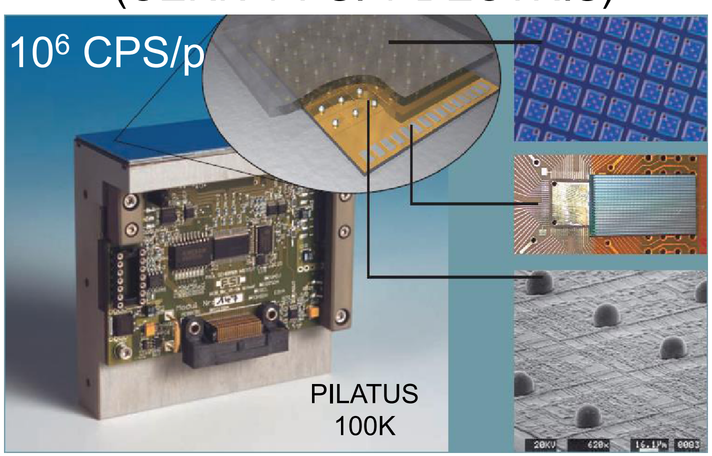

Si-sensor 2D array pn diodes

CMOS readout chip

In balls

Thanks to important advances in the x-ray detector technology it is now possible to simultaneously record high resolution images of x-ray photons at single OR multiple energy ranges through direct x-ray detection.

100K to 12M pixels (PILATUS: 172 μm, EIGER: 75 μm)

PILATUS3 900K-IPP in-vacuum detector for x-ray plasma spectroscopy

Pilatus detectors enable breakthrough of 100k pixels (min.) at single/multiple energy ranges

Operates in single photon counting mode

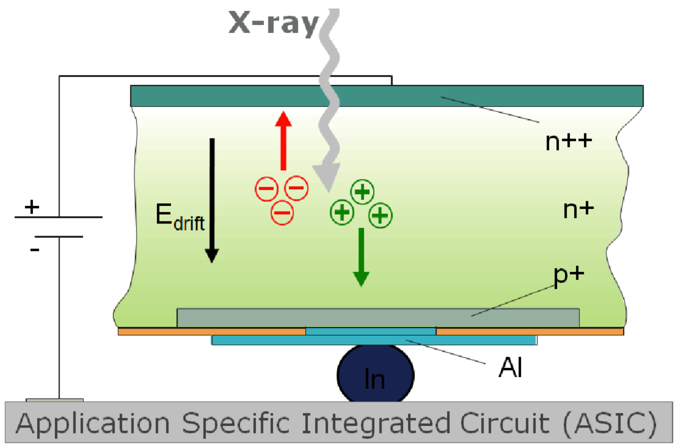

Photon counting circuit in **each pixel**

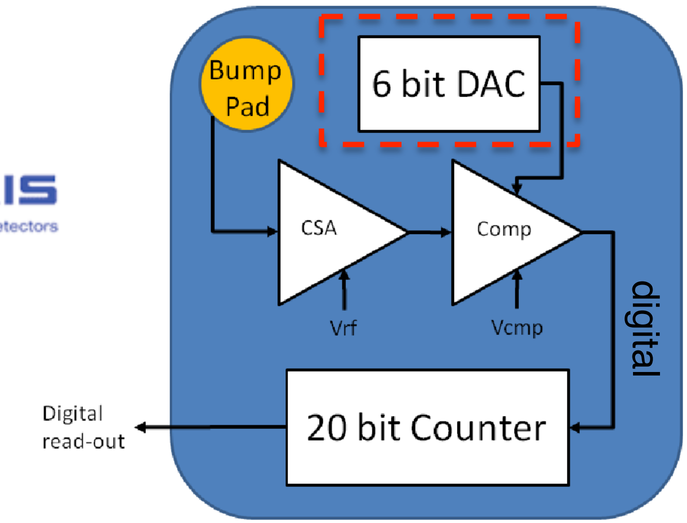

DECTRIS
Next Generation X-Ray Detectors

CMOS hybrid pixel technology developed originally for synchrotrons (CERN + PSI + DECTRIS)

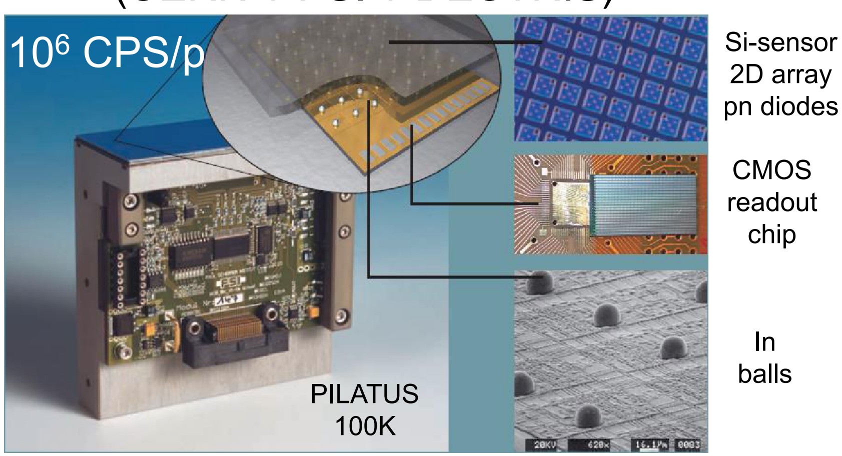

- New maximum frame rate of 500 Hz (1ms integration + 1 ms readout).
- New 10^7 CPS/p for PILATUS3
- The comparator voltage of the readout chip (V_{cmp}) controls the *global* threshold energy.
- The threshold energy can be individually *refined/ trimmed* using a built-in 6-bits DAC (V_{trim}).

He-like Ar spectra is available from the cold plasma edge to the hot core

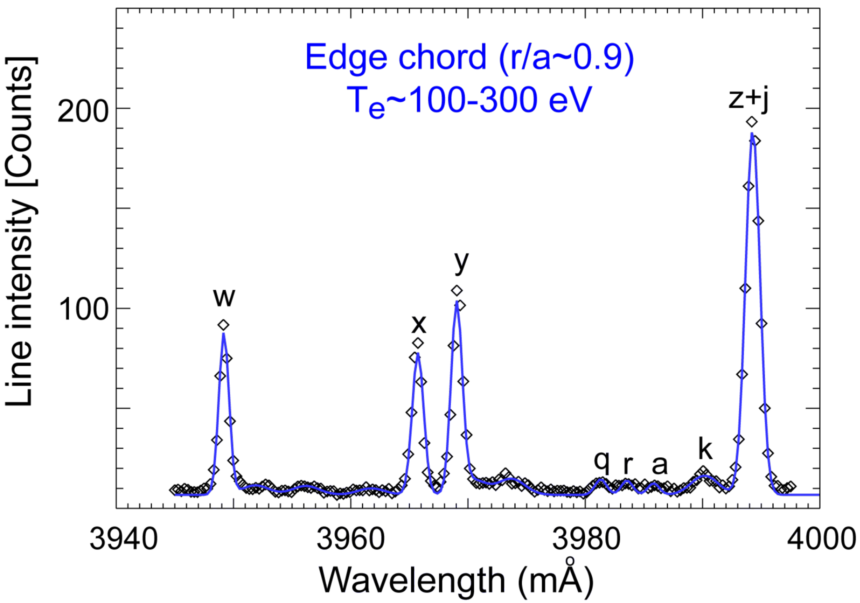

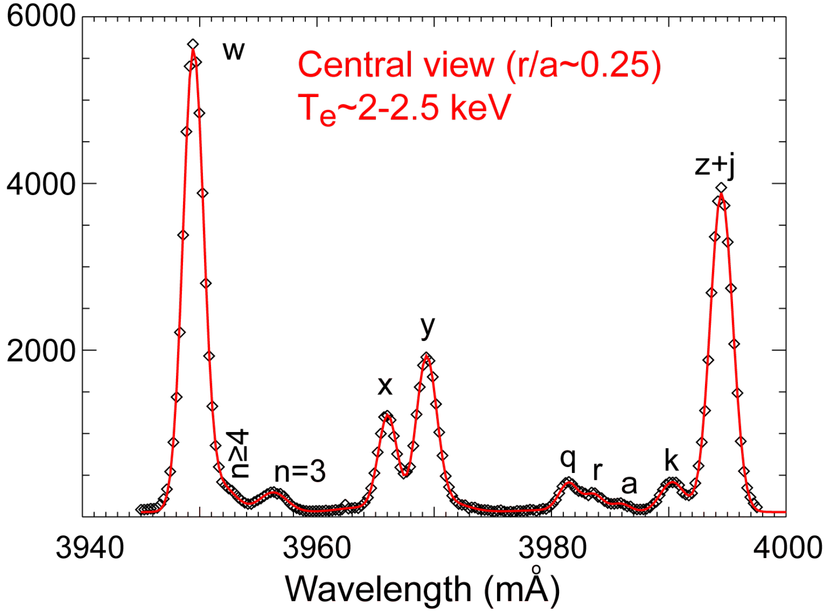

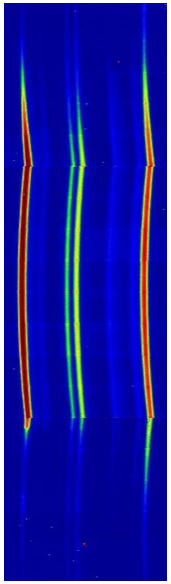

① Too cold at the edge ⇒ no excitation of dielectronic satelites.

② H-like Ar diffuse outward and recombine to produce the He-like ions.

③ Very narrow lines⇒low T_i as well.

① Enough to produce the resonant-like excitation of dielectronic satellites.

② Intensity of resonant w-line is f(T_e).

③ Much wider Doppler widh⇒higher T_i

Ion temperature profiles have been obtain in a variety of physics scenarios (L, H- and i-Mode)

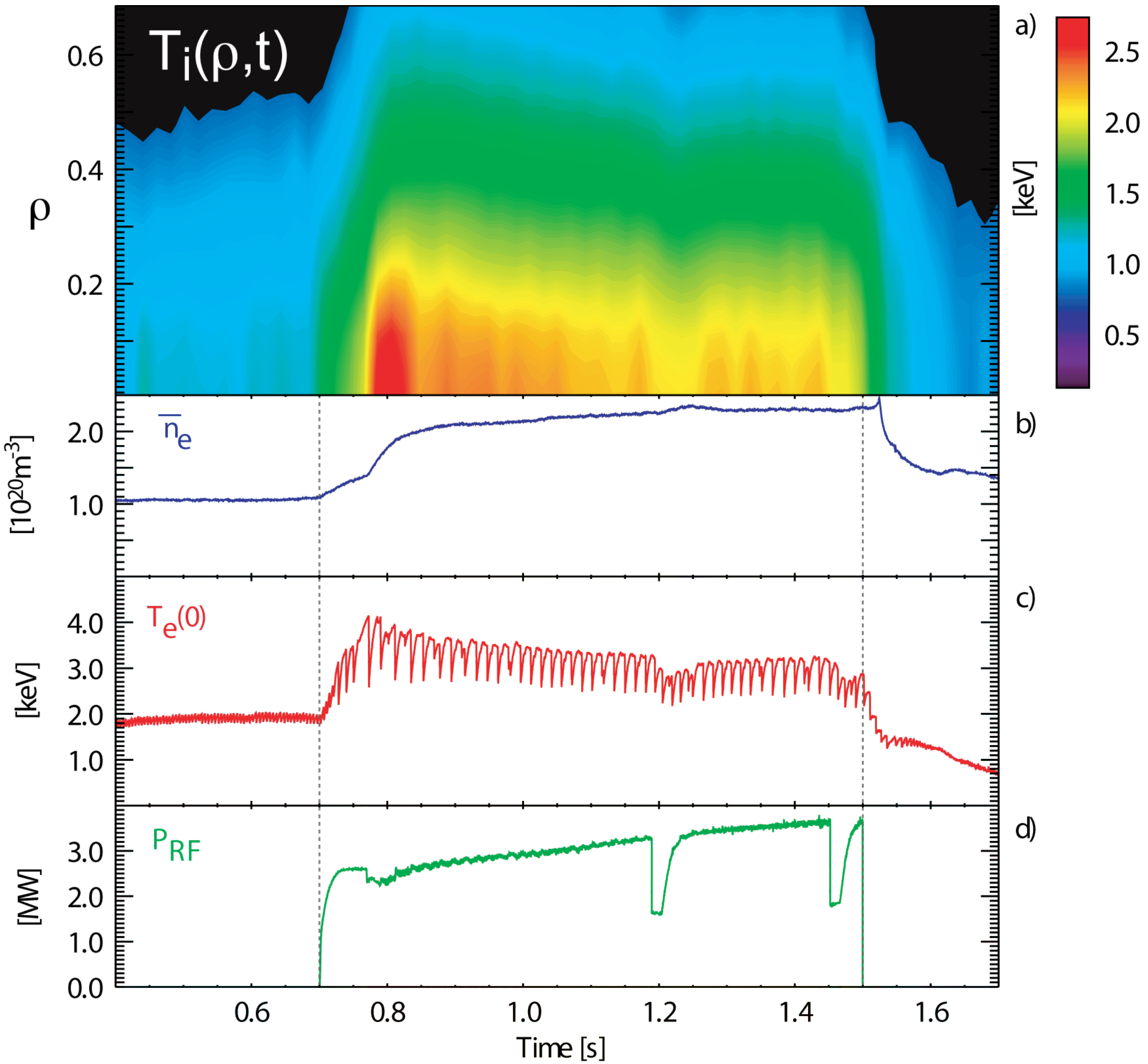

Electron temperature T_e-profiles can also be obtained using line-ratios

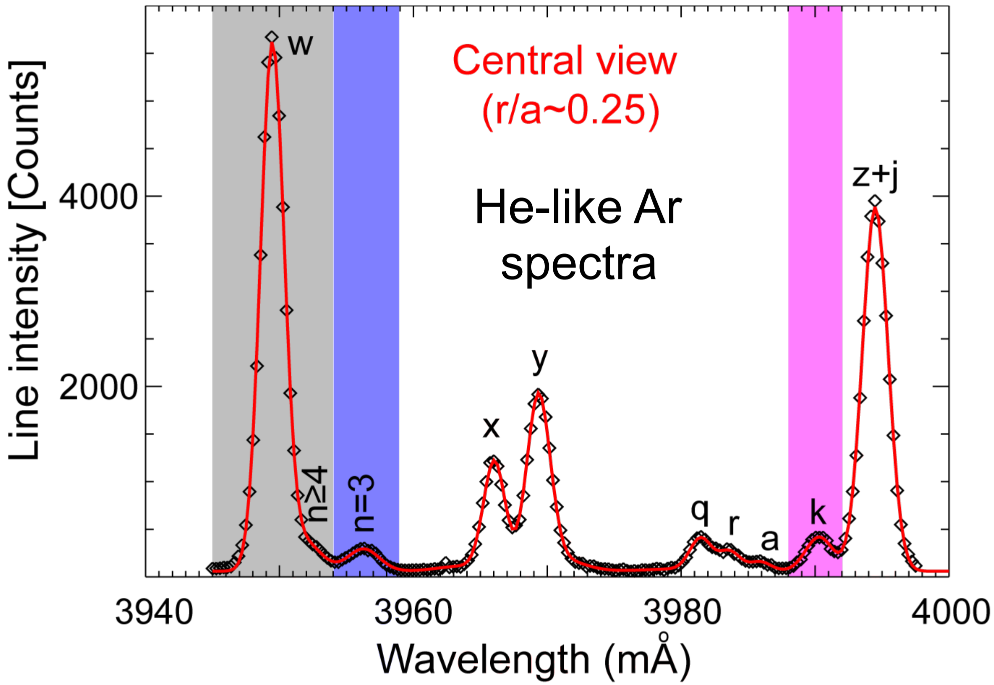

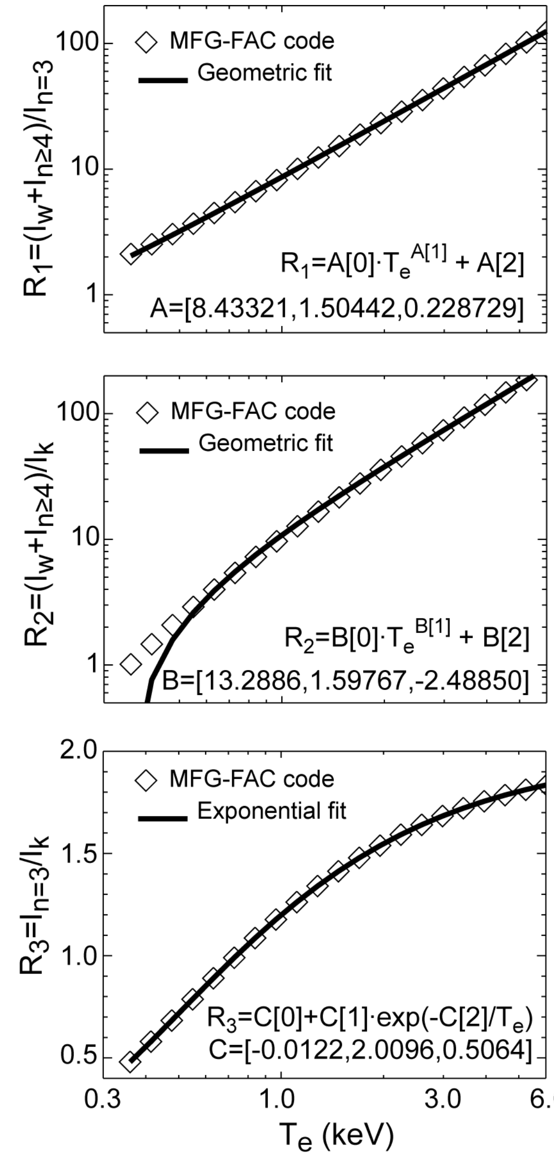

(L. Delgado-Aparicio, un-published)

Te-measurements based on the ratio of the resonance line-w and the dielectronic satellites "n=3" and "k"

① Technique applicable to Alcator C-Mod, NSTX-U, KSTAR, EAST, WEST, LHD and JT60SA.

② Considered to be a <u>secondary diagnostic technique</u> for the electron temperature (T_e) in ITER.

Three options in the x-ray range

① Conventional broadband x-ray measurements
(e.g. SXR tomography=>confinement, MHD, equilibrium).

② Doppler line-radiation x-ray measurements
(e.g. n_Z, T_e, T_i, v_ϕ, v_θ, => E_r).

③ Modern PHA & multi-energy measurements
(e.g. Z_{eff}, n_Z, T_e, $n_{e,fast}$).

Extract local plasma information !!!

New technology for developing multi-energy soft x-ray diagnostics is now available

CMOS hybrid pixel technology with excellent efficiency

Thanks to important advances in the x-ray detector technology it is now possible to simultaneously record high resolution images of x-ray photons at single OR multiple energy ranges through direct x-ray detection.

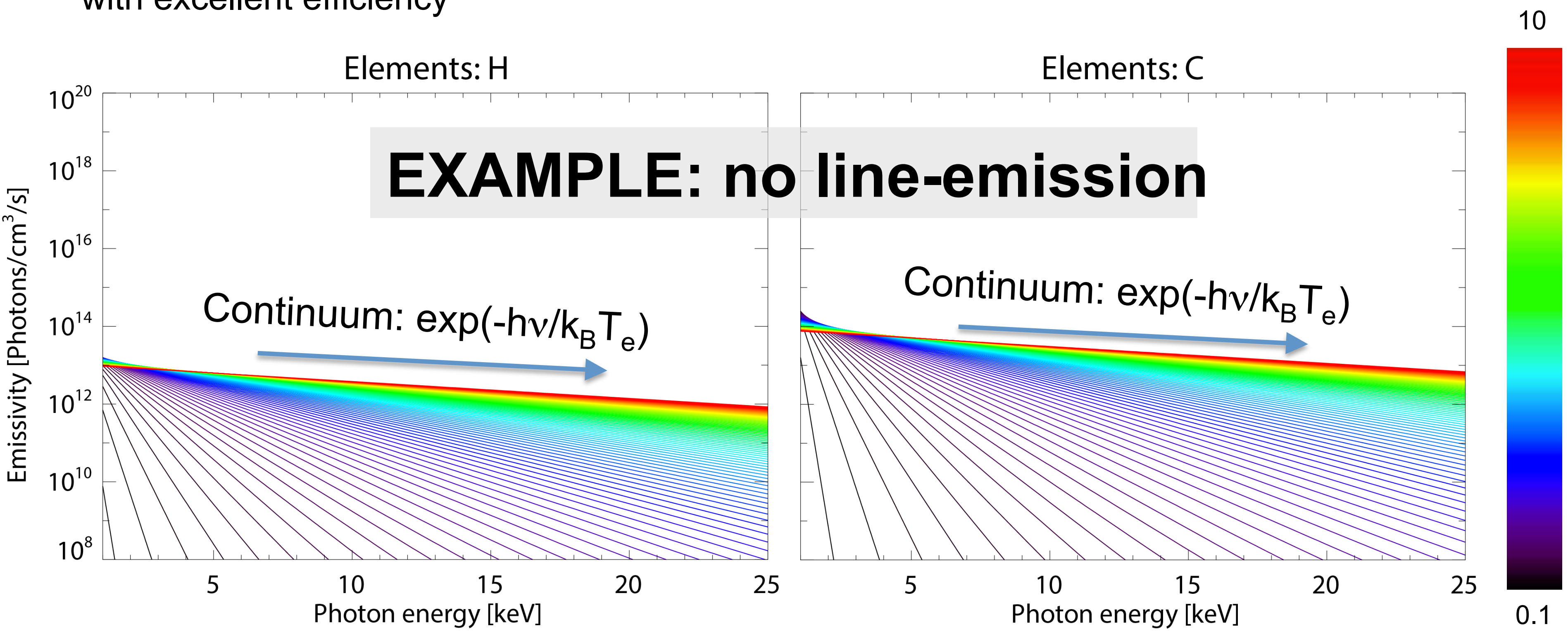

New technology for developing multi-energy soft x-ray diagnostics is now available

CMOS hybrid pixel technology with excellent efficiency

Thanks to important advances in the x-ray detector technology it is now possible to simultaneously record high resolution images of x-ray photons at single OR multiple energy ranges through direct x-ray detection.

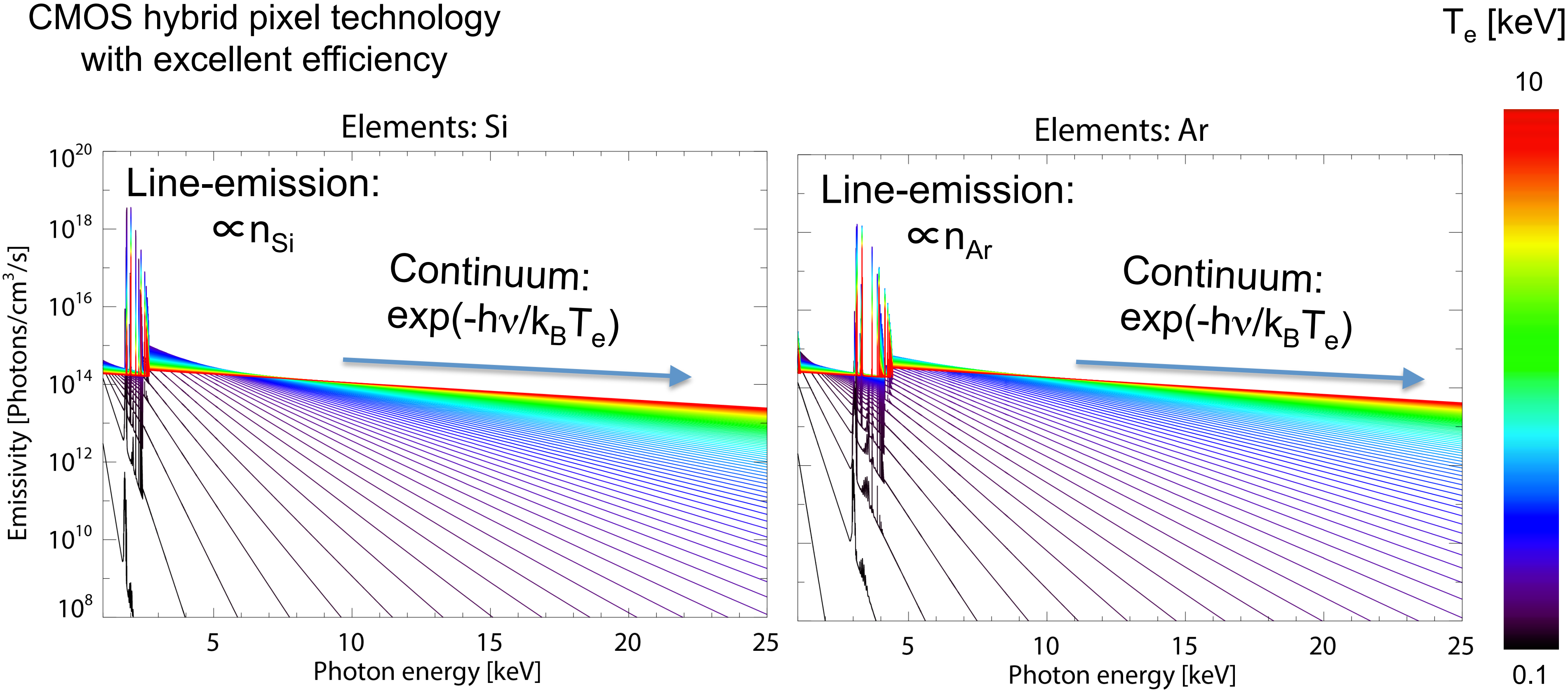

New technology for developing multi-energy soft x-ray diagnostics is now available

CMOS hybrid pixel technology with excellent efficiency

GOALS:

① Obtain n_Z & ΔZ_{eff} by sample or ***bracket*** line-radiation

② Obtain T_e, Z_{eff}, & $n_{e,fast}$ by ***sample*** the continuum-radiation

EXAMPLE: MOLYBDENUM

Mo-emission (Ne-, He- & H-like) between 2-5 and 17-22 keV ranges can be radially resolved

SOURCES: Mo/TZM (PFCs), Z-injector or LBO

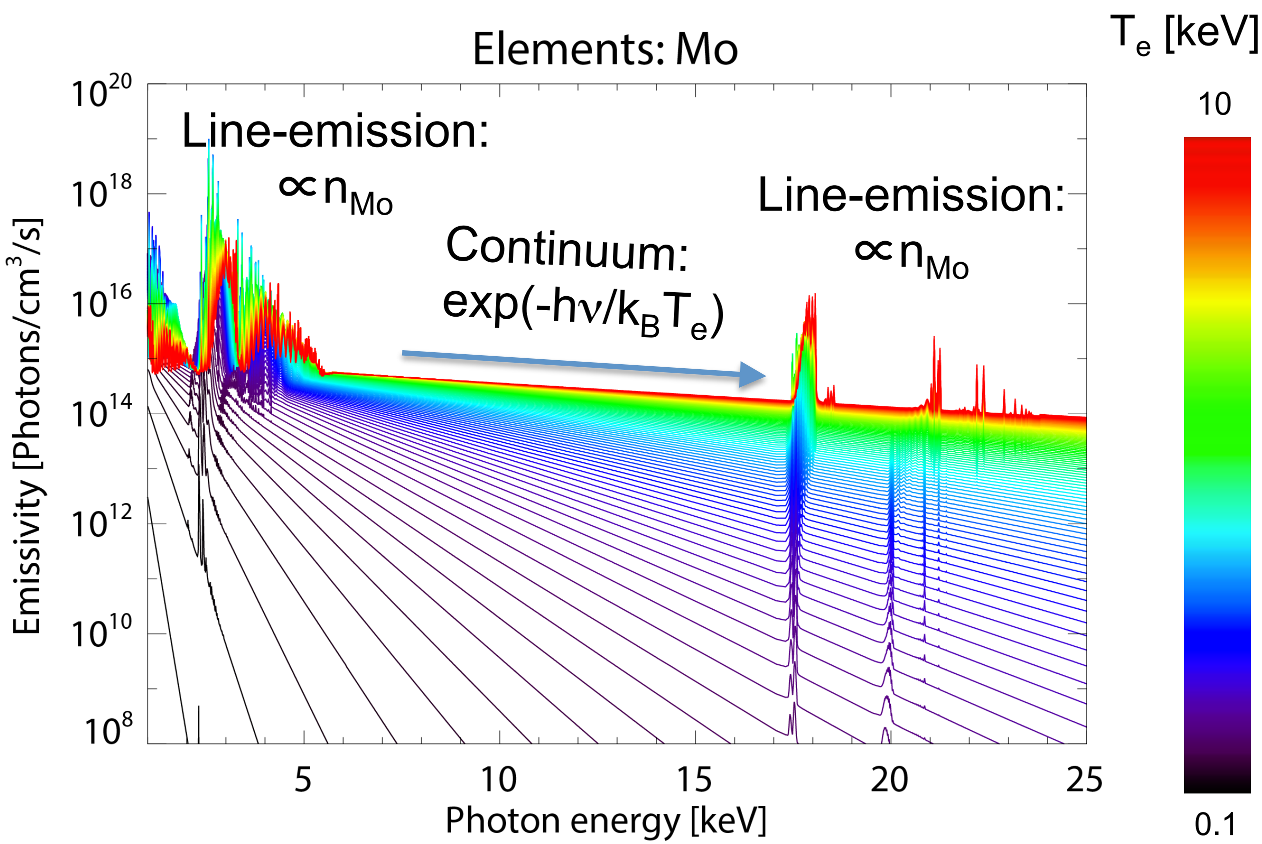

Motivation: Develop ME-SXR imaging for MCF plasmas with a unique capability

A unique opportunity of measuring, ***simultaneously***, a variety of important plasma properties:

a) central electron temperature ($T_{e,0}$) and profiles ($T_e(R,t)$)
b) medium- to high-Z impurity concentrations (Z_{eff}, n_Z =>ΔZ_{eff})
c) the birth of suprathermal e^- ($n_{e,fast}$)
d) plasma position (R_0, Z_0)

Especially applicable for:

Spherical tokamaks: No T_e ECE-measurements in STs due to low-B_ϕ

Burning plasmas: Complement other techniques such as TS and ECE

NSTX's 60 Hz Multi-point Thomson Scattering

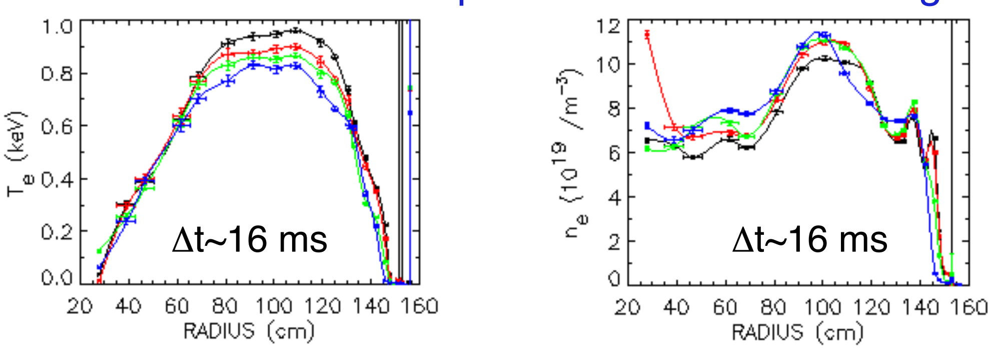

Tore Supra fast ECE data

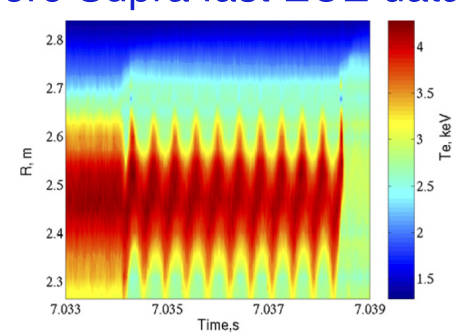

Motivation: Develop ME-SXR imaging for MCF plasmas with a unique capability

A unique opportunity of measuring, *simultaneously*, a variety of important plasma properties:

a) central electron temperature ($T_{e,0}$) and profiles ($T_e(R,t)$)

b) medium- to high-Z impurity concentrations (Z_{eff}, n_Z =>ΔZ_{eff})

c) the birth of suprathermal e^- ($n_{e,fast}$)

d) plasma position (R_0, Z_0)

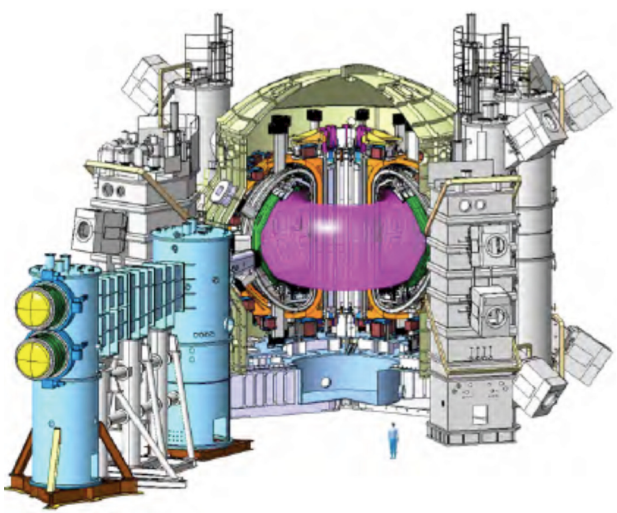

Think large: JT60SA, ITER & DEMO!

This technique should be explored also as a burning plasma diagnostic in-view of its simplicity and robustness.

e) $T_e(R,Z)$ => Ψ, J & q

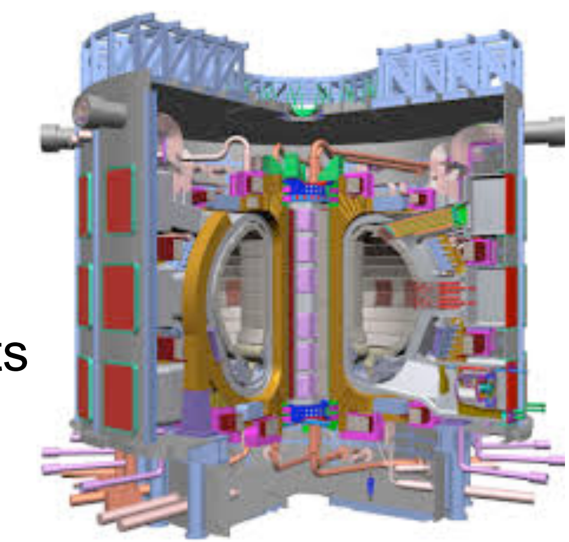

Photon counting ME-SXR systems use Si(Li), HgI_2, Si-Ge-CdTe diodes and SDDs

① Detectors in photon-counting mode

$(\langle T_e \rangle, \langle Z_{eff} \rangle, \langle n_{e,fast} \rangle, \langle n_Z \rangle)$

- Pulse height analysis (PHA)
- Good energy resolution (100-200 eV)
- Slow time-response (20-50 ms)
- Low efficiency at high-energies
- Very poor profile definition
- Still used in our community (HT7, TCV, HL-2A)

Y. Shi-RSI'04, Z. Y Chen - NIMA'04, PST'05, T. Madeira-EPS'05, P. Xu-PST'09, Y. Zhang-RSI'09, A. DuBois- RSI'15

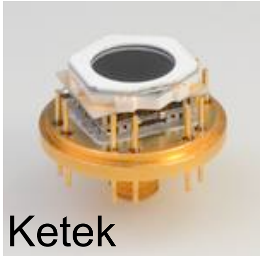

Single-chord spectrometers

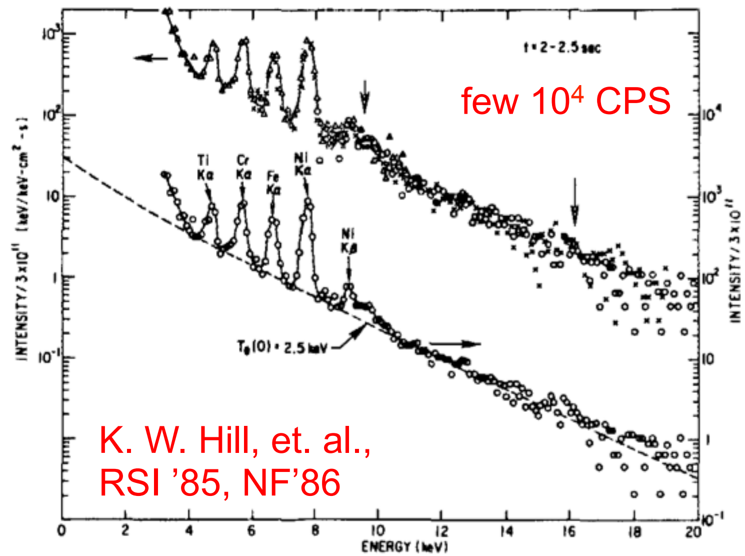

One spectrum per instrument

E. H. Silver-RSI'82, J. E. Rice-PRA'82

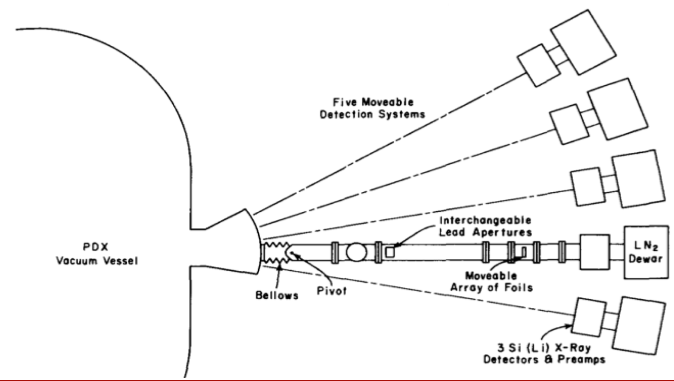

ME-SXR concepts in current mode used various filters, scintillators+PMTs, Si-diodes

② Multi-foil arrays in current-mode
(T_e and n_Z profiles)

- Better profile definition:
  - Line integrated measurements
  - Tomographic reconstructions
  - Tangential view is preferable
- Fast time-response (1 ms to 1 μs)
- Low efficiency at high-energies
- Easy to avoid low-Z emission.
- Poor energy resolution (1-5 keV)
- Still, good T_e measurements!

- WARNING: Difficult to interpret in the presence of medium- to high-Z impurities (e.g. Al, Fe, Mo, W)

L. Delgado-Aparicio, et. al., JAP'07, PPCF'07,'11, NF'09, '11

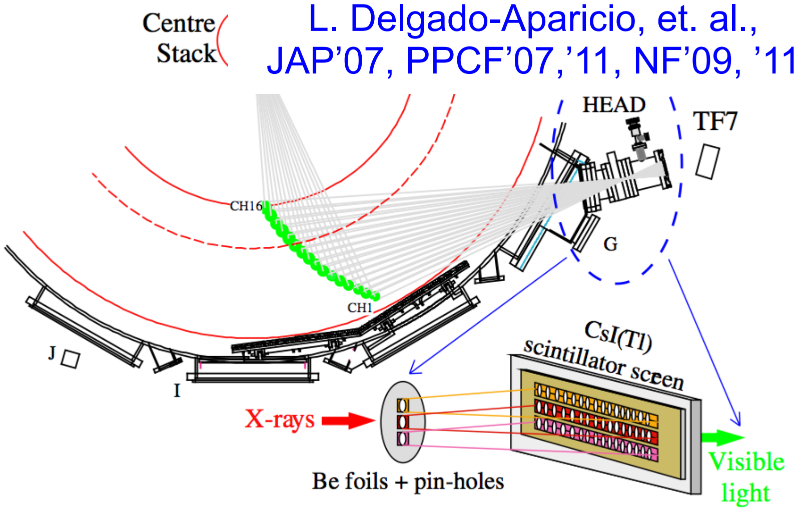

L. Delgado-Aparicio, et. al., RSI,'10, NF'11

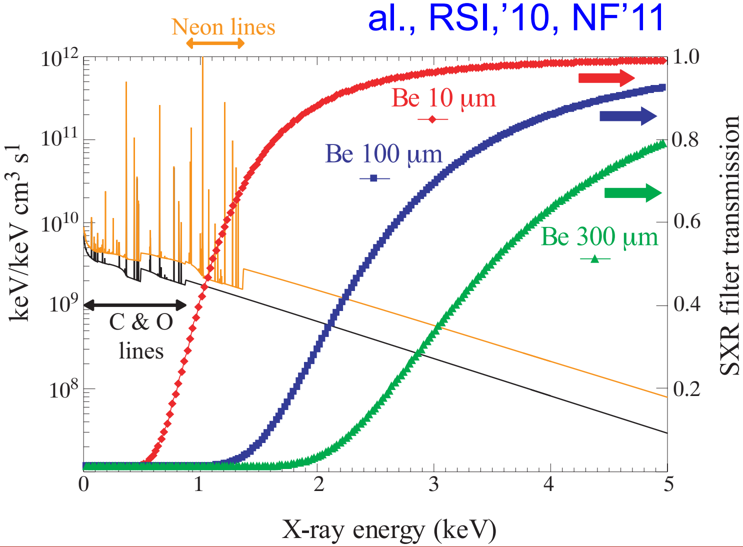

ME-SXR & Thomson Scattering "combo" provided fast $T_e(R,t)$ measurements in NSTX

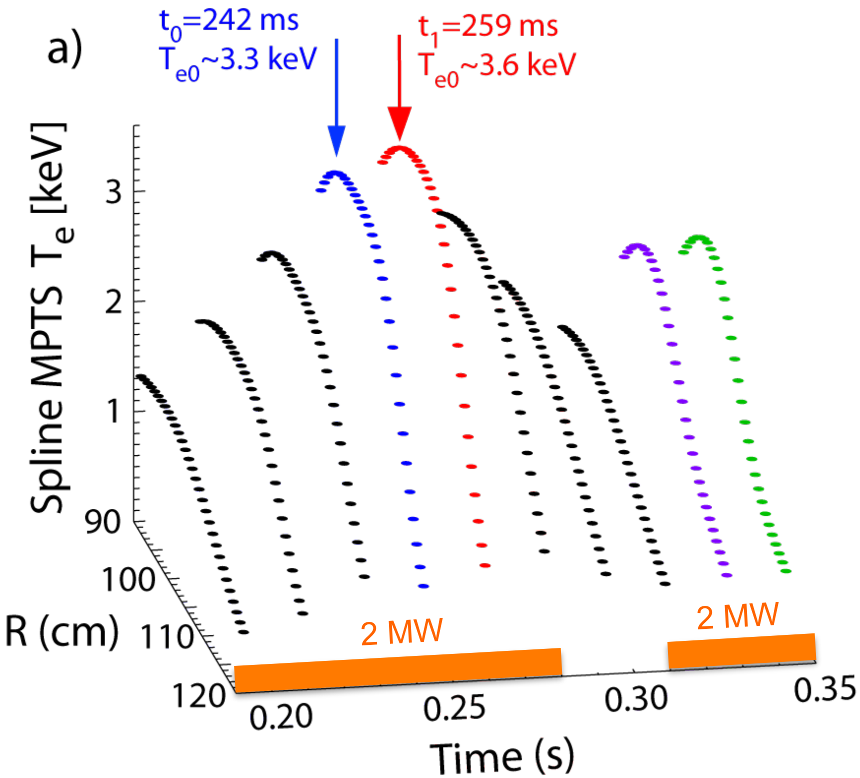

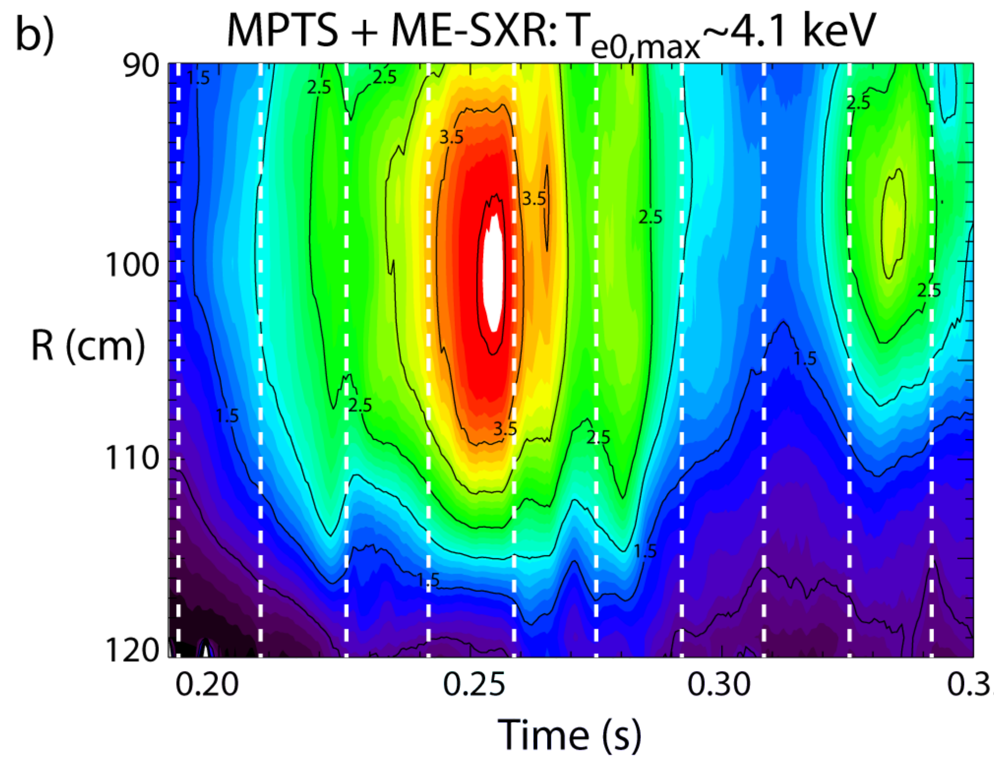

"Fast" SXR temperature measurements done in:

i. Steady state in Ohmic and NBI-heated scenarios (L. Delgado-Aparicio, et al., PPCF'07, D. J. Clayton, PPCF'13)

i. RF heated plasmas using HHFW waves (L. Delgado-Aparicio, et al., JAP'07)

ii. Plasmas with slow MHD [e.g. RWMs (L. Delgado-Aparicio, et al., PPCF'10)]

ME-SXR diode-based systems have been deployed in tokamaks and stellarators

RFX/MST-RFPs, Core
P. Franz, et al., NF'01, RSI'04, NF'13
M. McGarry, RSI'10, M. Galante, NF'15

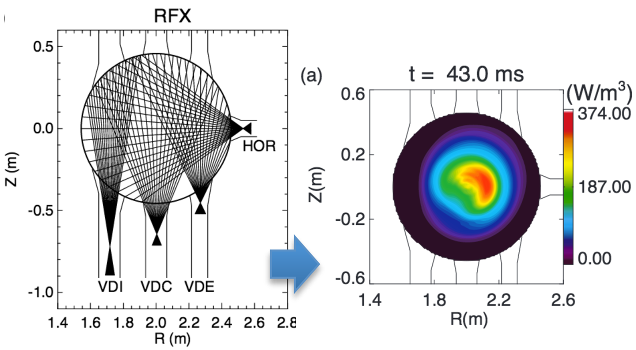

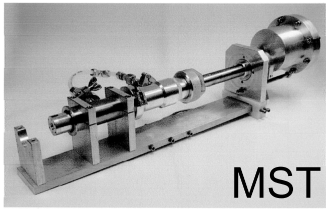

CTH, Core, J. L. Herfindal,
G. J. Hartwell, et al., RSI'14

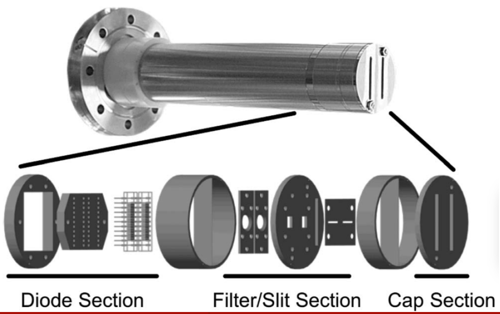

NSTX, Egde ME-SXR system
K. Tritz, et. al., RSI'12

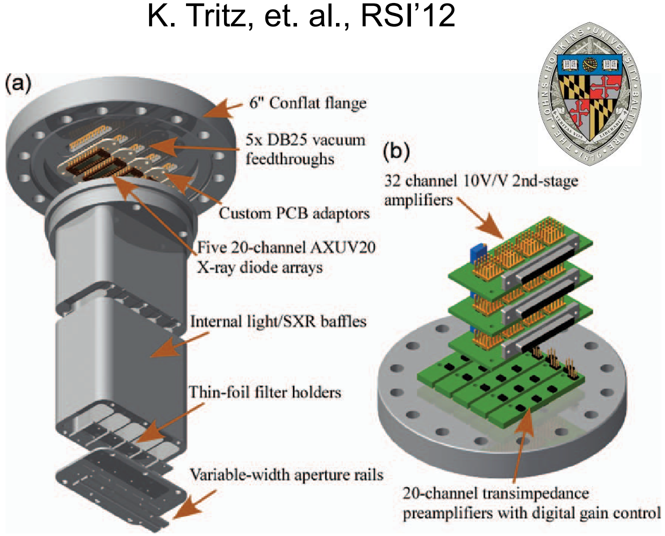

NSTX-U, Core & Edge ME system
K. Tritz, et. al., HTPD, 2014

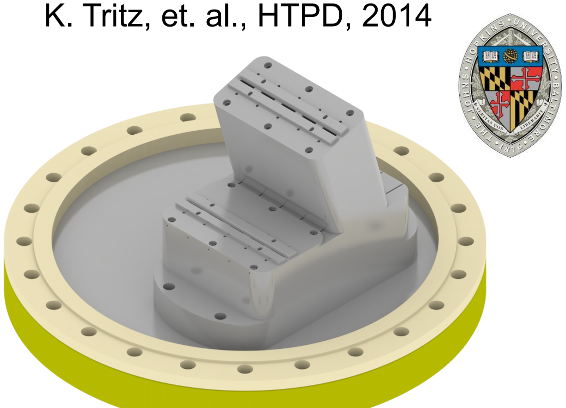

EAST, Edge ME-SXR system
Y. L. Li, K. Tritz, et. al., RSI'16

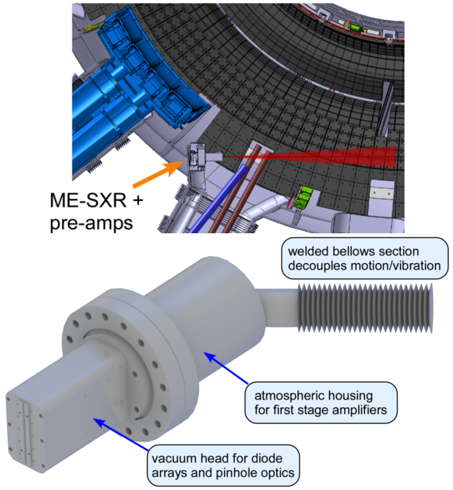

TJII, Core ME-SXR system
D. Baiao, et. al., RSI'12, '12

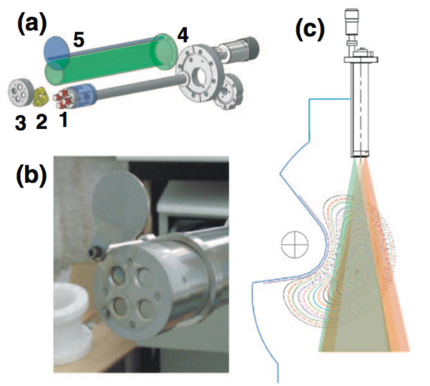

Pilatus detectors enable breakthrough of 100k pixels (min.) at single/multiple energy ranges

Operates in single photon counting mode

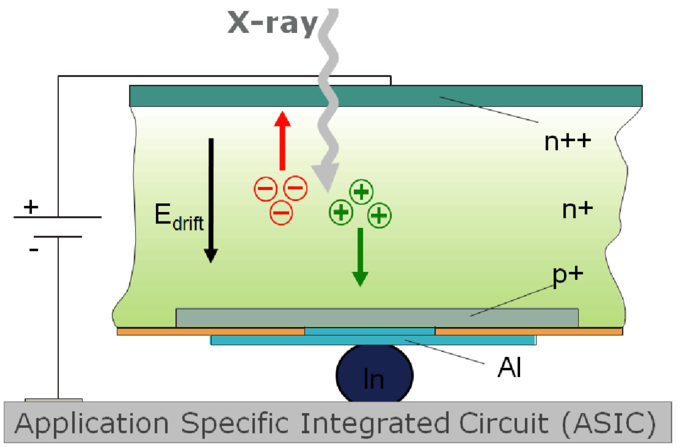

Photon counting circuit in **each pixel**

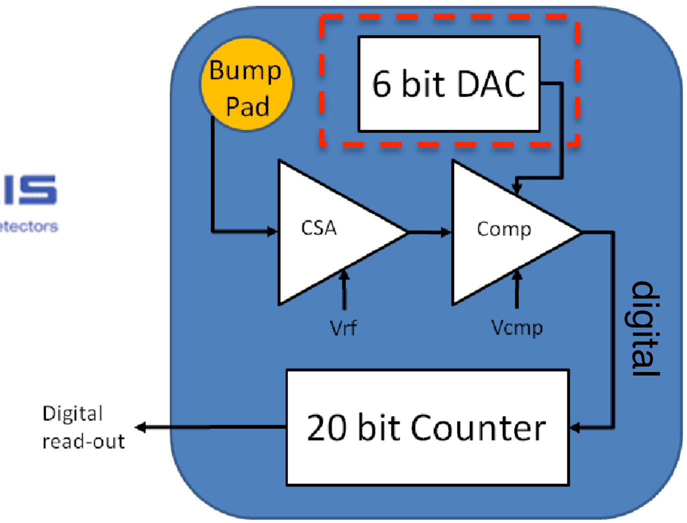

CMOS hybrid pixel technology developed originally for synchrotrons (CERN + PSI + DECTRIS)

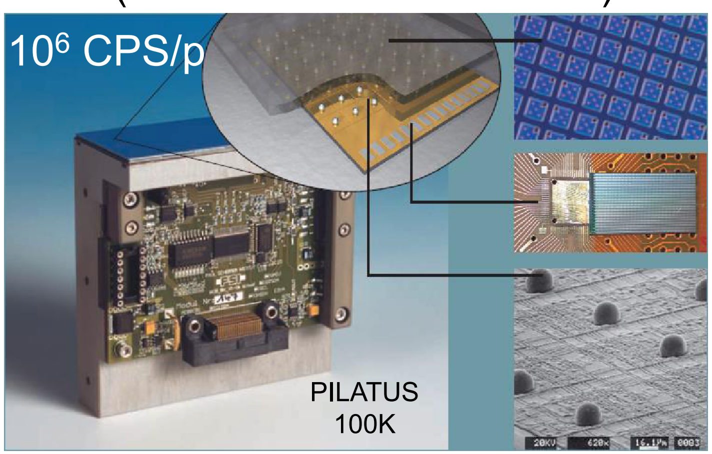

Si-sensor 2D array pn diodes

CMOS readout chip

In balls

- New maximum frame rate of 500 Hz (1ms integration + 1 ms readout).
- New 10^7 CPS/p for PILATUS3
- The comparator voltage of the readout chip (V_{cmp}) controls the *global* threshold energy.
- The threshold energy can be individually *refined/ trimmed* using a built-in 6-bits DAC (V_{trim}).

V_{comp} and V_{trim} allows individual coarse & fine tuning of energy range (per-pix): E_{width}~500 eV

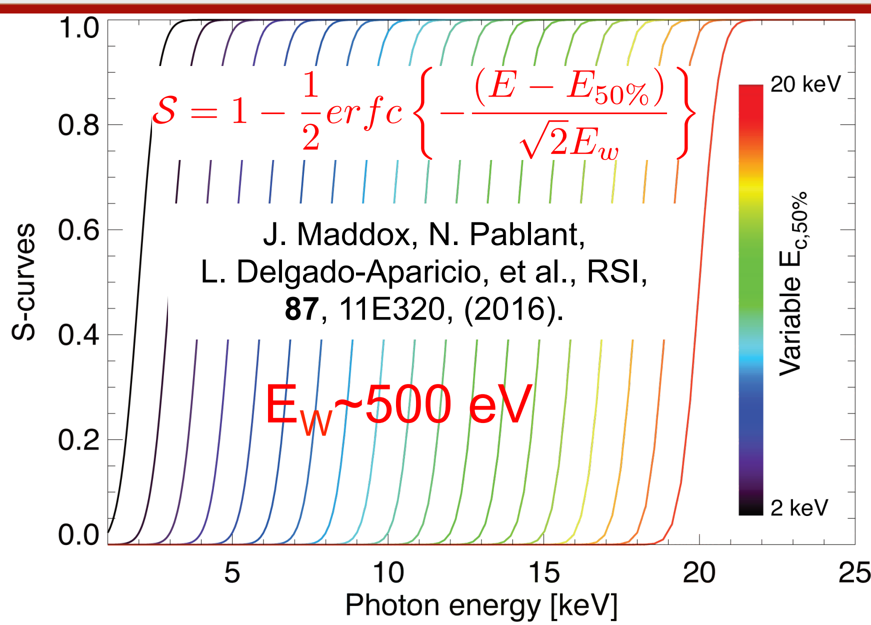

Photon counting circuit in **each pixel**

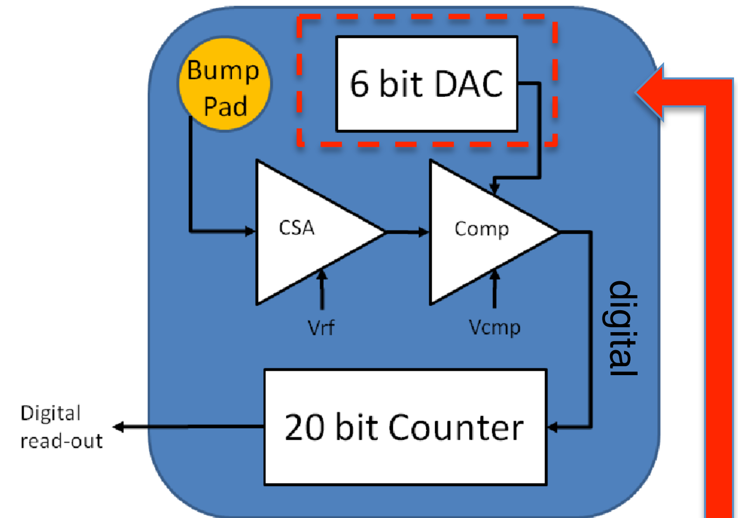

"Constant" width of electronic response is a great improvement over the use of filters

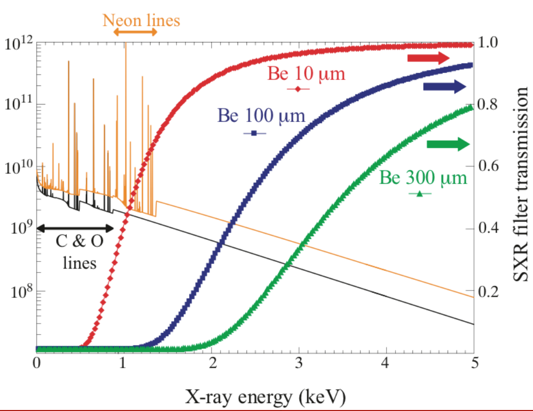

Filters:

$$\mathcal{T}(E) = \exp\left(-\frac{E_0^3}{E^3}\right)$$

$$\Rightarrow \frac{d\mathcal{T}}{dE}\Big|_{E_0} \sim \frac{1}{E_0}$$

L. Delgado-Aparicio, et. al., RSI,'10, NF'11

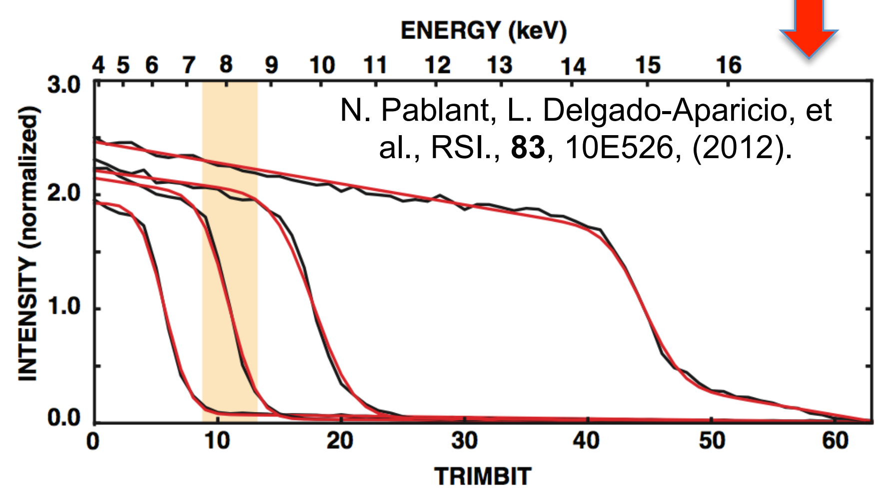

New ME-SXR imaging concept combined the best features from PHA & multi-foil methods

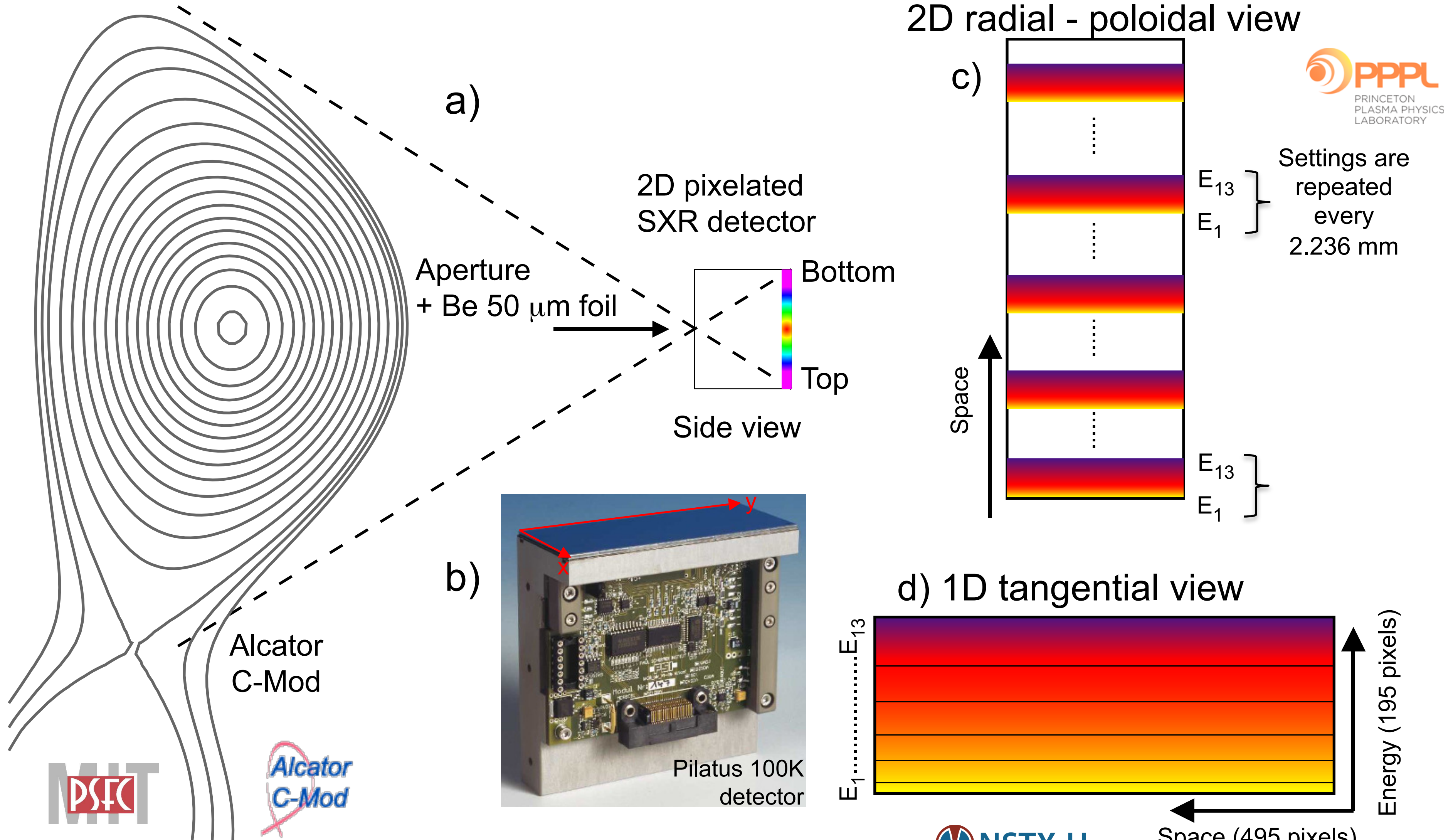

L. Delgado-Aparicio, et al., RSI, **87**, 11E204, (2016).

From sampling the continuum radiation from Ar & Mo one can measure T_e & $n_e^2 Z_{eff}$

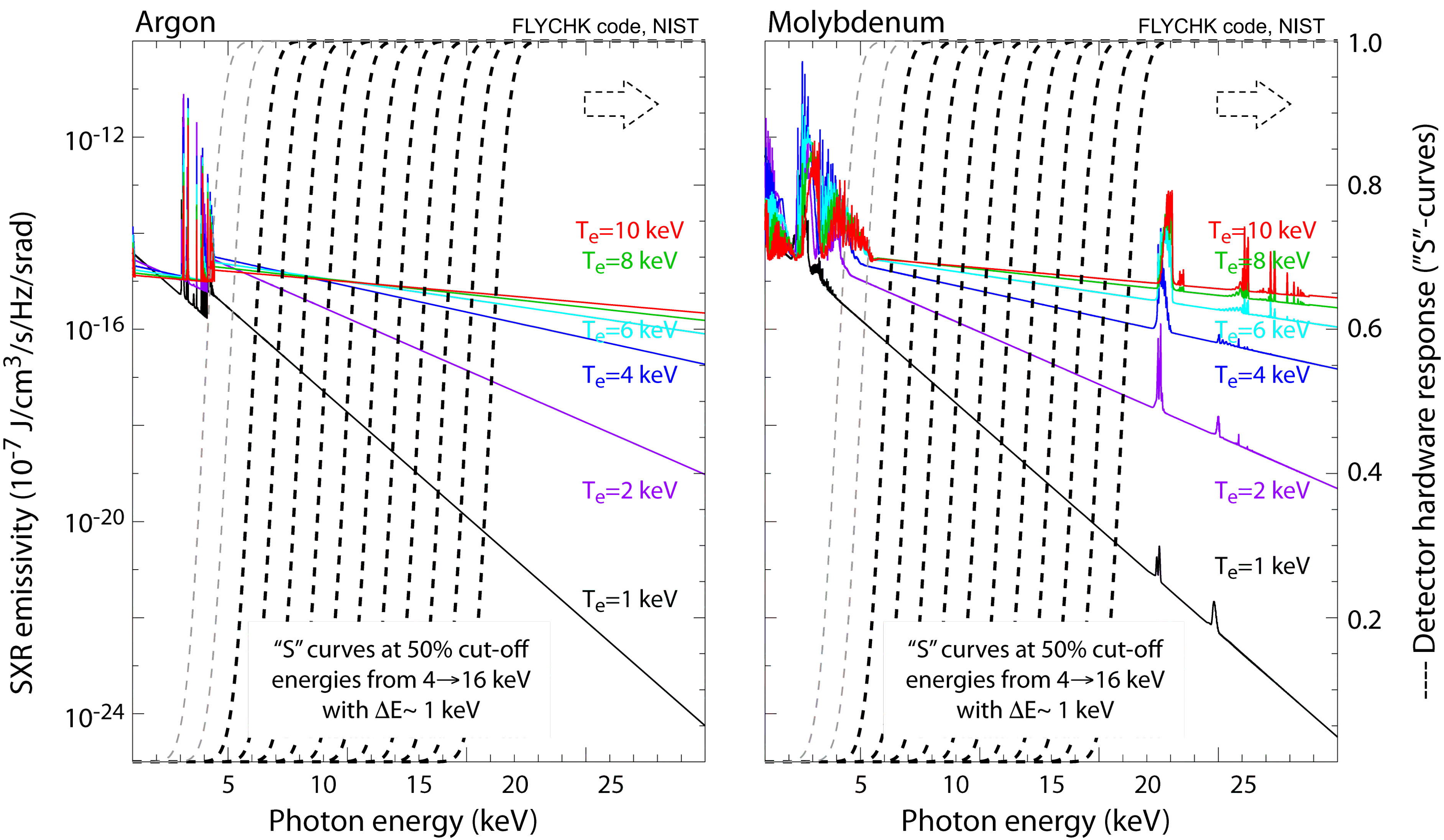

Goals #1&2: T_e^{SXR} profiles can be obtained using during Ohmic, ICRH & LHCD scenarios

- ICRH heats up ions & electrons.
- EEDF function is still Maxwellian
- Applicable to L or H-modes (including use of error fields)

- LHCD drives current and heat e^-
- LHCD present challenges for ECE
- Thin Si detectors are sensitive only to Maxwellian part of the EEDF

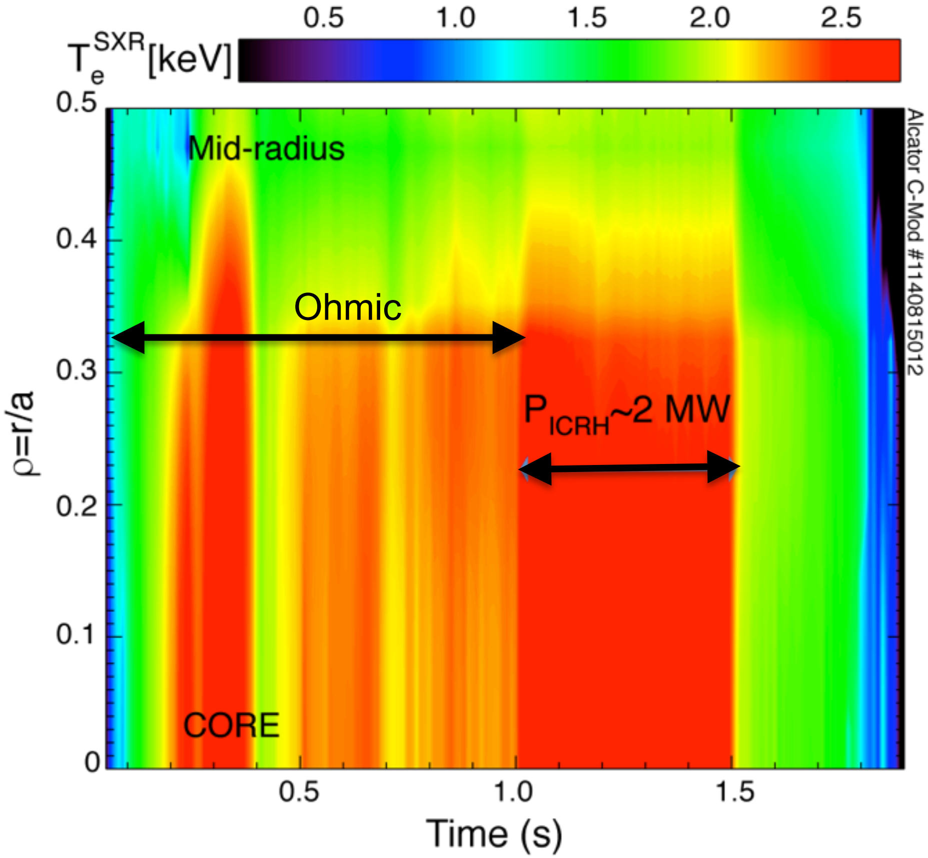

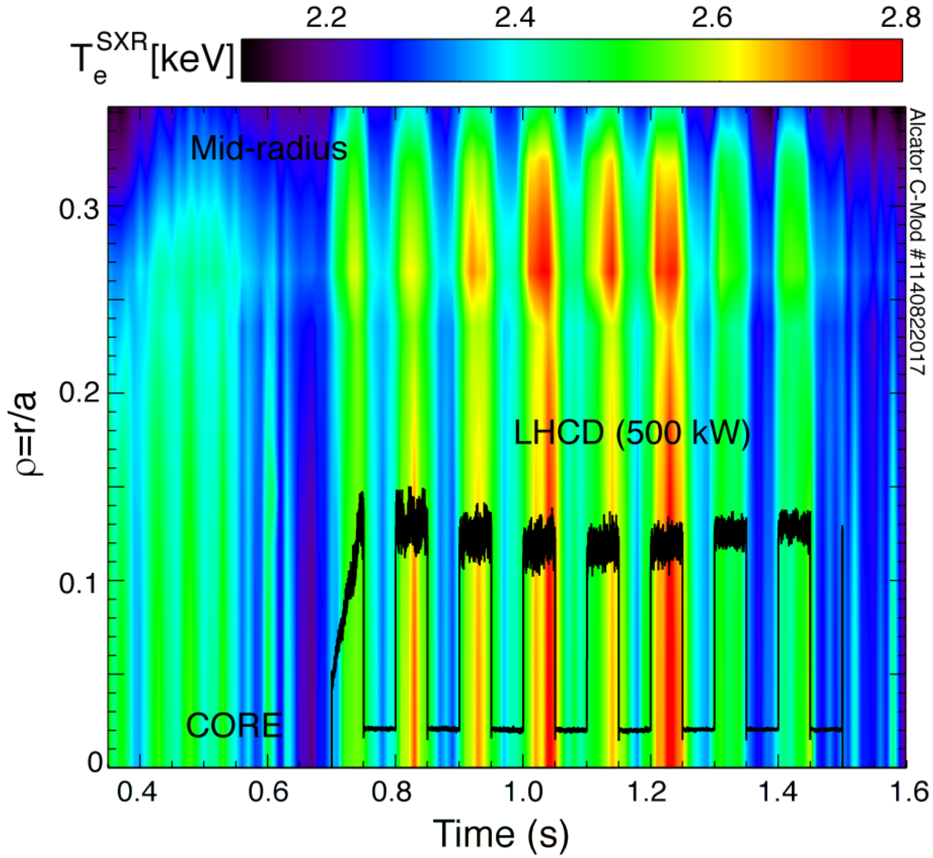

Goal #3: separate dynamic evolution of $T_e(R,t)$ from transient LBO contributions during LHCD

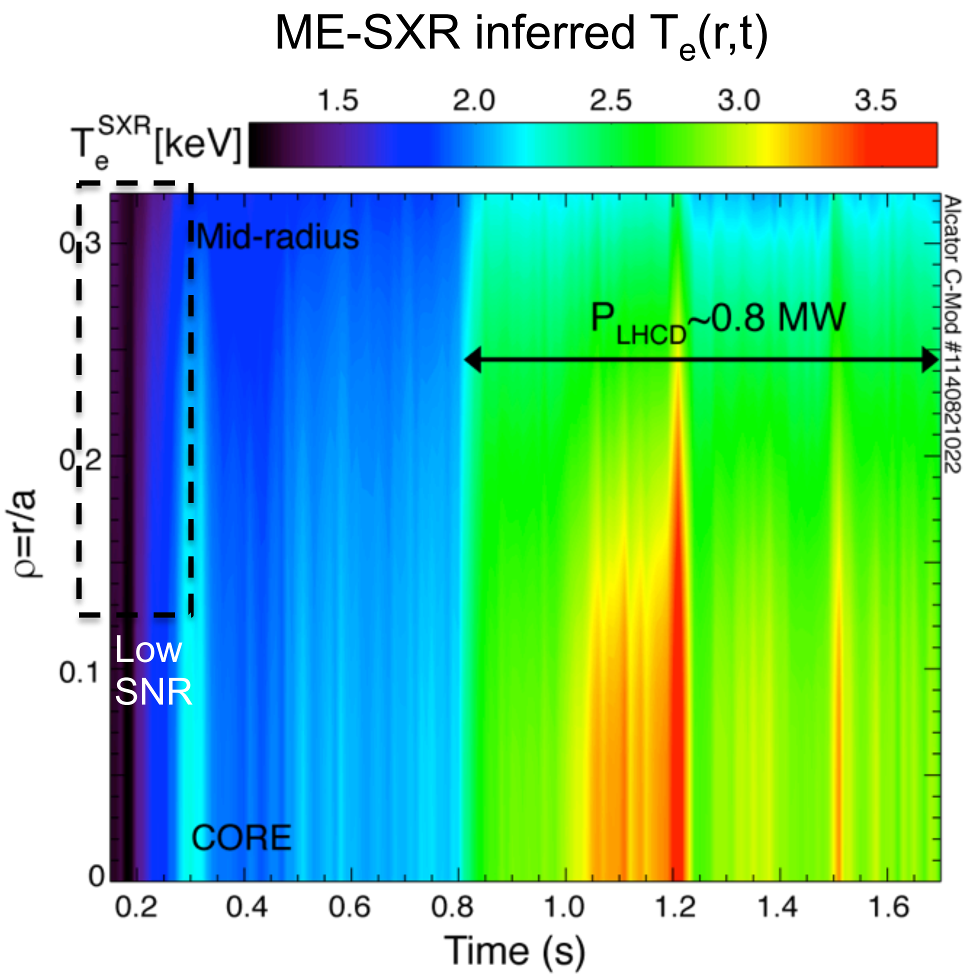

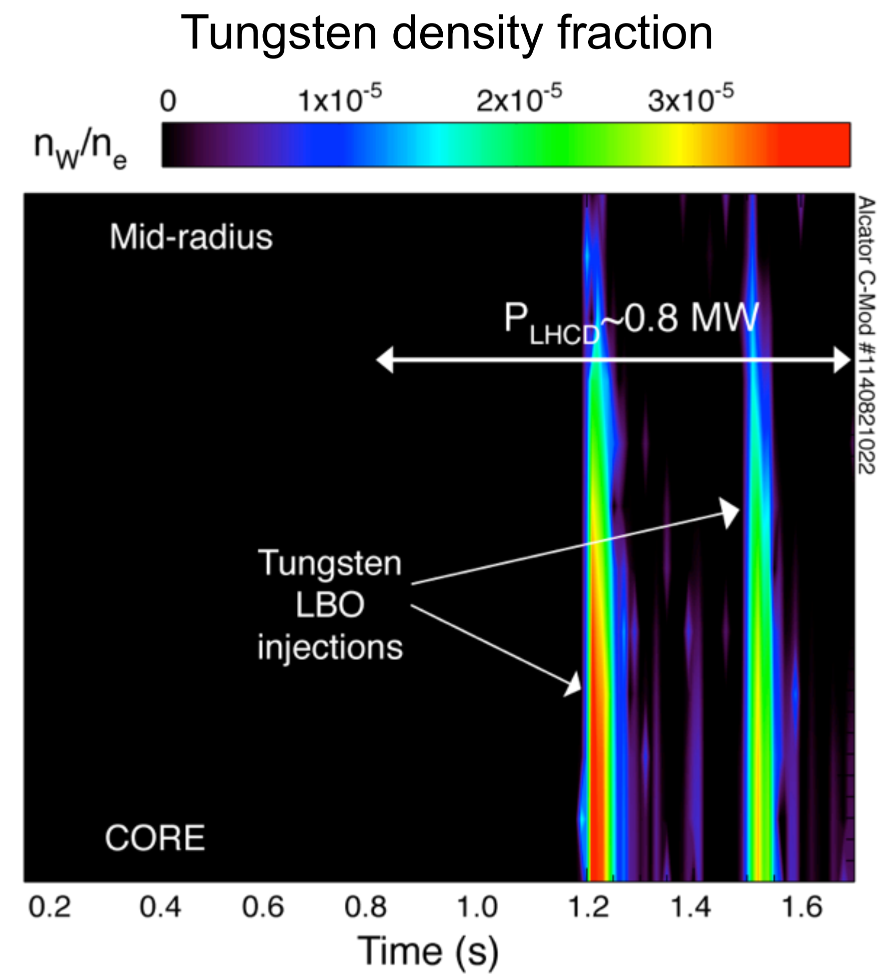

- Estimate n_Z/n_e using other diagnostics and compare
- Test Mo and W impurity transport in inductive & non-inductive scenarios

Summary 4: Modern diagnostics can help us resolve n_Z, $T_{e,i}$, $V_{\phi,\theta}$, Z_{eff} & $n_{e,fast}$ profiles

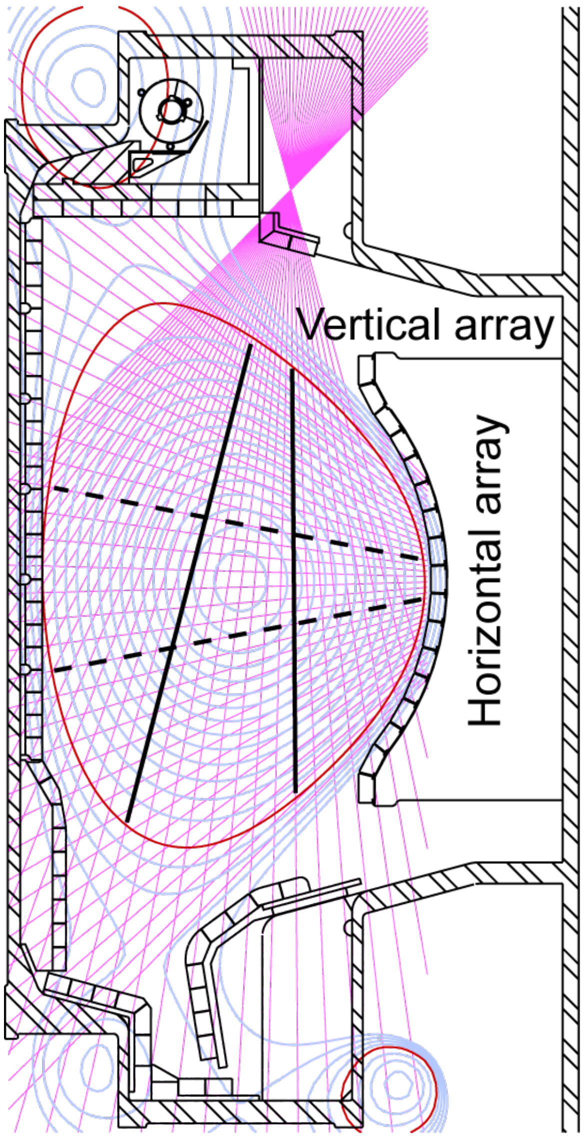

CXIS

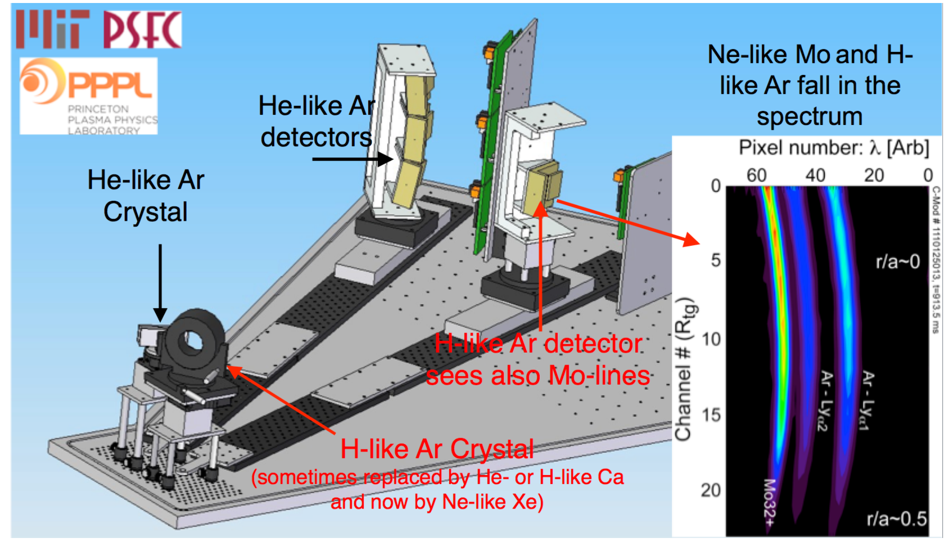

ME-SXR

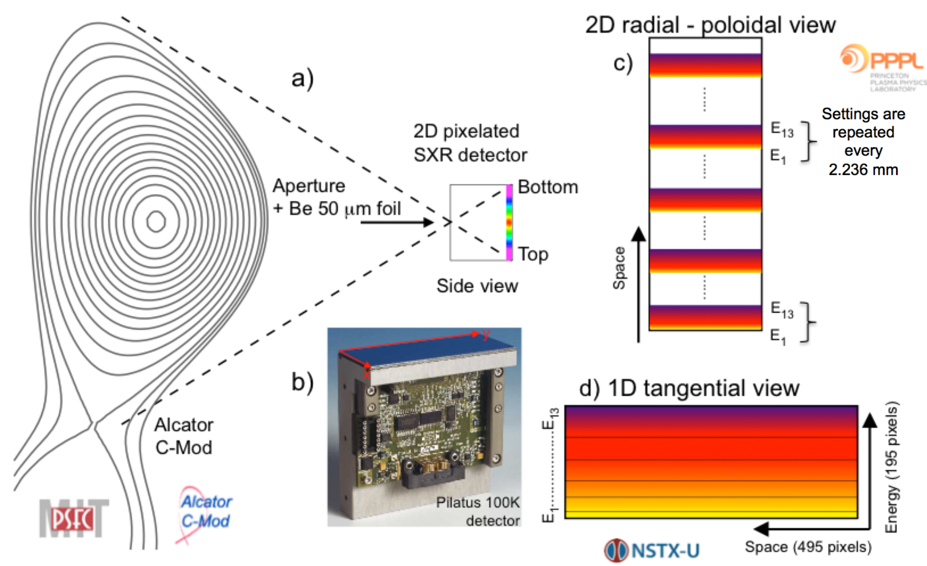

New core diagnostic systems will be installed in NSTX-U, MST, DIII-D, WEST, JT60SA to ITER

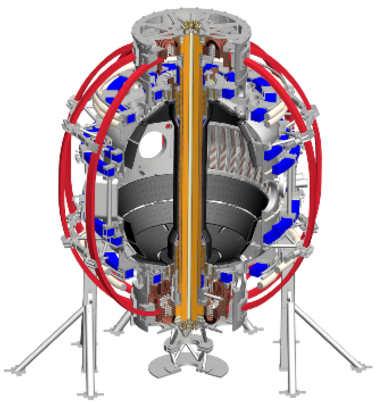

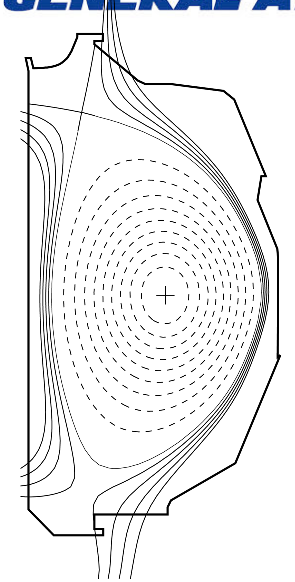

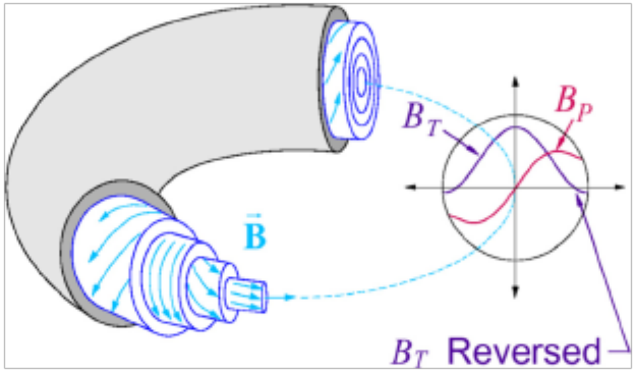

JT60SA

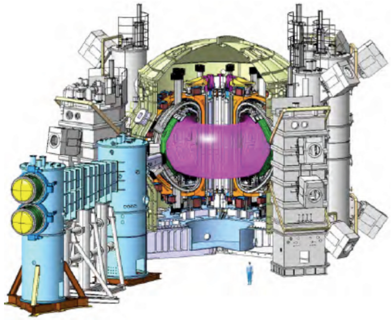

ITER

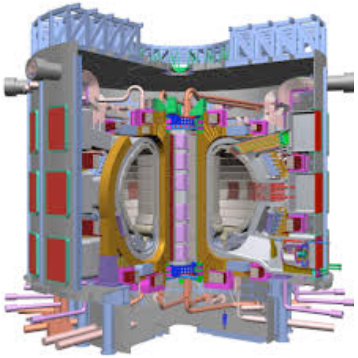

DEMO

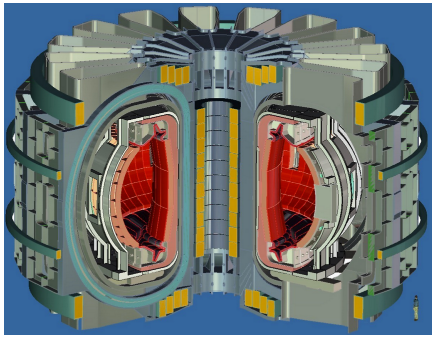

Summary

① With the selection of W for the divertor in ITER, understanding the sources, transport and confinement of high-Z impurities is crucial to ITER success.

② Avoid high-Z accumulation in the core is necessary to achieve and maintain high fusion performance in the presence of metal PFCs.

③ Reviewed the impact that low- to high-Z impurities have on the average plasma charge (Z_{eff}), resistivity and radiated power density (P_{rad}), and hence on transport, MHD instabilities and density limits.

④ A significant fraction of the power delivered to the plasma is lost in the form of radiation [even in an ideal pure H plasma].

⑤ In the x-ray range (subset of P_{rad}) could be as high as 90%.

⑥ Modern diagnostics in the visible, UV and x-ray range allow us to probe n_Z, $T_{e,i}$, $V_{\phi,\theta}$, Z_{eff} & $n_{e,fast}$ and their profiles!